8-9-2017 12:00 AM

Bubble-Induced Inverse Gas-Liquid-Solid Fluidized Bed

Xiliang Sun
The University of Western Ontario

Supervisor
Jesse Zhu
The University of Western Ontario

Recommended Citation

Abstract

Gas-liquid-solid fluidized beds have been widely applied in wastewater treatment, however, the current method of wastewater process has several limitations. Hence, an improved method is in demand. A 3.5 height and 0.1534m inner diameter column was used to study the hydrodynamic characteristics of a bubble-induced three-phase inverse fluidized bed. Air, water and three types of low-density particles were employed as gas, liquid and solid phases.

The hydrodynamic properties in the bubble-induced three-phase fluidized bed were investigated to provide the basic information for the industrial process, such as flow regime, bed expansion ratio and phase holdups. A flow regime map containing fixed bed, initial expansion, transition regime, complete fluidization and freeboard regime is presented. The bed expansion ratio behaves like the conventional fluidized bed. The axial profiles of the phase holdups show that with increasing gas velocity, liquid holdup has a downward trend, while gas holdup has an upward trend. Solids holdup is irrelevant with the gas velocity. Based on the Richardson-Zaki equation, a preliminary model between the solids holdup and superficial gas velocity was built.

Keywords

Acknowledgments

I would like to take this opportunity to express the gratitude and appreciation to those who have always been helping and supporting me in the academic and daily life.

My sincerest thank to my Supervisor Dr. Zhu, for believing in my potential, supporting me not only on research but also on daily life during my whole period of master study, and setting a role model for me, which ensured my successful fulfillment of this study.

My gratefulness is directed to Tian Nan for being a good friend and his help designing and constructing the experimental equipment and the report problems.

Many thanks to my friends in the research group, Jiaqi Huang, Yingjie Liu, Yupan Yun, Bowen Han, Haolong Wang, Xiaoyang Wei and Danni Bao, for their help, advice and friendship.

I really appreciate Mr.Wen's valuable advice in the experimental setups and George Zhang for his service.

Great gratitude is to my parents. Without their consistent and unreserved support, I could not have done this mission thus far a success.

Finally, my special thanks to my lovely boyfriend, Sida Zhou, for being the most stalwart supporter and faithful partner. I cannot thank him enough for loving and supporting me unconditionally.

Table of Contents

List of Tables

List of Figures

List of Appendices

Chapter 1

1   General Introduction

1.1   Introduction

Fluidization is solid particles are kept under suspension supported by the flow of fluid phase. At first, when the fluid is introduced into the static bed at a low velocity, fluid transits through the void between solid particles and particles remain as a static bed known as a fixed bed. The displacement of particles happens as increasing the fluid velocity, and it is known as an expanded bed. Now, particles are suspended with a higher velocity in the fluid and the drag force acts as a balancing force between the buoyancy and gravity. At a specific fluid velocity, the minimum fluidization velocity (Umf), the pressure drop through the bed is equal to the weight of the particles, which is a dynamic equilibrium. Under this situation, the bed is considered as a fluidized bed [Khan et al., 2014]. The phenomenon can be described as a mathematic equation [Yang, 2003]:

$$\Delta P = H_b(1-\varepsilon)(\rho_s - \rho_f)g$$

(1.1)

Fluidized beds have been used in many areas, especially in chemical and biochemical processing, like wastewater treatment. The efficient mixing and high mass/ heat transfer are the crucial factors in the fluidized bed [Bello et al., 2017].

Three-phase (Gas-liquid-solid) fluidized bed (TPFB) has been studied and it has many applications in chemical, petrochemical, pharmaceutical and biochemical industries [Fan,1989]. After employing particles, which density is lower than the liquid phase, as the solids phase, the fluidization system is known as an inverse three-phase fluidized bed (ITPFB). Compared to the conventional TPFB, the advantages of inverse fluidization contain simple reactor structure, convenient operation [Fan,1989], good fluidization at low fluid velocity, high rate of mass transfer [Fahim et al., 2013], high rate of heat transfer [Myre and Macchi, 2010] and effective control of biofilm thickness in biochemical treatment [Sokół and Woldeyes, 2011; Campos-Díaz et al., 2012]. With the development of inverse fluidized system, certain hydrodynamic characters have been

investigated with solid experimental results, such as flow regime [Han et al., 2000], pressure drop, bed expansion [Bendict et al., 1998; Kim and Kang, 2006], minimum fluidization velocity [Das et al., 2015], phase holdups [Shin et al., 2007;] and bubble behaviors [Narayanan et al., 2014; Hamdad et al., 2007]. Some other hydrodynamic characters such as mass and heat transfer coefficient have also been studied [Garcia-Ochoa and Gomez, 2009; Myre and Macchi, 2010].

A detailed literature review of the hydrodynamic of inverse fluidized bed previous study has been shown in Chapter 2.

1.2　Objectives

In this thesis, the following objectives should be achieved:

1. Basic concepts of the bubble-induced inverse gas-liquid-solid fluidized bed are first discussed to give a general background of this new technology.

2. Important hydrodynamic parameters related to reactor design and processes are discussed. As significant hydrodynamic characters determine the effectiveness of the fluidization process, flow regimes, bed expansion, and axial phase holdups will be studied in this thesis.

3. Based on the Richardson-Zaki equation, a preliminary model for the solids holdup and superficial gas velocity will be built.

1.3　Thesis structure

This thesis is based on the hydrodynamic characters of the bubble-induced inverse gas-liquid-solid fluidized bed.

Chapter 1 introduces the theoretical basis of fluidization and (inverse) three phase fluidized bed followed by the detailed literature review of hydrodynamic characters and applications in Chapter 2.

Schematics diagram of the inverse gas-liquid-solid fluidized bed is presented in Chapter 3. Moreover, the measurement methods and particle properties are also discussed.

According to different gas flow velocity, flow regimes can be separated as fixed bed regime, initial expansion regime, transition regime, complete fluidization regime and freeboard regime. The effects of the particle property and water level on transition gas velocities are studied in Chapter 4.

Chapter 5 is discussed about the effects of particles property and solids loading on the bed expansion ratio in the initial expansion regime and transition regime. While in the complete fluidization regime, the average phase holdups and local phase holdups were studied in Chapter 6 and Chapter 7, respectively.

Based on the Richardson-Zaki equation, a preliminary model related to the superficial gas velocity and phase holdup is introduced in Chapter 8. And some assumptions and discussions also be presented.

The conclusions and recommendations in Chapter 9 are described some main results of the thesis and some suggestions of the future work.

Chapter 2

2 Literature review

2.1 Introduction

Cleaning up the important source of water is a task of top priority. In Canada, over 150 billion liters of untreated and undertreated wastewater discharge into the waterways every year. Water is the source of life, in other word, water quality and human health have a close relationship. The current technology used in wastewater treatment is shown in Fig 2.1 [Lacroix et al., 2014]. However, the drawback of this process is that it requires large area but has low efficiency and long processing time. In addition, the main parts of this technique are the primary and secondary process and the aeration part. With the city development and population growth, this technique could not offer the clean water requirement in the future. Therefore, a new technology of wastewater treatment is in demand.
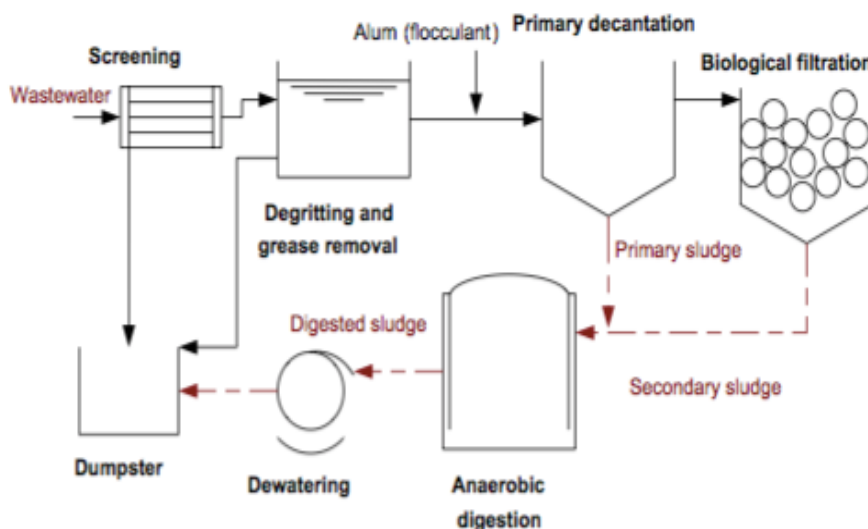
Figure 2.1 Simplified layout of wastewater treatment plant (WWTP).

The controlled part affected the wastewater treatment efficiency is the microorganism. In traditional wastewater treatment plant, bacteria suspend in the wastewater, thus the movement range is narrow and the reaction area is limited. If the bacteria attach then

grow on the surface of particles, the microorganism will move with the particles, which means the effective reaction area is larger than the suspended one.

Meanwhile, the sheer stress among particles can control the thickness of the biofilm, therefore a good mass transfer efficiency is achieved. Since the inverse fluidized bed can control the biofilm in a narrow range compared with the conventional one, the inverse fluidized bed reactor is more suitable for the wastewater treatment. Moreover, in the bubble-induced inverse fluidized bed, particles are fluidized only by an upward gas flow, which means there's no liquid flow in the system. Considering all kinds of situation, the bubble-induced inverse three-phase fluidized bed is employed as the new technology of wastewater treatment.

In inverse gas-liquid-solid fluidized bed, gas flows up and liquid goes downwards. Air, tap water and low-density particles are employed as gas phase, liquid phase and solids phase, respectively. As the density of particles is lower than the liquid, the particles floated on the top of the bed at first. After achieving the minimum fluidization velocity, the fixed bed disappears and the particles fluidize. Inverse fluidized bioreactors are employed in wastewater treatment in various industries [Nikolov and Karamanev, 1987; Karamanev and Nikolov, 1996]. Furthermore, some hydrodynamic characters in inverse fluidization have been studied to investigate the effects of different parameters.

2.2 Hydrodynamic characters in inverse fluidization

2.2.1 Flow regimes

There are two types of fluidizations, the liquid is continuous phase and gas is continuous phase, the former one is known as a fluidized bed, whereas the latter one is known as a turbulent bed [Fan et al., 1982a]. In inverse three-phase reactor, depending on different gas and liquid velocities, the flow regimes of larger particles can separate as (a) fixed bed (with or without local fluidization) with dispersed bubble regime; (b) bubbling fluidized bed regime; (c) transition regime and (d) slugging fluidized bed regime (Fig 2.2). [Fan et al., 1982b] When liquid and gas velocity are at a low rate, only a few particles move, however, most of the particles are stationary, as the drag force of the particles cannot balance the net gravity, which is known as the fixed bed. In the bubbling fluidized bed

regime, bed expansion ratio is influenced by the liquid velocity and gas velocity. At the constant liquid velocity, the bubble size and frequency do not change with increasing the gas velocity, however, the gas holdup through the bed increases while the liquid holdup decreases. Meanwhile, the sectional area of liquid decreases. On the other hand, at constant gas flow rate, increasing the liquid flow rate improves the linear liquid velocity, which encourages the particles to move with the liquid and leads to the initial expansion. The transition regime is narrow and difficult to control. The specialty in this regime is that bubbles become coalescence and the bubble size and frequency changes. In slugging fluidized bed regime, bubble impacts the particles, meanwhile, particles also have an influence on the bubble size and movement. The interaction effect between bubbles and particles occurs constantly.
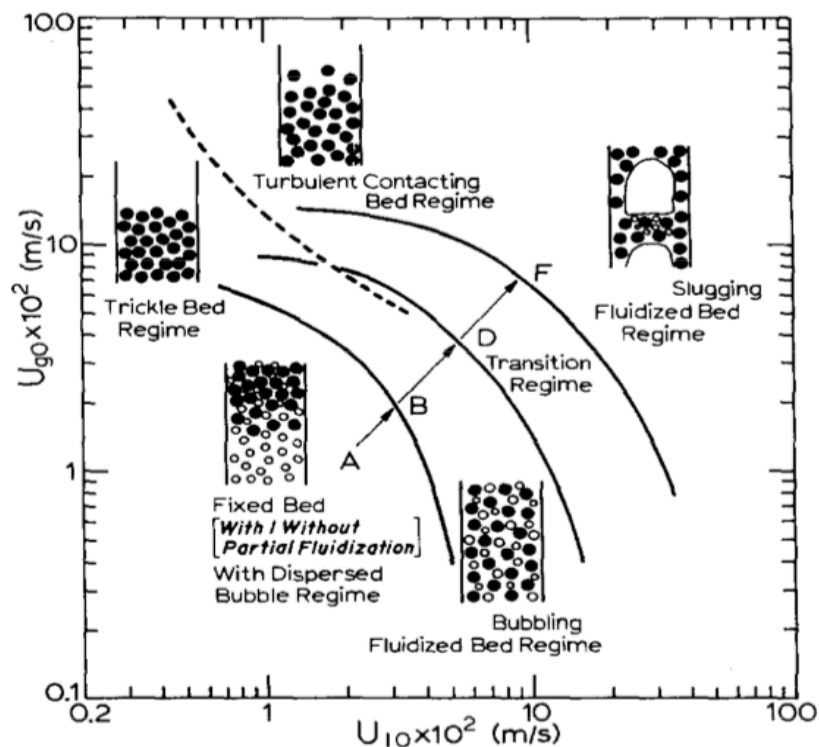
Figure 2.2 Flow regime diagram for a countercurrent gas-liquid-solid fluidized bed. Polyethylene hollow spheres, d=0.01m, ρ_s =388kg/m³; — liquid as a continuous phase, — — gas as a continuous phase.

In addition, for smaller particles, flow regime can separate three parts: (a) fixed or partial fluidized bed; (b) bubbling bed; (c) coalescing bubbling flow [Buffière and Moletta, 1999]. A schematic diagram of flow regimes is shown in Fig 2.3.
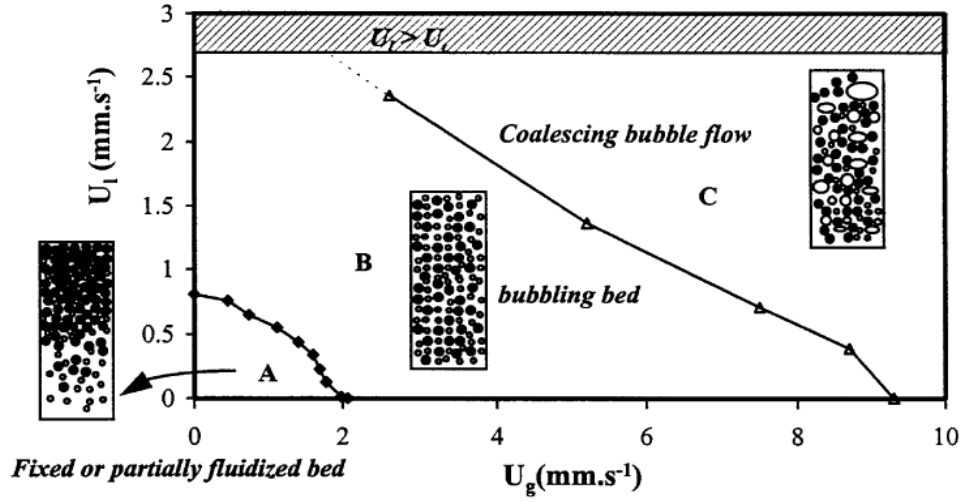
Figure 2.3 Flow regime map of inverse three-phase fluidized bed using small spherical particles, d=0.175mm, ρ_s=690kg/m^3 (A) fixed or partially fluidized bed; (B) bubbling bed; (C)fluidized bed with the transition to coalescing bubble flow.

2.2.2　Pressure gradient

Pressure gradient is one of the significant parameters to calculate the energy and power expenditure. Briens et al. reported the minimum fluidization liquid velocity (Ulmf) can be obtained by measuring the static pressure drop through a three-phase inverse fluidized bed [Briens et al., 1997]. With the basic principle of inverse fluidization, the pressure gradient through the bed is equal to the density of bed multiplies gravitational acceleration. Eq.2.1 expresses the pressure gradient in inverse three-phase (gas-liquid-solid) fluidized bed; the frictional pressure gradient in inverse two-phase (liquid-solid) fluidized bed has represented in Eq.2.2.

$$\left(-\frac{\Delta P}{\Delta z}\right)_{bed} = \rho_{bed}g = \left(\rho_s\varepsilon_s + \rho_l\varepsilon_l + \rho_g\varepsilon_g\right)g \tag{2.1}$$

$$\left(-\frac{\Delta P}{\Delta z}\right)_{f,ls} = \varepsilon_s(\rho_s - \rho_l)g \tag{2.2}$$

If it assumes the force of fluidization only by the liquid [Zhang et al., 1995; Zhang et al., 1998], Eq2.1 and Eq2.2 are combined to obtain Eq2.3.

$$\left(-\frac{\Delta P}{\Delta z}\right)_{bed} = \left(\varepsilon_s + \varepsilon_l\right)\rho_l g + \varepsilon_g \rho_g g + \left(-\frac{\Delta P}{\Delta z}\right)_{f,ls} \tag{2.3}$$

However, a different consequence can be acquired by assuming the force on the solid parts is provided by the liquid-gas mixture [Lee et al., 2000]. For a fixed bed, $\left(-\dfrac{\Delta P}{\Delta z}\right)_{f,ls}$ can be expressed by the Ergun equation [Ergun, 1952], then applied to the two-phase interaction. Neglecting the term $\varepsilon_g \rho_g g$ in Eq2.3, a final representation of pressure gradient is given below

$$\frac{1}{\rho_l g}\left(-\frac{\Delta P}{\Delta z}\right)_{bed} = 1 - \varepsilon_g - \frac{150\varepsilon_s^2 \mu_l U_l}{\Phi^2 d_p^2 \varepsilon_l^3 \rho_l g} - \frac{1.75\varepsilon_s U_l^2}{\varepsilon_l^3 \Phi d_p g} \tag{2.4}$$

Buffière and Moletta found 4 parameters *a,b,c,d* to fit the experimental data for the collision frequency and particle pressure under the given equation [Buffière and Moletta, 2000]:

$$Model = a\left[F\left(\frac{\varepsilon_s}{\varepsilon_{s0}}\right)\right]^b U_g^c \left(\frac{\varepsilon_s}{\varepsilon_{s0}}\right)^d \tag{2.5}$$

The optimum values obtained are

$a = 305700, b = 1.01(\approx 1), c = 1.02(\approx 1), d = 0.99(\approx 1)$ for collision frequency;

$a = 423, b = 1, c = 1.14, d = 0.75$ for the dimensionless particle pressure.

2.2.3   Minimum fluidization velocity

Minimum fluidization velocity is one of the conclusive parameters for the design of the three-phase fluidized bed [Zhu et al., 2007]. The definition is when the pressure gradient through the bed reaches the minimum, the superficial velocity is the minimum liquid fluidization velocity (U_{lmf}) [Cho et al., 2002]. In addition, the minimum liquid fluidization velocity also can be measured when the drag force balances the gravity and buoyancy of the particle [Lee et al., 2000].

Lee reported although U_{lmf} decreases as gas velocity increases, the patterns sometimes display concave-downward, sometimes concave-upward and sometimes S-shape behavior. The difference may be caused by the effects of liquid motion induced by rising bubbles and solids agglomerates attached to bubbles. Furthermore, U_{lmf} with wetting agent is lower than U_{lmf} without wetting agent, this phenomenon is attributed to the wetting agent that is effective to eliminate the bubble attached to the particles [Lee et al., 2000]. Das investigated with four different type particles and four different concentration non-Newtonian liquids and obtained that with increasing the bed weight, the pressure drop increases, however, the minimum inverse fluidization velocity is almost constant, which means the U_{lmf} is independent of solids loading. Meanwhile, U_{lmf} has no relevance with the column diameter. Ultimately, Das summarized that U_{lmf} is only determined by Reynolds number (Re) and Archimedes number (Ar) and particle properties (such as particle size, density, and sphericity) [Das, 2010].

2.2.4   Phase holdups

Phase holdup is one of the important hydrodynamic characteristics of the three-phase fluidized bed, which decides the fluidization efficiency within the fluidized bed. At present, the measurements of different phase holdups are various.

The well-established method of calculating the solids holdup is given below

$$\varepsilon_s = \frac{M}{\frac{\pi}{4} d_p^2 \rho_s H_{bed}} \tag{2.6}$$

Fan reported that in the inverse bubbling regime the liquid flow rate on gas holdup (ε_g) could be neglected. By comparison, in the conventional three-phase fluidized bed with large particles, the gas holdup decreases with an increasing liquid flow rate. Additionally, in the inverse slugging fluidized regime, the gas holdup has an opposite trend compared with the conventional bed. The empirical equations of the gas holdup in inverse bubbling regime and inverse slugging regime are given by [Fan et al., 1982a]:

$$\varepsilon_g = 0.322 \varepsilon^{1.35} (U_{go} / U_{l0})^{0.18} \tag{2.7}$$

for the inverse bubbling fluidized bed regime and

$$\varepsilon_g = 2.43 U_{g0}^{0.704} U_{l0}^{0.25} \tag{2.8}$$

for the inverse slugging fluidized bed regime.

Furthermore, Shin et al. suggested that the variation of liquid holdup is complex, gas holdup and solids holdup decreases with increasing the liquid viscosity. In addition, Shin et al. summarized that the physical properties and operating conditions then got some corrected equations of gas holdup and liquid holdup. Meanwhile, an equation related the solids holdup calculation is also given below [Shin et al., 2007]

$$\varepsilon_g = 5.517 U_g^{0.383} U_l^{0.426} \mu_l^{-0.071} (\frac{\rho_s}{\rho_l})^{11.357} \tag{2.9}$$

$$\varepsilon_l = 4.014 U_g^{0.136} U_l^{0.155} \mu_l^{0.056} (\frac{\rho_s}{\rho_l})^{2.009} \tag{2.10}$$

$$1 - \varepsilon_s = 5.568 U_g^{0.158} U_l^{0.169} \mu_l^{0.048} (\frac{\rho_s}{\rho_l})^{2.762} \tag{2.11}$$

Kim and Kang studied the bubble parameters and got gas holdup correlated as [Kim and Kang, 2006]

$$\varepsilon_g = 1.18 U_g^{0.235} U_l^{0.335} \mu_l^{0.391} (\frac{\rho_s}{\rho_l})^{3.61} \tag{2.12}$$

Bandaru et al. investigated the hydrodynamic of inverse three-phase fluidized bed and found that at low liquid velocity, the bed is packed at the top and the axial solids holdup is constant. At higher liquid velocity, the solids holdup gradually decreases from the top to the bottom of the bed. The axial variation of gas holdup along the height of the column is almost uniform within the range of liquid and gas velocities studied. Besides, it is experimentally observed that more solids distributed at the top and some at the bottom of the bed. Based on this observation, Bandaru et al. suggested considering the actual

variation of phase holdups in the bed is rather than assuming an average phase holdup of the entire bed [Bandaru et al., 2007].

Unfortunately, as the local holdup is related with lots of influencing factors, the accurate value is not easy to measure, thus there are a few related articles written about the local holdup studies.

2.2.5　Bed expansion

The general definition of fluidized bed expansion ratio is the ratio of bed height after the expansion and initial bed height. The bed expansion ratio can speculate the hydrodynamic in fluidized bed after change operating conditions. Bed expansion is a complex parameter affecting various kind of fluid mechanics. Furthermore, if bed expansion can be predicted by equations, it would be useful in actual operation design.

Despite bed expansion is important in fluidized bed design, not much of work has been reported in the literature for the detail experiments. Sau et al. have developed several empirical equations for bed expansion ratio in gas-solid tapered fluidized bed. The models for different types of particles were obtained and are given as follows [Sau et al., 2010].

For spherical particles:

$$R = 2.811(\frac{D_0}{D_1})^{0.05}(\frac{h_s}{D_0})^{-0.027}(\frac{d_p}{D_0})^{-0.463}(\frac{\rho_s}{\rho_f})^{-0.236}(\frac{U-U_{mf}}{U_{mf}})^{0.157} \qquad (2.13)$$

and for non-spherical particles:

$$R = 10.967(\frac{D_0}{D_1})^{0.119}(\frac{h_s}{D_0})^{-0.233}(\frac{d_p}{D_0})^{-0.091}(\frac{\rho_s}{\rho_f})^{-0.225}(\frac{U-U_{mf}}{U_{mf}})^{0.261} \qquad (2.14)$$

Furthermore, the Richardson and Zaki model is the most popular one in the fluidized bed due to its simplicity and its good agreement with experimental data. The basic R-Z equation is given by following [Richardson and Zaki, 1954]:

$$\frac{U}{U_i} = \varepsilon^n \tag{2.15}$$

Fan et al. studied the bed expansion of inverse fluidized bed based on R-Z equation and got the n values equations [Fan et al., 1982a]

$$n = 15 \mathrm{Re}^{-0.35} e^{3.9\frac{d_p}{D}} \tag{2.16}$$

for 350 < Re < 1250, and

$$n = 8.6 \mathrm{Re}^{-0.2} e^{-0.75\frac{d_p}{D}} \tag{2.17}$$

for Re > 1250. The article does not mention about how to determine the superficial fluid velocity U_i, but supposedly this has been done using the well-known standard drag curve.

2.2.6   Particle property

There's no author considering the particle property effect on fluidized efficiency. Therefore, after analyzing the data the articles mentioned, some conclusion can be obtained.

The particles with a density close to liquid required lower minimum fluidization velocity, which can be explained that particles move with liquid and smaller density difference results in less energy required to support the fluidization of particles [Buffière and Moletta, 1999].

2.2.7   Bubble behaviors

Bubble behaviors are one of the important parameters in three-phase fluidized bed research and design, which can be used for bed operating regime division and determine the flow structure. Bubble behavior directly determines the axial-radial phase holdup in the bed distribution, interaction and interphase heat and mass transfer efficiency.

In inverse three-phase fluidized bed, bubble size increases along with flow superficial velocity and liquid viscosity; while, decreases with increasing solids loading [Narayanan,

2014]. Bubble rising velocity increases with increasing superficial gas velocity or increasing liquid viscosity; decreases when the superficial liquid velocity increases [Kim and Kang, 2006; Son et al., 2007]. Bubble rising velocity has a positive correlation with the solids loading [Son et al., 2007]. Bubble frequency has a positive correlation with flow superficial velocity, while has a negative correlation relationship with liquid viscosity [Kim and Kang, 2006; Son et al., 2007]. Son et al. studied and found that bubble size, bubble rising velocity and frequency has been well correlated based on the concept of gas drift flux by means of dual electrical resistivity probe system. The equations are given by [Son et al., 2007].

$$L_b = 0.117(\frac{U_g + U_l}{1 - \varepsilon_g})^{0.446}(\frac{\rho_s}{\rho_l})^{-2.78}\mu_l^{0.191} \tag{2.18}$$

$$U_b = 0.108(\frac{U_g + U_l}{1 - \varepsilon_g})^{-0.219}(\frac{\rho_s}{\rho_l})^{-2.98}\mu_l^{0.076} \tag{2.19}$$

$$F_b = 30.846(\frac{U_g + U_l}{1 - \varepsilon_g})^{0.404}(\frac{\rho_s}{\rho_l})^{6.732}\mu_l^{-0.002} \tag{2.20}$$

Hamdad et al found that adding surfactants (ethanol) can reduce the minimum superficial gas velocity, inhibit bubble coalescence and decrease bubble rising velocity, consequently, increase gas holdup. The principle is same as adding surfactants in a conventional three-phase bed [Hamdad et al., 2007]. However, different surfactants have various influences on bubbles. For the larger bubbles, additives like sodium chloride (NaCl), sodium phosphate dibasic (Na_2HPO_3) and benzoic acid reduce the gas holdup. A possible explanation was given by Briens et al., who stated that the additives stabilize bubbles surfaces, inhibiting the splitting caused by shear force, as a result, reduce gas holdup. In conclusion, the surfactant has two main fractions: one is inhibiting bubble split which reduces gas holdup, while the other one is inhibiting bubble coalescence which increases gas holdup [Briens et al., 1999].

The reports of the axial and radial local bubble distribution are not too much, however, it is an important parameter in studying bubble behaviors. Similarly, different structure

types of gas distributor, column diameter and pressure gradient may affect the bubble behaviors, while, the articles about this field are not getting much attention recently.

2.2.8   Residence time distribution (RTD)

Residence time distribution can reveal the existing problems on the reactors then improve the design of the reactor. However, this area doesn't draw much attention.

Sánchez et al. investigated the fraction influence on residence time distribution and liquid mixing within a tracer used as a solution of potassium chloride (KCl). RTD curves with different solids fractions are presented in the dimensionless form *E(θ)* [Sánchez et al., 2005].

$$E(\theta) = \frac{C(\theta)}{(Q/V)\sum C_i \Delta t_i} = \frac{C(\theta)}{(\sum C_i \Delta t_i)t_a} \tag{2.21}$$

where

$$\theta = t / t_a \tag{2.22}$$

2.2.9   Mass transfer property

The internal mass transfer between reactor and substance is one of the important parameters in design and industries application. Inverse three-phase fluidized bed mainly includes the gas-liquid phase mass transfer and liquid-solid phase mass transfer.

In aerobic bioprocessing, oxygen is the key part as its low solubility in aqueous solutions but a continuous supply is needed. Mass transfer of gas-liquid interface is a complicated process, which is strongly influenced by the hydrodynamic conditions in the reactor. The mass transfer coefficient (k_L) can be estimated by many equations. Some of them are based on experiments, while others are theoretical. The theoretical model can be divided into two-film model, penetration model, renewed surface model, and film-penetration model [Garcia-Ochoa and Gomez, 2009].

In inverse three-phase fluidized bed, Whitman's two-film model is used widely (Fig.2.4). For the low-solubility gas (oxygen) and liquid interface mass transfer, the oxygen mass transfer rate per unit of reactor volume, N_{O2}, is obtained by the product of overall flux and the gas-liquid interfacial area per unit of liquid volume, a.:

$$N_{O_2} = aJ = k_l a(C^* - C_l)$$
(2.23)

In this equation, due to the oxygen is soluble in water slightly, the Henry constant H is very high. It is commonly accepted that the resistance on the liquid side of the interface is more than in the gas side, thus the resistance on the gas side can usually be neglected. Combined Eq2.19, the overall mass transport coefficient (K_l) is equal to the local coefficient (k_l).

$$\frac{1}{K_l} = \frac{1}{Hk_g} + \frac{1}{k_l}$$
(2.24)
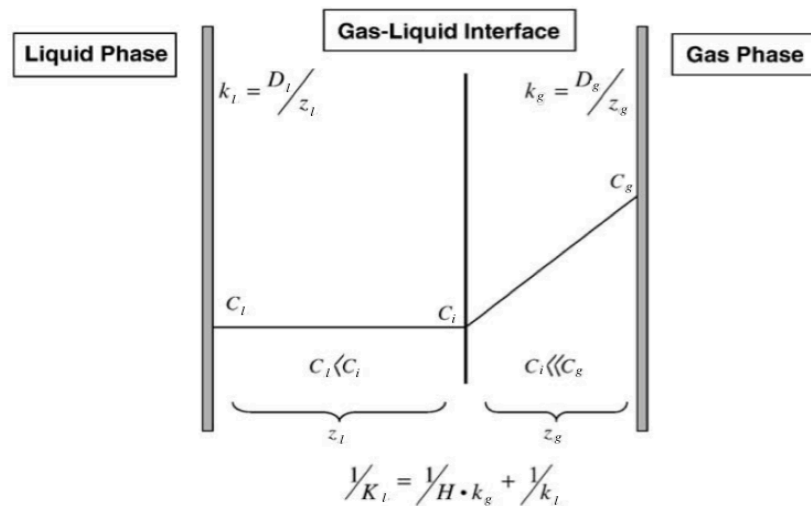
Figure 2.4 Schematic representation of the gas-liquid interface, concentration, mass transfer coefficients K_l, k_l and kg according to two-film theory.

Meanwhile, because of the difficulty of measuring k_l and a separately, the product $k_l a$ can be measured instead of two factors called volumetric gas-liquid mass transfer coefficient.

Hamdad et al. reported that $k_l a$ has a positive relationship with gas velocity but do not have a significant change in liquid velocity. Increasing gas velocity enhanced gas holdup and intensity of turbulence, while liquid velocity has little effect on bubble coalescence and gas holdup. Moreover, increasing solids loading decreases values of $k_l a$ at gas velocities over 20mm/s. This phenomenon is primarily due to decrease the gas holdup then a decrease in a happens [Hamdad et al., 2007].

Fahim observed that $k_l a$ is proportional to superficial gas (up to175%) and liquid velocity (up to 24%) both in a model and real fermentation conditions. Furthermore, the oxygen transfer in inverse three-phase fluidized bed is higher than in other bioreactors. And combined different conditions, an empirical equation is given by [Fahim, 2013]

$$k_l a (\frac{\mu_g}{\rho_g g^2})^{\frac{1}{3}} = 4.345 * 10^{-7} \left[u_g (\frac{\rho_g}{\mu_g g})^{\frac{1}{3}} \right]^{0.526} \left[u_l (\frac{\rho_g}{\mu_g g})^{\frac{1}{3}} \right]^{0.446} \left[\sigma (\frac{\rho_g}{\mu_g^4 g})^{\frac{1}{3}} \right]^{0.579} \qquad (2.25)$$

2.2.10   Heat transfer property

Temperature control is the key part of reactors not only controlled temperature can maintain the optimal reaction rate, but also temperature can affect the fluid property like density, viscosity, and diffusivity. In addition, temperature also has an influence on microorganisms that need a compatible environment to live and grow. In a word, the understanding of heat transfer phenomenon is necessary for industrial applications. Heat transfer coefficient (h) is investigated to perform the character of surface-to-bed or wall-to-bed heat transfer.

The immersed heater-to-bed heat transfer coefficient is measured when flow velocity is higher than the minimum fluidization velocity. The heat transfer increases with an increasing gas velocity because increasing gas velocity causes increasing bubble size and rising velocity, which lead to an increase of turbulence. Liquid velocity has a negative effect on heat transfer due to the solids holdup decreases at higher liquid velocity resulted in the contact surface area decreases. For the inverse three-phase fluidized bed, modified Nusselt number with or without liquid velocity is calculated as follows, respectively [Cho et al., 2002].

With liquid velocity inverse three-phase fluidized bed,

$$Nu = \frac{hd_p(1-\varepsilon_s)}{k_l\varepsilon_s} = 0.084(\frac{C_p\mu_l}{k_l})(\frac{d_p\rho_l U_g}{\mu_l\varepsilon_s})^{0.944} \qquad (2.26)$$

without liquid velocity inverse three-phase fluidized bed,

$$Nu = \frac{hd_p(1-\varepsilon_s)}{k_l\varepsilon_s} = 0.050(\frac{C_p\mu_l}{k_l})(\frac{d_p\rho_l(U_g+U_l)}{\mu_l\varepsilon_s})^{0.810}$$

(2.27)

Average surface-to-bed heat transfer coefficient increases with gas velocity, same as the heater-to-bed heat transfer coefficient. Since bubble size and bubble rising velocity increases with gas velocity, which enhances the turbulence through the bed. Average heat transfer coefficient increases at low solids loadings, however, decreases after a point of solids loading. This trend is related to the probe surface renew frequency. Increasing solids loading means more contact between particles and fluid, which results in a higher rate of fluid transfer around the probe. Above that point of concentration, higher solids loading of the liquid-solid phase causes an apparent viscosity increase, hence, the heat transfer coefficient decreases. Combined various parameters, Son et al got an experimental Nusselt number equation which is confirmed by Myre and Macchi 's experiment [Myre and Macchi, 2010].

$$h = C\left[k_l\rho_l C_{pl}\left\{\frac{[(U_l+U_g)(\rho_l\varepsilon_l+\rho_g\varepsilon_g+\rho_s\varepsilon_s)-(U_g\rho_g)]g}{\varepsilon_l\mu_l}\right\}^{\frac{1}{2}}\right]^{\frac{1}{2}} \qquad (2.28)$$

$$Nu = \frac{hd_p(1-\varepsilon_s)}{k_l\varepsilon_s} \qquad (2.29)$$

2.3 Hydrodynamic characters in bubble-induced inverse three-phase fluidized bed

Despite bubble-induced inverse three-phase fluidized bed has lots of advantages and usefulness, not much work has been reported in the literature for understanding certain important characteristics, especially phase holdups, bed expansion ratio and particle property effects and so on.

Chapter 3

3 Experimental apparatus and measurement methods

3.1 The structure of bubble-induced inverse gas-liquid-solid fluidized bed

A schematic diagram of the bubble induced inverse gas-liquid-solid fluidized bed is shown in Fig 3.1. A PVC column was employed as the main part with 0.1524m inner diameter and 3.5m height. Air, tap water and low-density particles were employed as gas, liquid, and solids phase, respectively. In addition, solids phase included three types of particles, including 904kg/m^3 polypropylene, spheroid; 930kg/m^3 polyethylene, cylinder; and 950kg/m^3 polypropylene, cylinder. To reduce the effect of plasticizer, solid particles were washed with tap water several times and watered before using at least 4 hours.
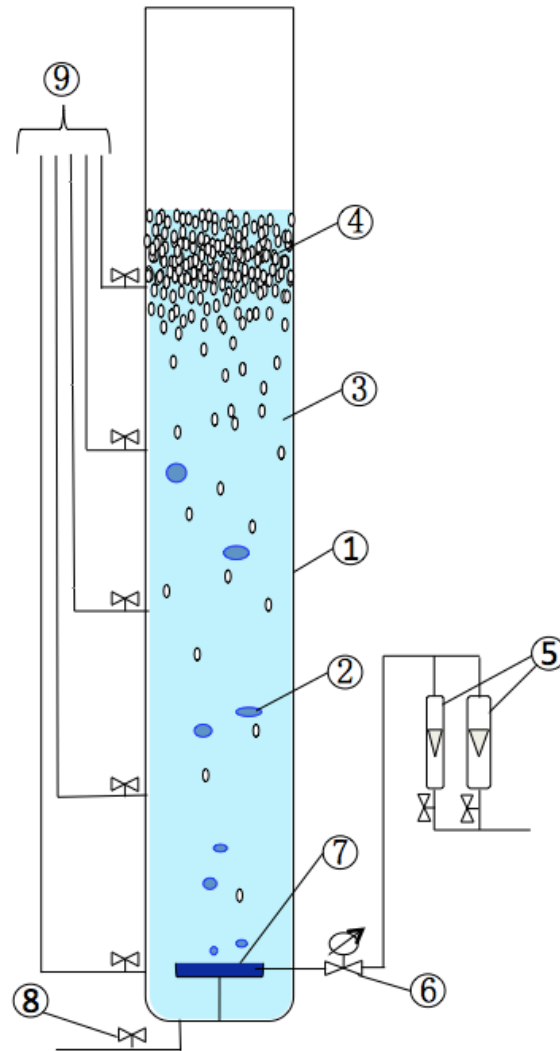
Figure 3.1 Schematic diagram of gas-driven inverse gas-liquid-solid fluidized bed. (1) column, (2) bubble, (3) liquid, (4) solid particles, (5) rotameters, (6) pressure gauge, (7) gas distributor, (8) liquid inlet/outlet valve, (9) manometer.

3.2 Experimental procedure

To avoid the possibility of air binding which results in the sudden break, the gas velocity decreases after complete fluidizing at high gas velocity.

Before starting the experiment, equally spaced pressure taps arranged through the column and connected to the manometers, meanwhile, manometers should be calibrated before experiments. To avoid the particles entering the pressure measurement lines, a stainless-steel screen was soldered to the cross surface of each pressure tap.

At first, the liquid was introduced from the inlet valve to the column until the determined height. As there's no water release, the liquid inlet/outlet valve should remain close during the experiment. Then, premeasured particles were added through the top of the column. Air was measured with the gas rotameters before being introduced through the gas distributor. Two different range gas rotameters were used to satisfy various operating conditions.

The solids concentration also called solids loadings were determined by the ratio of static bed height (H_0) to total height of column (H_{total}), varying from 5% to 20% (volume fraction).

Moreover, gas distributor was made of porous quartz with an 8.7cm outer diameter and a 2.7cm inner diameter (Fig3.2). The bubbles are small by using porous quartz, which can guarantee the good fluidization in the system. In addition, a pressure gauge was connected between the rotameters and gas distributor to measure the inlet gas pressure.
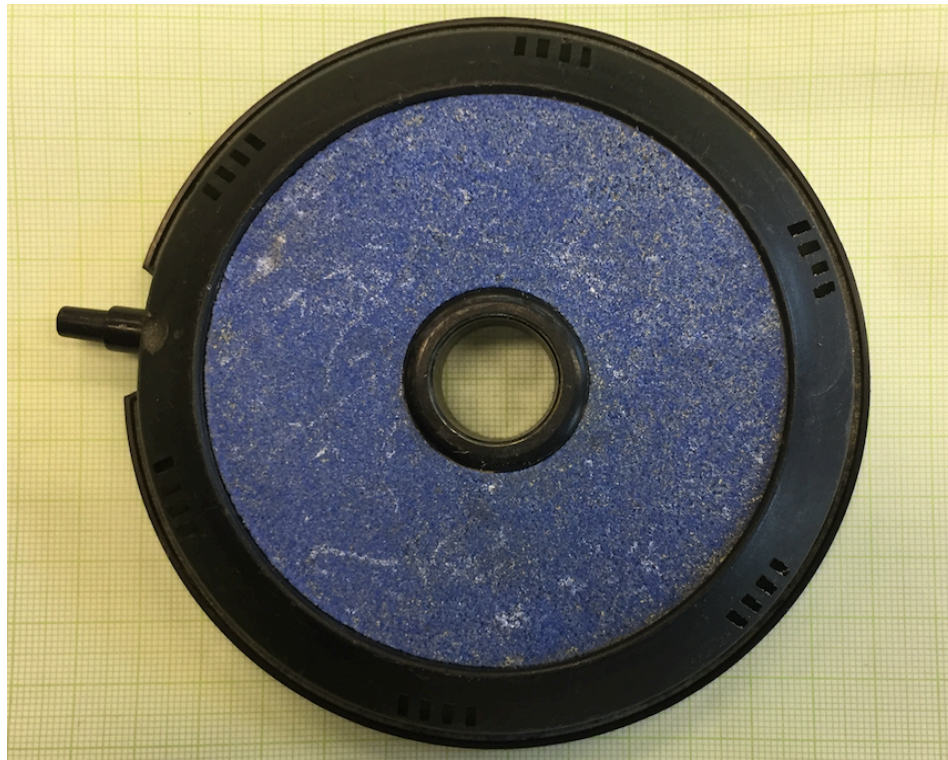
Figure 3.2 Picture of gas distributor.

3.3 Measurement procedures

Main hydrodynamic parameters measured in this study includes superficial gas velocity
(U_g), pressure drop, average phase holdups (ε), local solids holdup (ε_s), bed expansion
ratio (R) and so on. The measuring devices are listed in Table 3.1.

Table 3.1 Measurement methods of main hydrodynamic parameters

Parameters	**Measuring devices**
Superficial gas velocity	Gas rotameter, pressure gauge
Pressure drop	Pressure taps, manometer
Average phase holdups	Pressure taps, manometer
Local solids holdup	Pressure taps, manometer
Bed expansion ratio	Photography

3.3.1 Measurement of superficial gas velocity

The superficial gas velocity is measured by the gas rotameter combined with the pressure
gauge between rotameter and gas distributor.

After combined the pressure gauge, the calibrated gas flow rate was calculated by the
following equation

$$P_{ac}V_{ac} = nRT \tag{3.1}$$

$$P_{st}V_{st} = nRT \tag{3.2}$$

the term of "nRT" is same in Eq3.1 and Eq3.2, then V_{ac} can be obtained by

$$V_{ac} = \frac{P_{st}V_{st}}{P_{ac}} \tag{3.3}$$

Furthermore, as gas flow rate is related to the column diameter, superficial gas velocity is used instead of the gas flow rate. Superficial gas velocity is an artificial one, which is calculated under the hypothesis that gas is the only one flowing in the given cross section area. Superficial gas velocity is calculated by the following equation.

$$U_g = \frac{Q_g}{\frac{\pi}{4}D^2}$$ (3.4)

There's common that P_{ac} is equal to 1atm, under the circumstance, V_{ac} (1atm) was shown in Fig 3.4. P_{st} increases with increasing gas velocity, so, the slope in Fig3.4 has an upward bend.
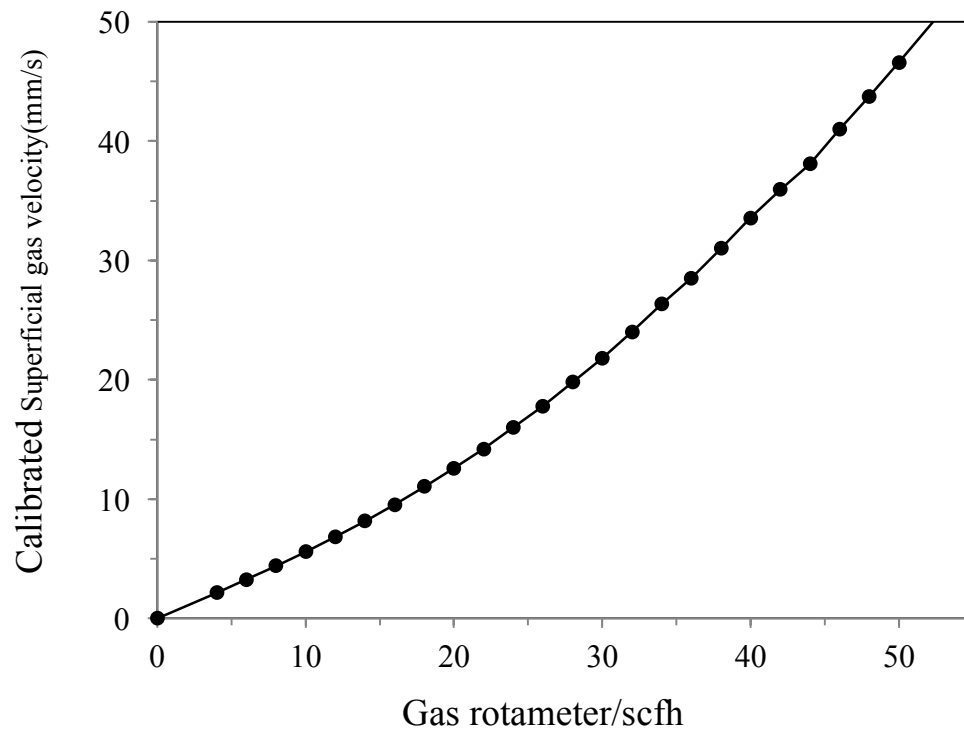
Figure 3.3 Calibration curve of gas rotameter considering pressure gauge.

3.3.2   Measurement of pressure drop

Pressure drop is measured by the equal mounted pressure taps and manometer. Photographs are employed for calculating the different height as they can record the

height within extremely short time to decrease the impact of water level fluctuates. Besides, the use of image, not only the time differences but also the personal reading errors are reduced.

Moreover, to minimize the personal reading errors, three images are taken to get the average pressure drop.

3.3.3   Measurement of average phase holdups

Average phase holdup is studied in the complete fluidization regime. To calculate the average phase holdups, a pressure balance between the top pressure tap and bottom pressure tap is given as

$$\rho_l g \Delta h + \rho_m g \Delta H = \rho_l g \Delta H \qquad (3.5)$$
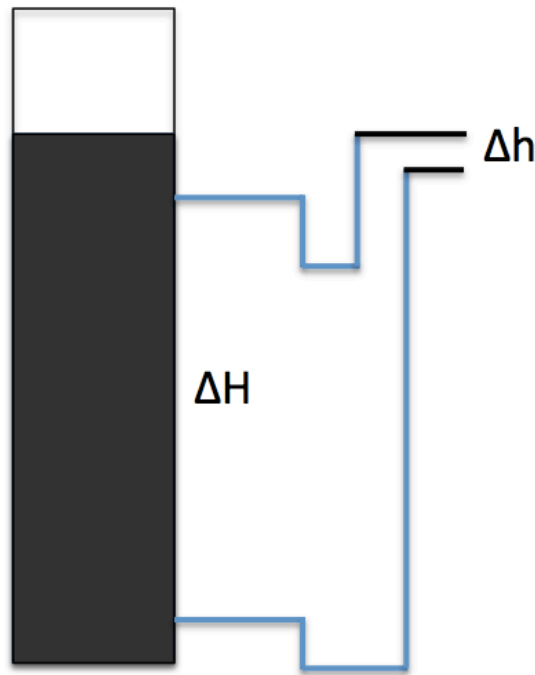
Figure 3.4 Schematic diagram of pressure drop through the column.

Meanwhile, mixture of gas, liquid and solid phase can be calculated by

$$\rho_m = \rho_s \varepsilon_s + \rho_l \varepsilon_l + \rho_g \varepsilon_g \qquad (3.6)$$

and it is known that the amount of adding three phase holdups is equal to one.

$$\varepsilon_s + \varepsilon_l + \varepsilon_g = 1 \tag{3.7}$$

Liquid was added when decrease gas velocity to remain the total bed height unchanged (visually), thus pressure taps are measured the pressure difference in fixed height through the column. The amount of added liquid is recorded to calculate the average liquid holdup.

$$\varepsilon_l = \frac{V_{water}}{V_{bed}} \tag{3.8}$$

Therefore, with four equations and four unknown variables, column mixture density can be expressed by pressure drop, while gas holdup (ε_g) and solid holdup (ε_s) can use liquid holdup (ε_l) and column mixture density to calculate.

$$\varepsilon_g = \frac{(\rho_s - \rho_m) - (\rho_s - \rho_l)\varepsilon_l}{(\rho_s - \rho_g)} \tag{3.9}$$

$$\varepsilon_s = \frac{(\rho_m - \rho_g) + (\rho_g - \rho_l)\varepsilon_l}{(\rho_s - \rho_g)} \tag{3.10}$$

3.3.4   Measurement of local phase holdups

For the local phase holdups, the main assumption of this model is that the axial liquid distribution in the column is uniform, which means the local liquid holdup is equal to the average liquid holdup.

$$\varepsilon_{l,local} = \varepsilon_{l,total} \tag{3.11}$$

Gas holdup (ε_g) and solids holdup (ε_s) can be obtained by the same equation of average phase holdups.

3.4 Particle properties

The physical properties of the 3 types of particles employed in bubble-induced ITPFB are shown in Table 3.2. The density of particles is determined by the average of 50 samples. The appearance of particles shown in Fig 3.6. The terminal particle velocity is determined by the following equation (Karamanev, 1996):

$$U_t = \sqrt{\frac{4(\rho_p - \rho_l)g d_p}{3\rho_l C_D}}$$

(3.12)

for free rising particles,

$$C_D = \frac{432}{Ar}(1 + 0.0470 Ar^{\frac{2}{3}}) + \frac{0.517}{1 + 154 Ar^{-\frac{1}{3}}}$$

(3.13)

for $\quad Ar < 1.18 * 10^6 d_p^2$

(3.14)

$$C_D = 0.95$$

(3.15)

for $\quad Ar > 1.18 * 10^6 d_p^2$

(3.16)

$$Ar = \frac{g d_p^3 \rho_l (\rho_l - \rho_p)}{\mu^2}$$

(3.17)
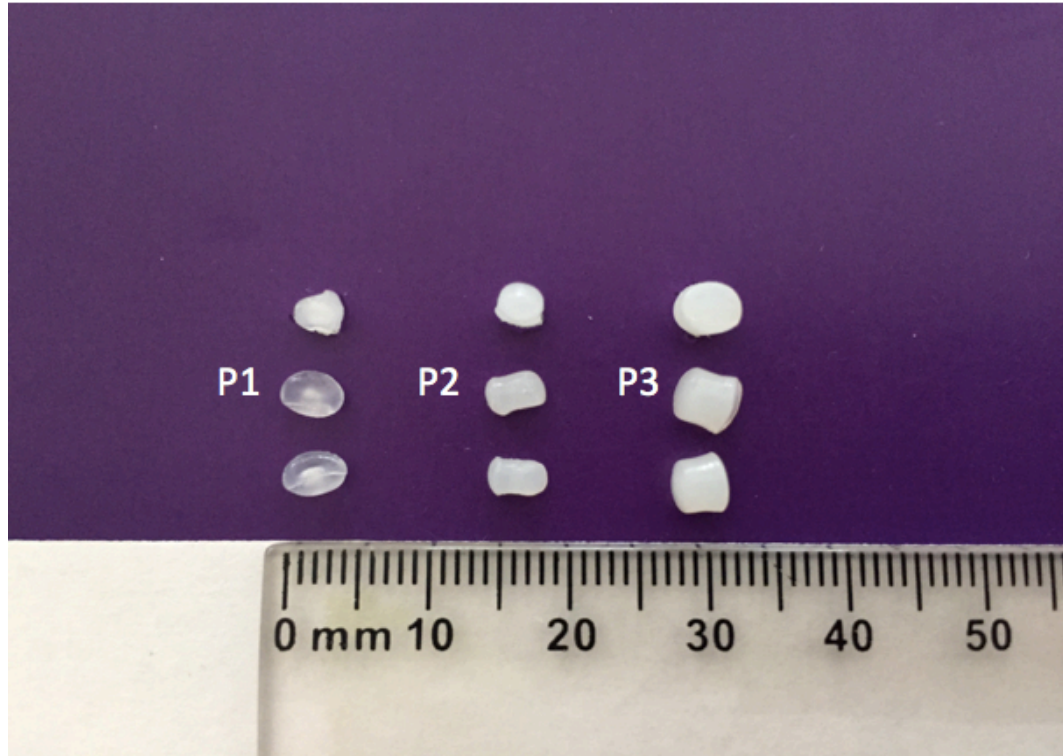
Figure 3.5 The appearance of three types of particles.

Table 3.2 Physical properties of particles used in bubble-induced ITPFB.

Particles	Shape	ρ_s (kg/m^3)	ε	Sphere Φ	d_p (mm)	U_t (cm/s)
P1	Spheroid	904	0.359	0.988	3.5	6.74
P2	Cylinder	930	0.353	0.841	3.5	5.73
P3	Cylinder	950	0.365	0.874	4.6	5.53

Chapter 4

4   Experimental investigation of flow regimes

In an inverse three-phase fluidized system, the liquid is considered as continuous phase while gas is the dispersed phase, generally. Based on the experimental phenomenon and some literature about the gas velocity definition [Fan et al., 1982b, Buffière and Moletta, 1999], three transitional gas velocities have been recorded as initial fluidization velocity (U_{g1}), full expansion velocity (U_{g2}) and complete fluidization velocity (U_{g3}).

Based on the experimental phenomenon, different flow regimes are presented depending on different gas velocities. The main method to analyze the flow regimes was visual observation. A schematic representation of the flow regimes with different gas velocities is shown in Fig 4.1. At first, particles, which densities are lower than liquid's density, were fixed at the top of the column when there's no gas flow rate. After the gas was introduced through the gas distributor, the lowest fixed particles began to fluidize. This gas velocity is called as initial fluidization velocity (U_{g1}). When superficial gas velocity was beyond U_{g1}, packed bed was gradually broken from the bottom to the top. The transform was too fast to control, therefore an initial fluidization velocity was used to instead of the minimum fluidization velocity that was the minimum superficial gas velocity required to keep all particles in action. With continuing increasing the gas velocity, particles were full distributed through the whole column. However, the solids distribution was not uniform in this regime. Some particles can reach the bottom, while most particles were fluidized at the top. In other words, solids concentration was diminishing from the top to the bottom through the column gradually. In this regime, full expansion velocity (U_{g2}) was achieved when some particles reached the bottom of the column. With further increasing the gas velocity, the difference of the solids concentration was reduced then disappeared, which means solid particles were uniformly distributed through the column with higher gas velocities, while the minimum gas velocity to maintain this situation is known as complete fluidization velocity (U_{g3}). Based on the experimental phenomenon, the particles were moved into the lower position with a further increased gas velocity. In other words, particles were not uniformly

distributed through the bed again, while only gas and liquid still existed at the top of the column when superficial gas velocity was beyond top freeboard velocity (U_{g4}). As the value of Ug4 was higher than the velocity range in this project, the detailed investigation will be studied in the future.

The effects of particle properties and solids loadings on three specific gas velocities were discussed in the following parts.
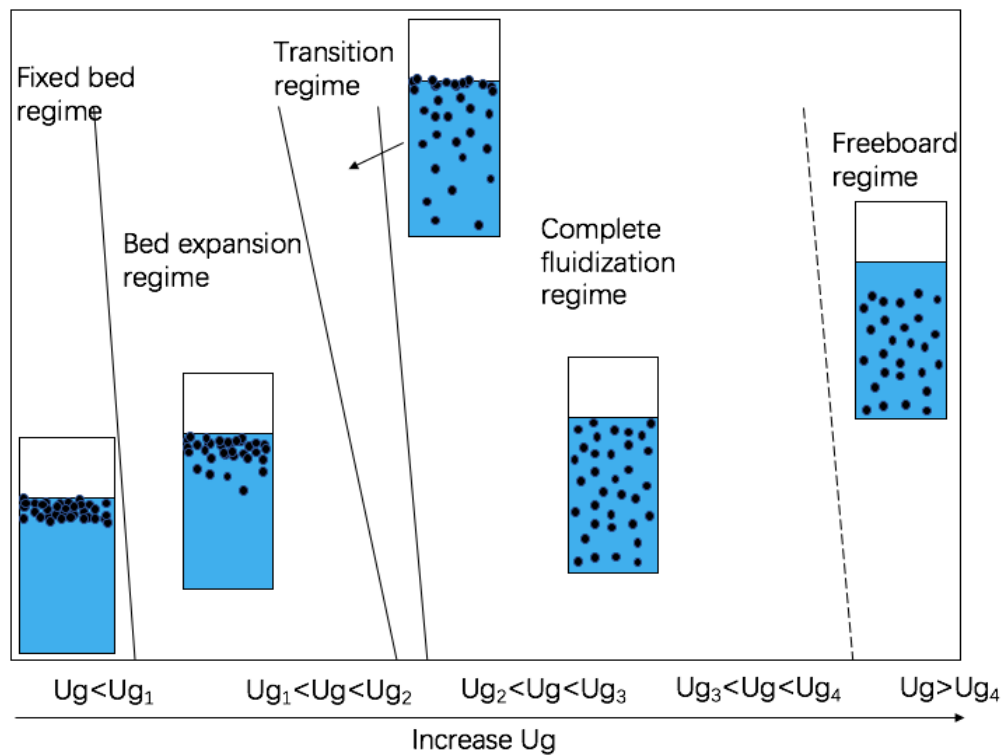
Figure 4.1 Flow regimes map in bubble-induced inverse three-phase fluidized bed.

4.1 Initial fluidization velocity (U_{g1})

Initial fluidization velocity is the minimum superficial gas velocity required to break the fixed bed, while the particles in the lower position begin to fluidize. The variations of the initial fluidization velocity (U_{g1}) with solids loadings for 3 types of particles are shown in Fig 4.2. Initial fluidization velocity (U_{g1}) decreases with increasing the solids loading for P2 (930 kg/m^3) and P3 (950 kg/m^3) because particles fluidization is controlled by the liquid as particles density is closed to liquid density, while liquid pattern is determined by the gas flow rate because no liquid goes in or out during the experiment. In this situation,

particle fluidization is indirectly controlled by gas flow rate. With increasing the solids loadings, more particles immerse into the water and the lowest particles are more closed to the gas distributor, which means easier to begin to fluidize. However, U_{gl} for P1 (904 kg/m^3) doesn't decrease with increasing solids loadings, the reason is that P1 is easy to form an aggregation. Aggregation begins serious with increasing solids loading, which means P1 requires higher gas flow rate to break the aggregation. The required gas flow rate is higher than the diminished one caused by increasing solids loading.

U_{gl} for P2 is lower than U_{gl} for P3 though the density of P3 is closer to liquid density than P2. Because the diameter of P3 is larger than the diameter of P2, the gas velocity of P3 required to fluidized is higher than P2 requirement, which means, at a same gas flow rate, P2 is easier to fluidize than P3.
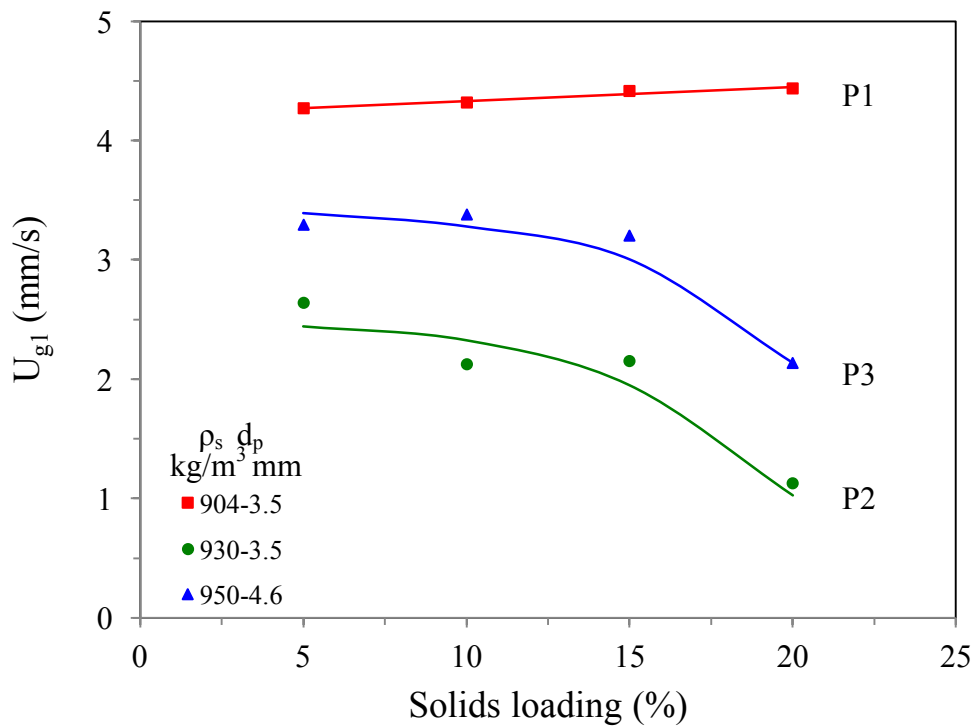
Figure 4.2 Initial fluidization velocity (U_{gl}) as a function of solids loading for three types of particles.

4.2 Full expansion velocity (U_{g2})

Full expansion velocity is the superficial gas velocity when some particles have reached the bottom of the column, however, the distribution of solids concentration is not uniform. The variations of the full expansion velocity (U_{g2}) with solids loadings for 3 types of particles are shown in Fig 4.3. For all particles, full expansion velocity (U_{g2}) decreases then keeps constant with increasing solids loadings, because gas flow rate drives liquid movement which actuates particles fluidization indirectly. With increasing solids loading, more particles immerse into the water, which means the low-position particles are closer to the gas distributor. At same gas velocity, the particles begin to fluidize then reach the bottom, whereas, some particles still fix at the top of the bed. The drag force for each particle to reach the bottom is same, so, the U_{g2} keeps constant with increasing solids loadings when the required gas flow rate is obtained.

U_{g2} for P2 is lower than U_{g2} for P3 though the density of P3 is closer to liquid density than P2. Because the diameter of P3 is larger than the diameter of P2, the required fluidization velocity of P3 is higher than P2, which means, at a same gas flow rate, P2 is easier to fluidize than P3.
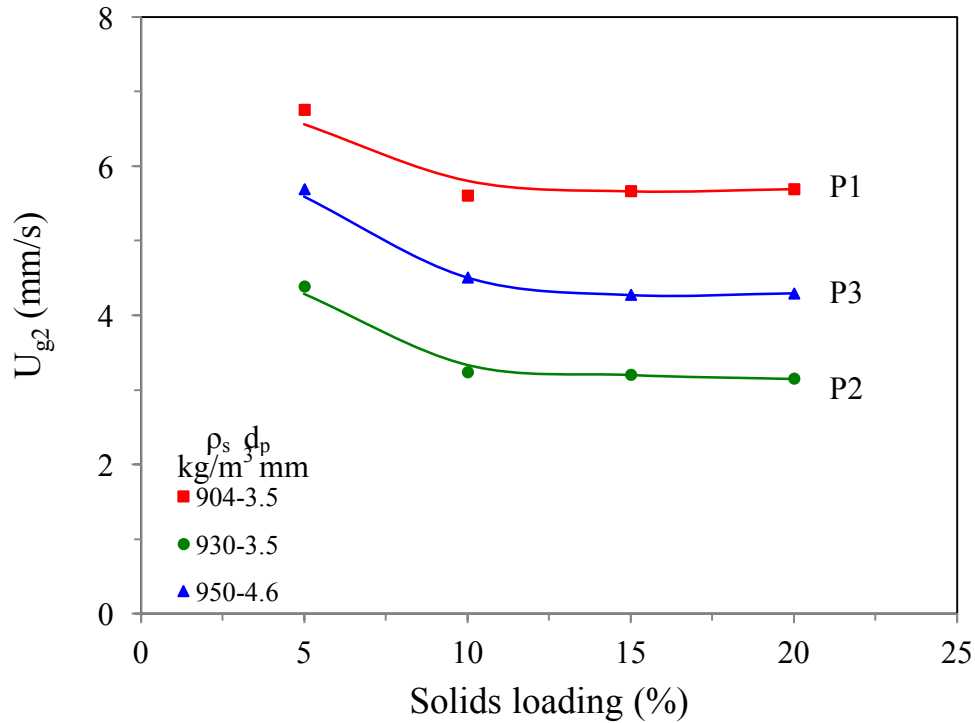
Figure 4.3 Full expansion velocity (U_{g2}) as a function of solids loading for three types of particles.

4.3 Complete fluidization velocity (U_{g3})

Complete fluidization velocity is the superficial gas velocity required when the fixed bed is broken. The variations of the complete fluidization velocity (U_{g3}) with solids loadings for 3 types of particles are shown in Fig 4.4. For all particles, complete fluidization velocity decreases with an increase solids loading, because higher solids loading means more particles immerse into the water and the lowest particles are closed to the gas distributor. As mentioned in U_{g1} and U_{g2}, gas flow rate drives particles fluidization indirectly. At the same solids loading, particles which density is closed to liquid require lower superficial gas velocity to fluidize. For this reason, the complete fluidization velocity for P1 is much higher than P2 and P3.

U_{g3} for P2 is lower than U_{g3} for P3 though the density of P3 is closer to liquid density than P2. As mentioned in U_{g1} and U_{g2}, P3 is larger than P2, which means P3 requires higher fluidization velocity than P2. Furthermore, the degree of the size influence on U_{g2} and U_{g3} is different.
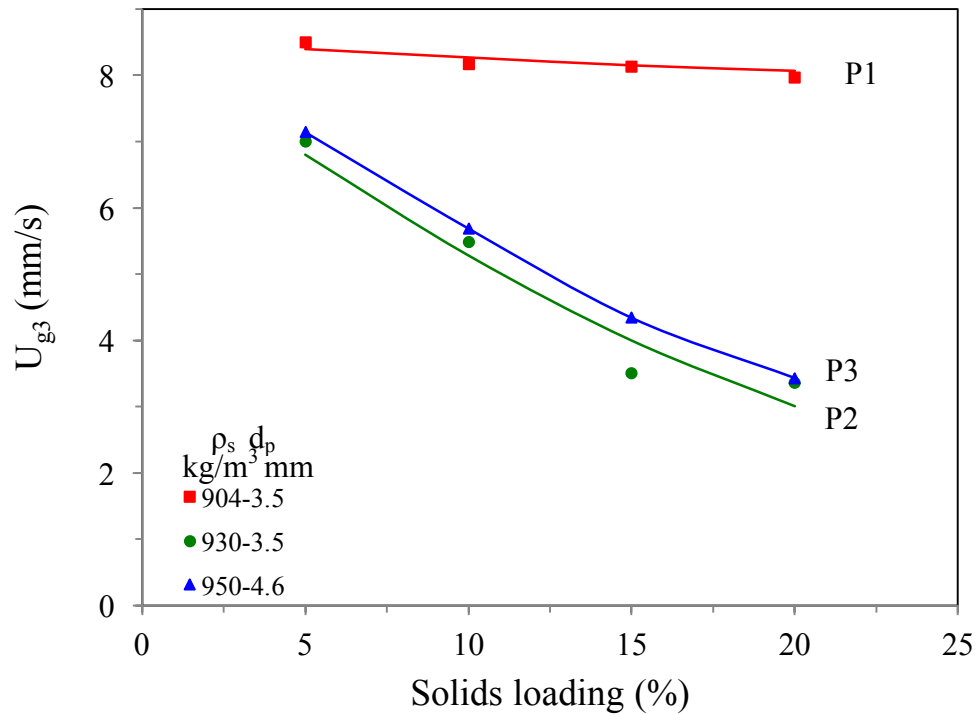
Figure 4.4 Complete fluidization velocity (U_{g2}) as a function of solids loading for three types of particles.

4.4 Flow regimes

In bubble-induced inverse gas-liquid-solid fluidized bed, depending on the superficial gas velocity and water level, flow regimes can separate into fixed bed regime, initial expansion regime, transition regime and complete fluidization regime, and freeboard regime. Based on the experimental phenomenon, the value of U_{g2} is equal or greater than 50mm/s.

The superficial gas velocity varied with particle densities are shown in Fig 4.5. With increasing the density of particle, all three superficial fluidization velocities decrease because the particles whose density is close to the density of liquid are easier to fluidize.
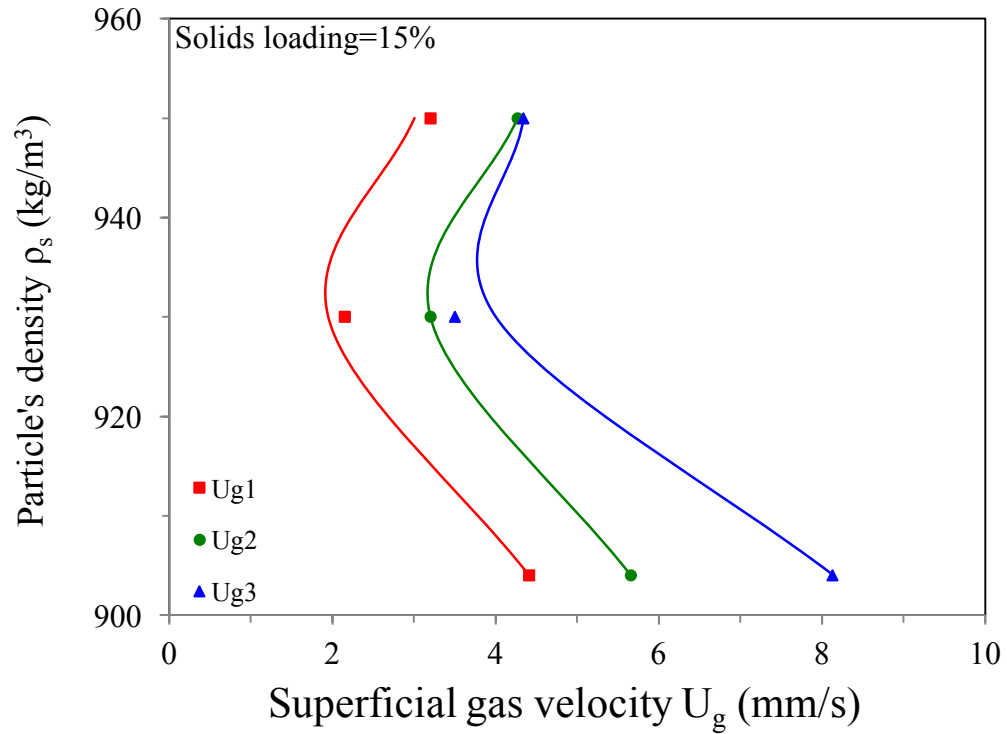
Figure 4.5 Superficial gas velocity varied with particle's densities.

The superficial gas velocity varied with particle densities are shown in Fig 4.6. For three particles, initial fluidization velocity (U_{g1}) is lower than full expansion velocity (U_{g2}) that is lower than complete fluidization velocity (U_{g3}). With increasing solids loadings, initial fluidization velocity and complete fluidization velocity decrease because more particles immerse into water and the lowest position particles are close to the gas distributor. The full expansion velocity decreases at first then remains constant, thus the possible reason is that the required superficial gas velocity is obtained.
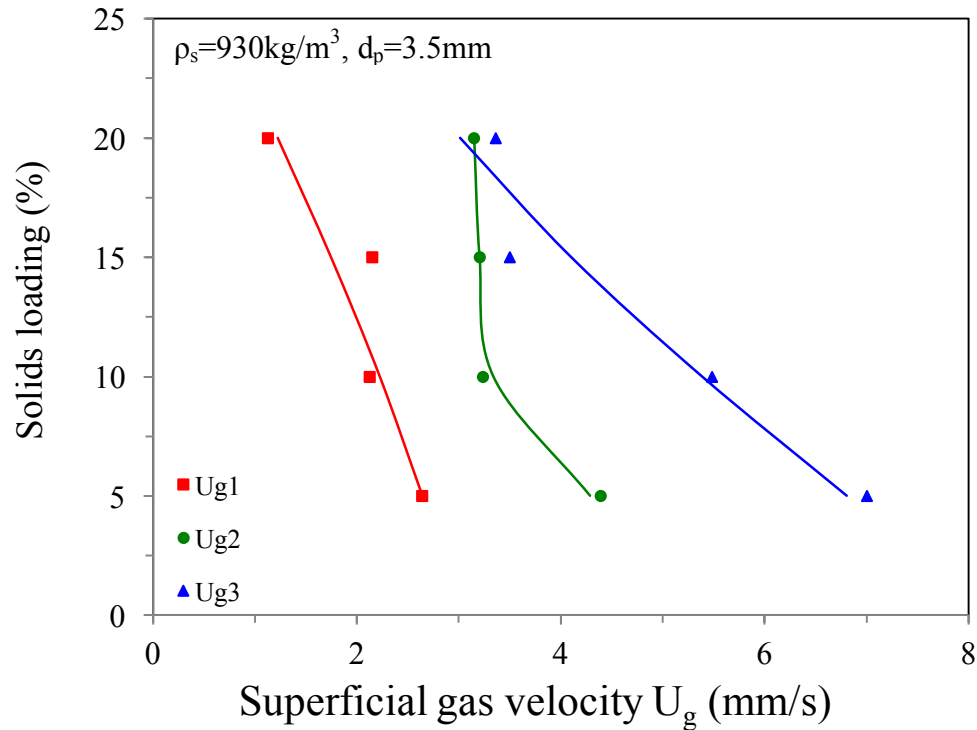
Figure 4.6 Superficial gas velocity varied with solids loadings.

The superficial gas velocity varied with water level for 3 types of particles are shown in Fig 4.7. For three particles, initial fluidization velocity (U_{g1}) is less than full expansion velocity (U_{g2}) that is less than complete fluidization velocity (U_{g3}). At same solids loading (5%), with increasing particles density, all three special gas velocities (U_{g1}, U_{g2} *and* U_{g3}) decrease because particles whose density is close to the liquid are easy to fluidize. Meanwhile, the size of particles also affects the fluidization velocity. At the same solids loading (5%), bigger particles require higher gas flow rate. In addition, with increasing water level, three special superficial fluidization velocities increase because bubble coalescence results in fluid density decrease.
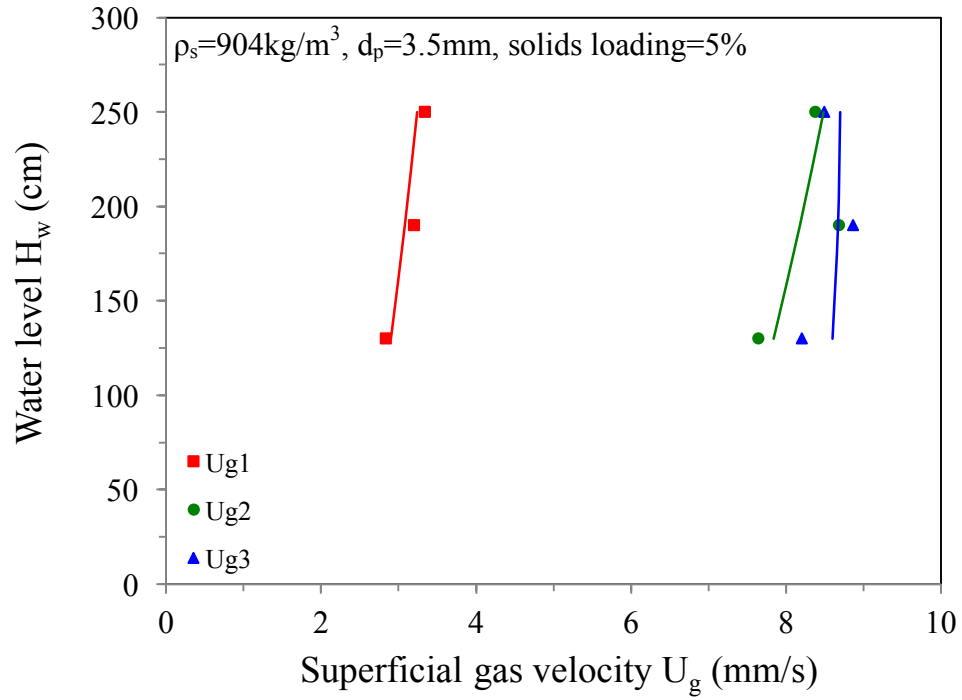
(a)
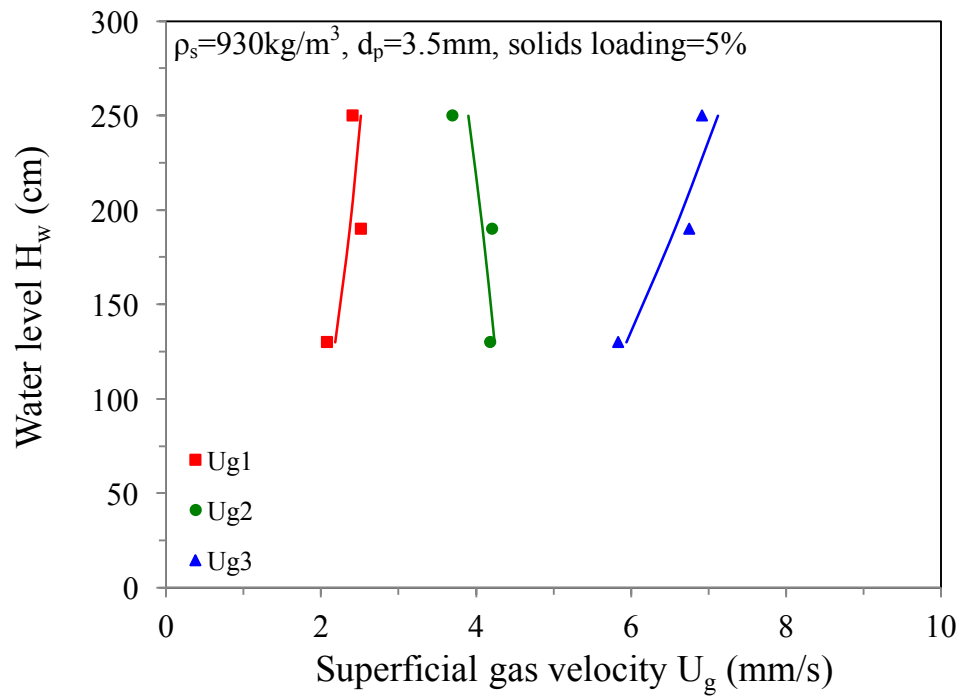
(b)
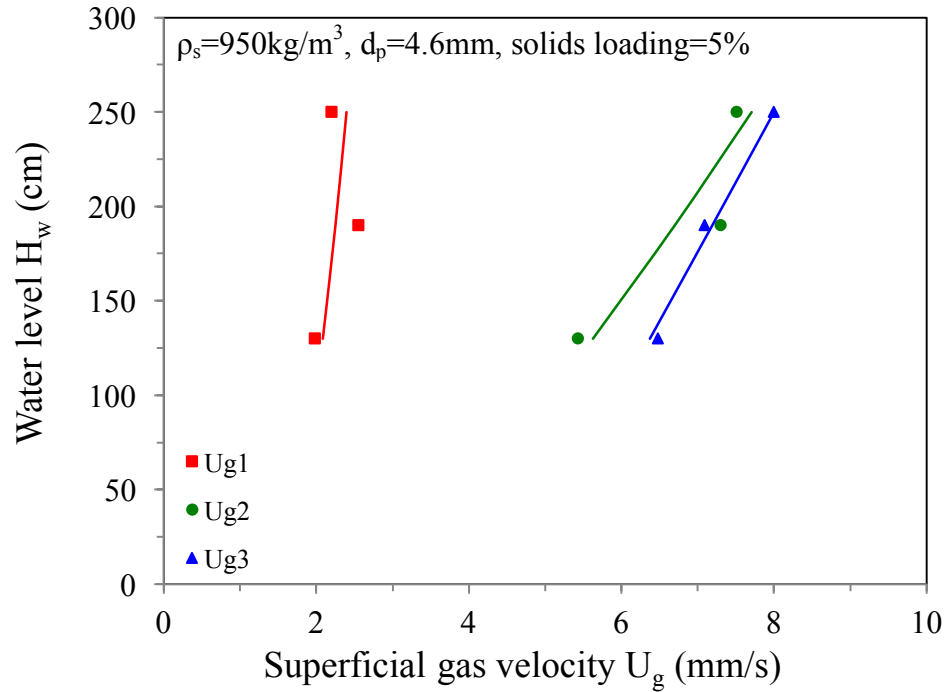
(c)

Figure 4.7 Superficial gas velocity varied with water level for three types of particles: (a) 904kg/m^3, (b) 930kg/m^3 and (c) 950kg/m^3.

The superficial gas velocity varied with water level for 3 solids loadings are shown in Fig 4.8. For three solids loadings, initial fluidization velocity (U_{g1}) is lower than full expansion velocity (U_{g2}) that is lower than uniform fluidization velocity (U_{g3}). For particle P2 (930 kg/m^3), with increasing solids loading, all three special gas velocities (U_{g1}, U_{g2} and U_{g3}) decrease because more particles immerse into water with higher solids loading.
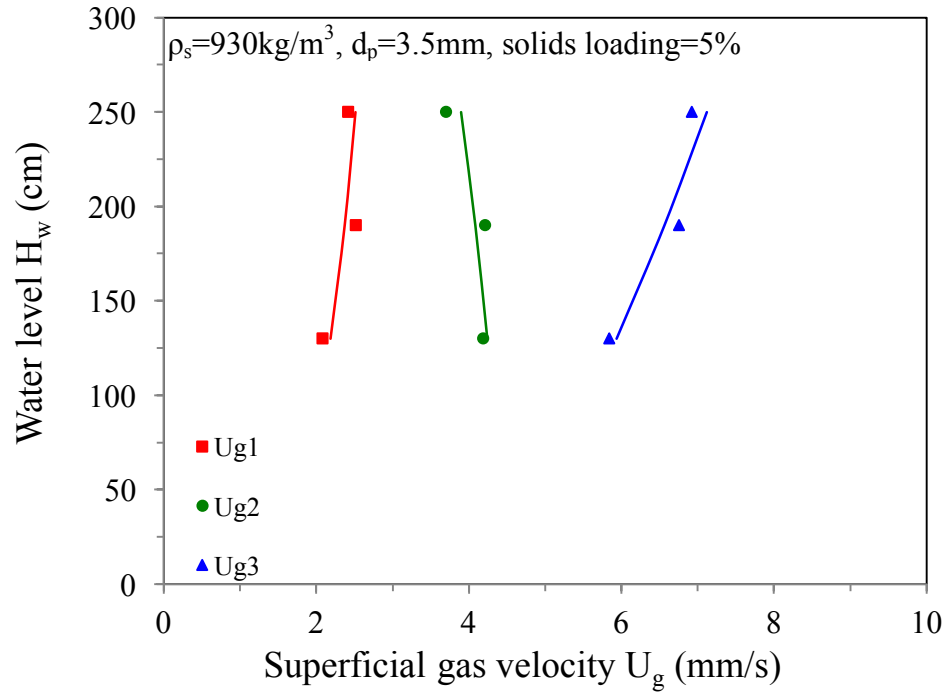
(a)
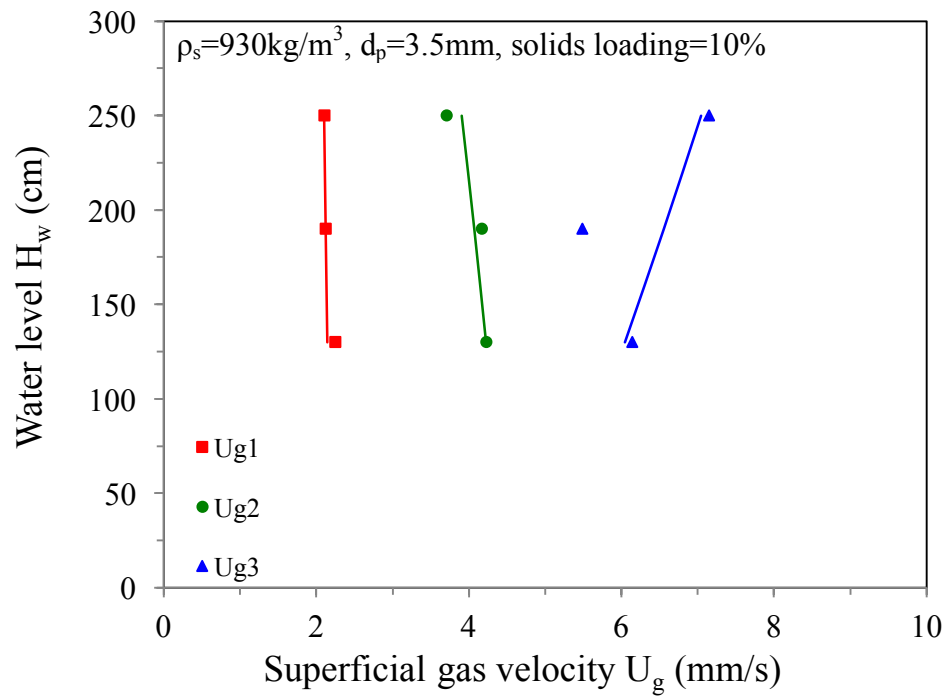
(b)
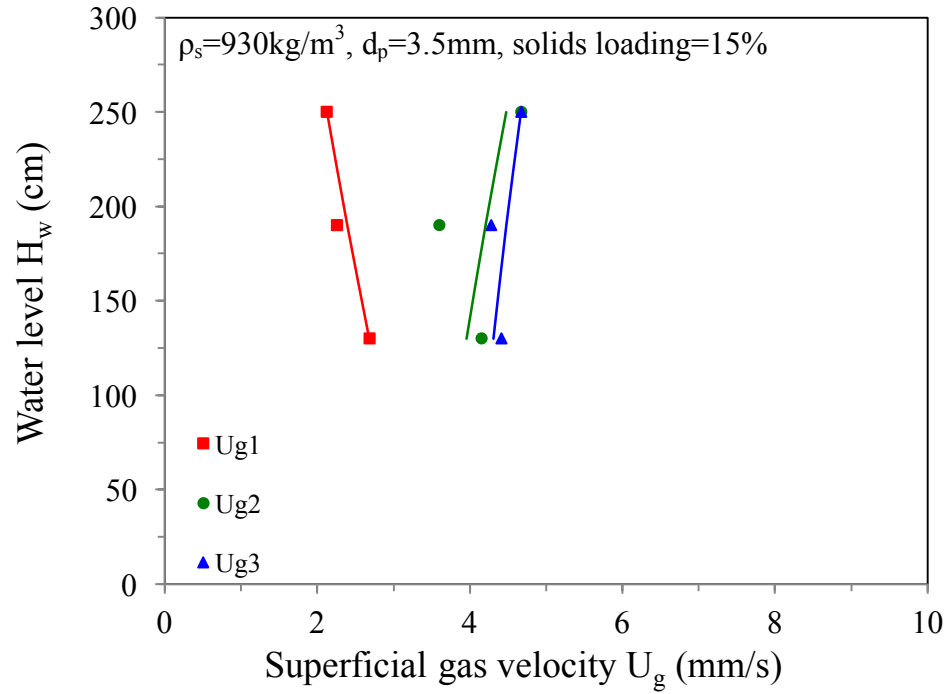
(c)

Figure 4.8 Superficial gas velocity varied with water level for three solids loadings: (a) 5%, (b) 10% and (c) 15%.

Chapter 5

5   Experimental investigation on bed expansion

Bed expansion in the inverse fluidization is a critical factor that assists in scaling up fluidized bed and the design of reactors for industrial applications.

The general definition of bed expansion ratio is using the following equation:

$$R = H_{total} / H_0$$

Initial bed height (H_0) is the fixed bed height after full fluidization, in case some particles attach to the wall. Total bed height (H_{total}) is measured as the distance between the highest and lowest particle positions. In addition, the lowest layer doesn't behavior like a horizontal lane (Fig5.1). The lowest particle position is determined by the average position between the top and bottom particles in Fig5.1.
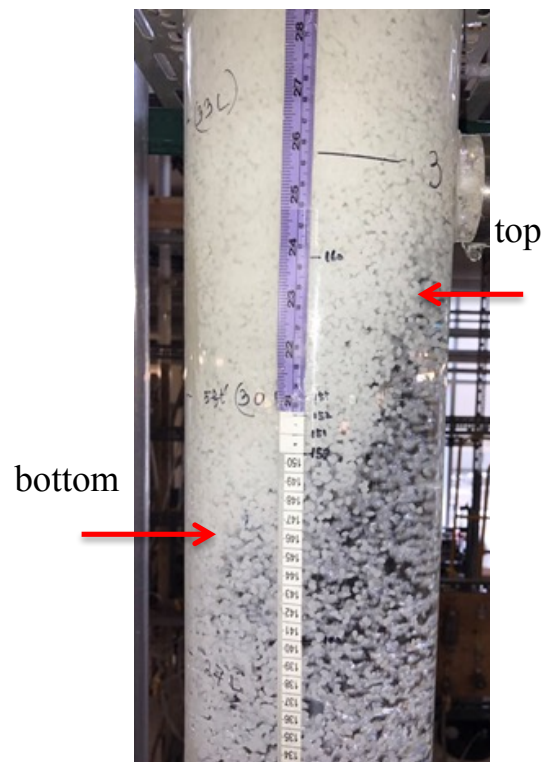
Figure 5.1 The selection of lowest layer of the expansion bed.

5.1 The effect of particle property on bed expansion ratio

Three different particles are employed to investigate the bed expansion ratio, including 904kg/m^3, 3.5mm; 930kg/m^3, 3.5mm and 950kg/m^3, 4.6mm. The variations of bed expansion ratio as a function of superficial gas velocity for three different particles are shown in Fig 5.2. It is observed that the bed remains fixed until a certain gas flow rate (U_{g1}), subsequently increases with gas flow rate for different solid densities and initial water level. Since at lower gas flow rate, drag force caused by the downward flow cannot balance the net buoyancy of the particles acting in the opposite direction. Therefore, the particles keep as the packed bed at the top of the column. With increasing the gas flow rate, a condition (downward drag force=upward net buoyancy) is obtained where the lowest position of the particles begin to fluidize. The velocity corresponding to the flow rate is referred as initial fluidization velocity (U_{g1}). With further increasing the gas flow rate, more and more particles separate from the packed bed then fluidize, meanwhile, bed expansion ratio increases as drag force increases with increasing gas flow rate. When some particles reach the bottom of the bed, the velocity corresponding to this gas flow rate is termed as the full expansion velocity (U_{g2}). As the limit of the column height, the bed expansion ratio keeps constant after the full expansion velocity. Furthermore, in three initial water levels (130cm, 190cm and 250cm), the patterns of the bed expansion ratio are like each other, which means the influence of the initial water level can be neglected.

In addition, P1 (904kg/m^3) has the highest initial fluidization velocity and full expansion velocity as the difference between the density of P1 and liquid is the biggest among three particles. Also, P2 and P3 have almost same initial fluidization velocity and full expansion velocity, the reason is that the difference between the density of P2 and liquid is higher than the P3, however, P3 has larger size than P2. Combined the effect of the density and size, the trend of the bed expansion ratio of P2 and P3 is similar.
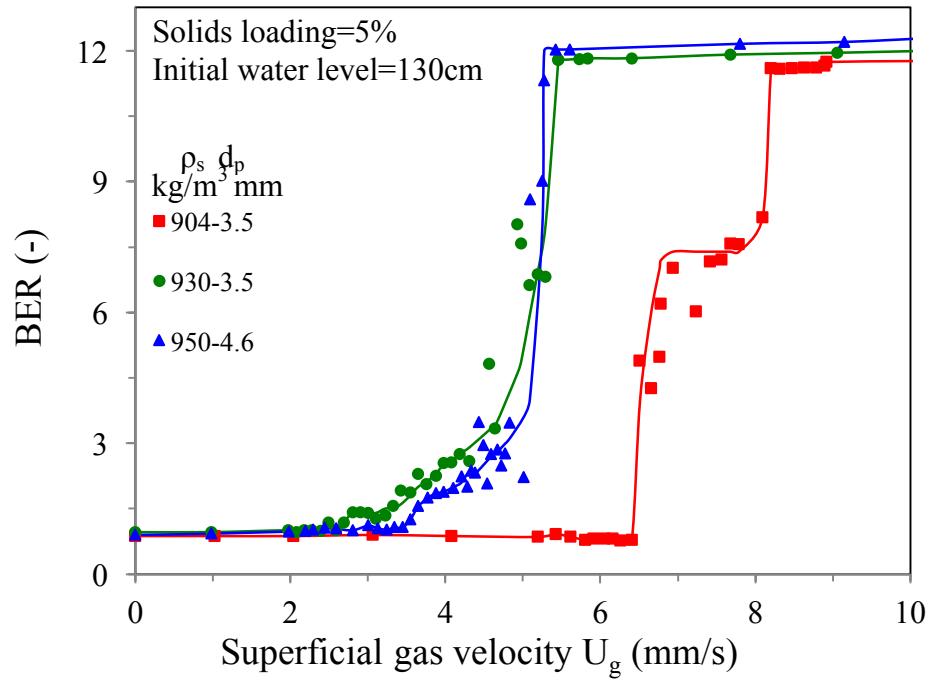
(a)
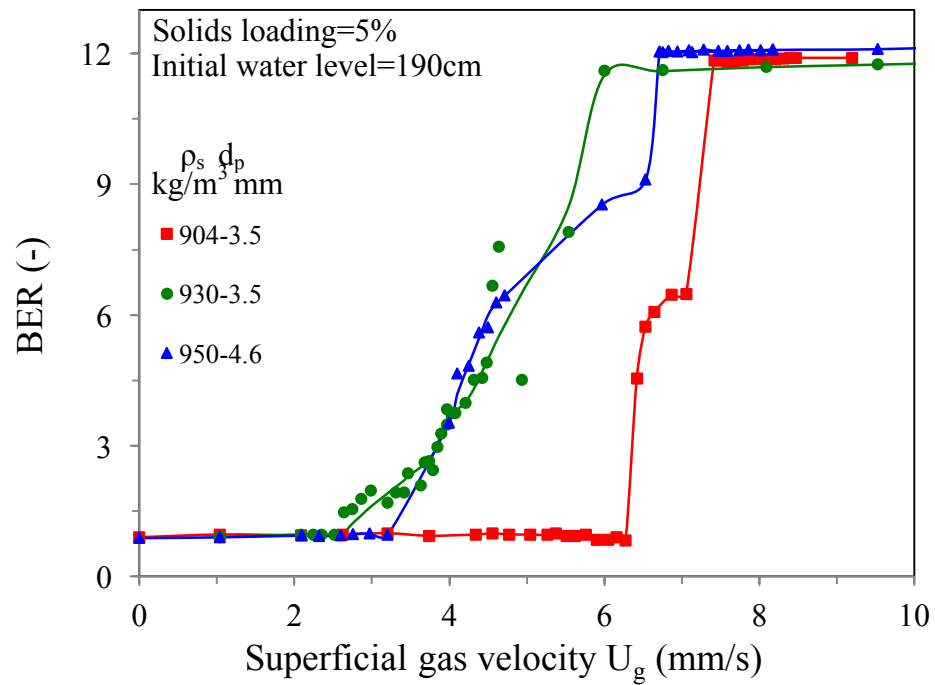
(b)
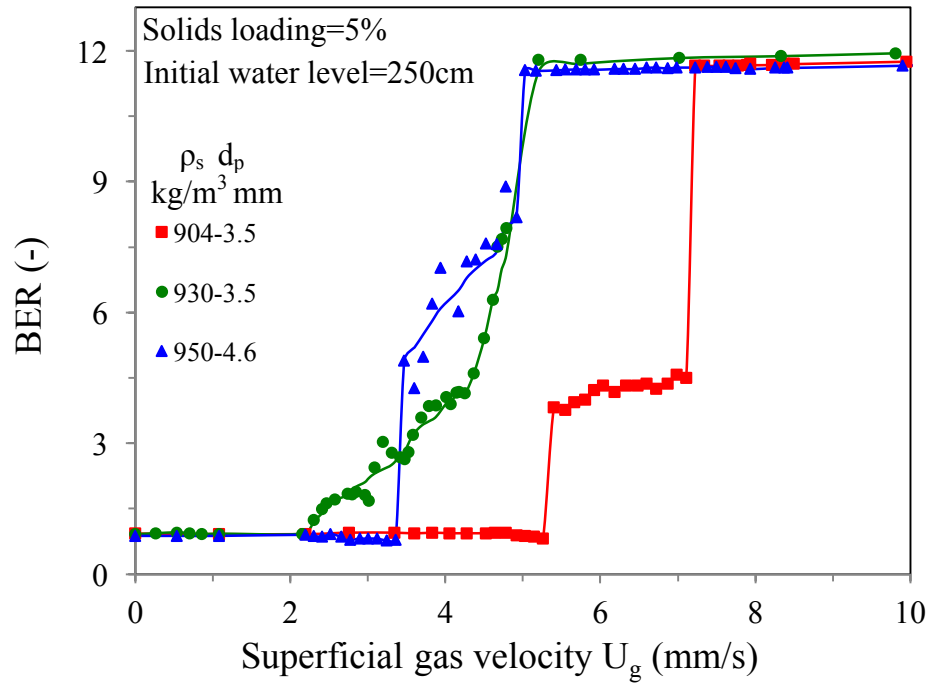
(c)

Figure 5.2 The variations of bed expansion ratio as a function of superficial gas velocity for three different particles: (a) 130cm, (b) 190cm and (c) 250cm.

5.2 The effect of water level on bed expansion ratio

Three different particles are employed to investigate the effect of water level on bed expansion ratio, including 904kg/m^3, 3.5mm; 930kg/m^3, 3.5mm and 950kg/m^3, 4.6mm. The variations of bed expansion ratio as a function of superficial gas velocity for three water levels with three different particles are shown in Fig 5.3. It is observed from the figure that the bed remains as fixed until a certain gas flow rate, which is termed as the initial fluidization velocity. Thus, with further increasing the gas flow rate, bed expansion increases as more and more particles begin to fluidize. After some of the particles reach the bottom, this gas flow rate corresponding to the gas velocity is referred as the full expansion velocity. When the gas flow rate is higher than the full expansion velocity, as the limit of the total column height, the bed expansion ratio remains constant. The particles have the same trends as the trend in Fig 5.2.

With increasing the initial water level, the initial fluidization velocity and full expansion velocity is almost same, which verifies the view that got in Fig 5.2. In addition, compared with the effect of water level on P1, P2 and P3, a general conclusion can be obtained that the effect of the initial water level can be neglected.
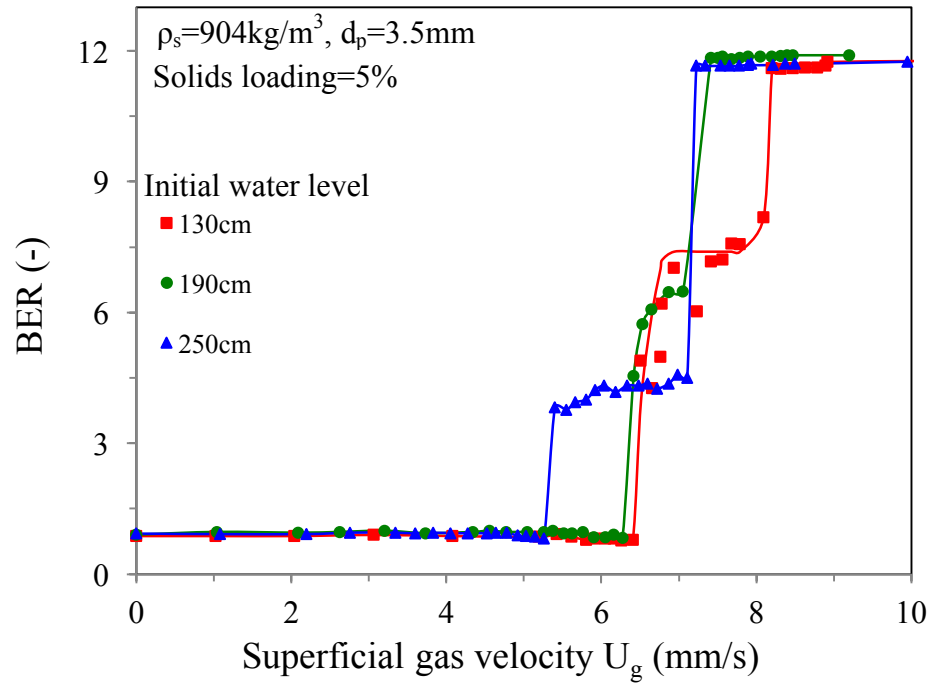
(a)
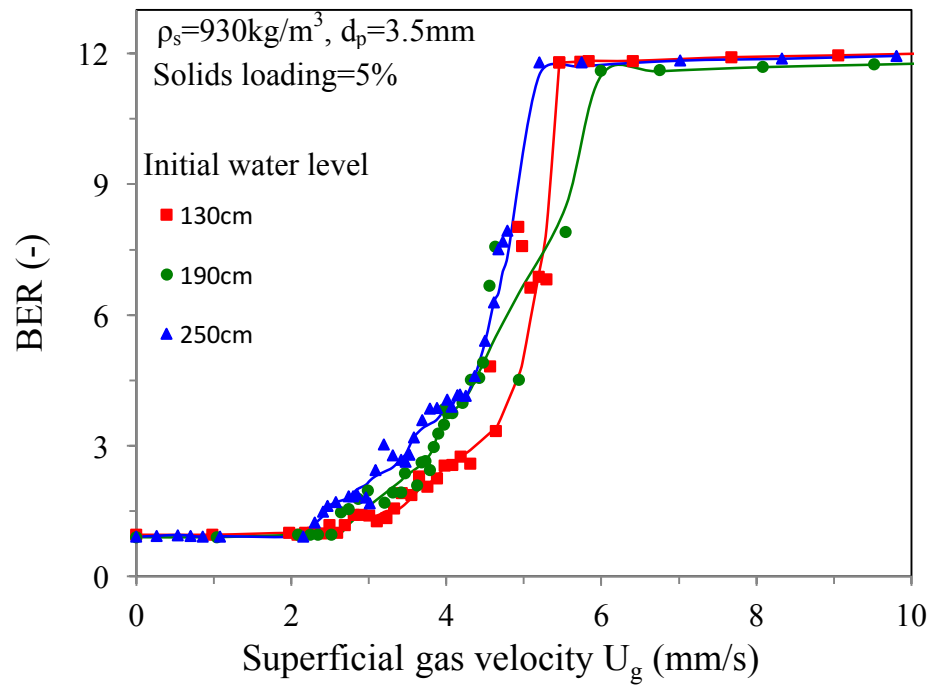
(b)
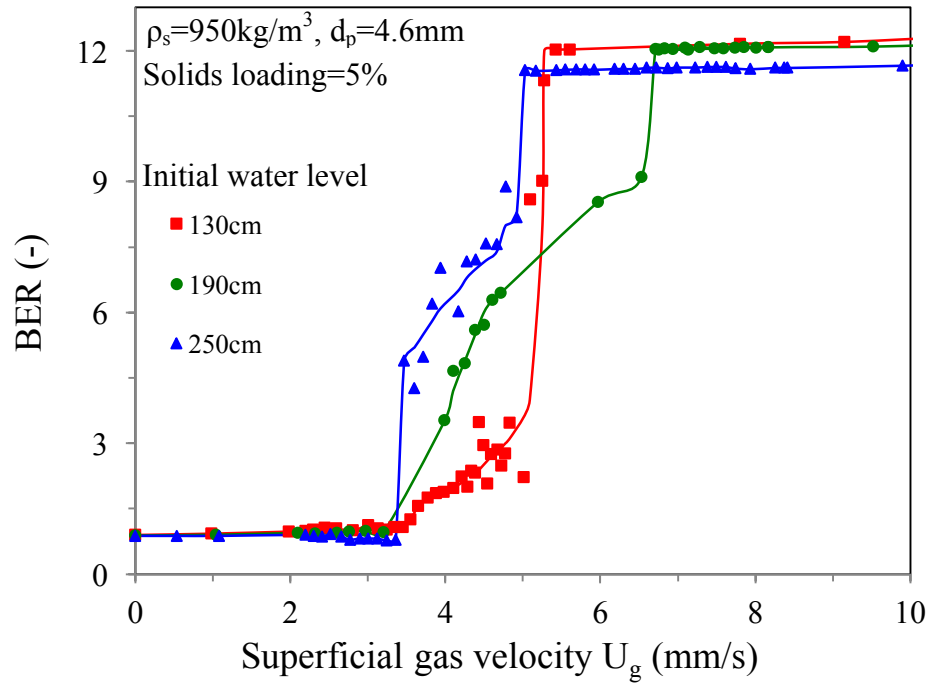
(c)

Figure 5.3 The variations of bed expansion ratio as a function of superficial gas velocity for three water levels with three different particles: (a) 904kg/m^3, (b) 930kg/m^3 and (c) 950kg/m^3.

5.3   The effect of solids loading on bed expansion ratio

P2 (930kg/m^3) has been employed to investigate the effect of solids loading on bed expansion ratio. The variations of bed expansion ratio as a function of superficial gas velocity for three solids loadings are shown in Fig 5.4. It is observed from the figure that with increasing the gas flow rate to the initial fluidization velocity, the fixed bed begins to fluidize; because when the gas velocity reaches the initial fluidization velocity, the upward force equals to the downward force. With further increasing the gas flow rate, the bed expansion ratio increases as more and more particles keep in motion. Due to the limit of the total height of the column, the maximum bed expansion ratio is achieved. This gas flow rate is referred as the full expansion velocity.
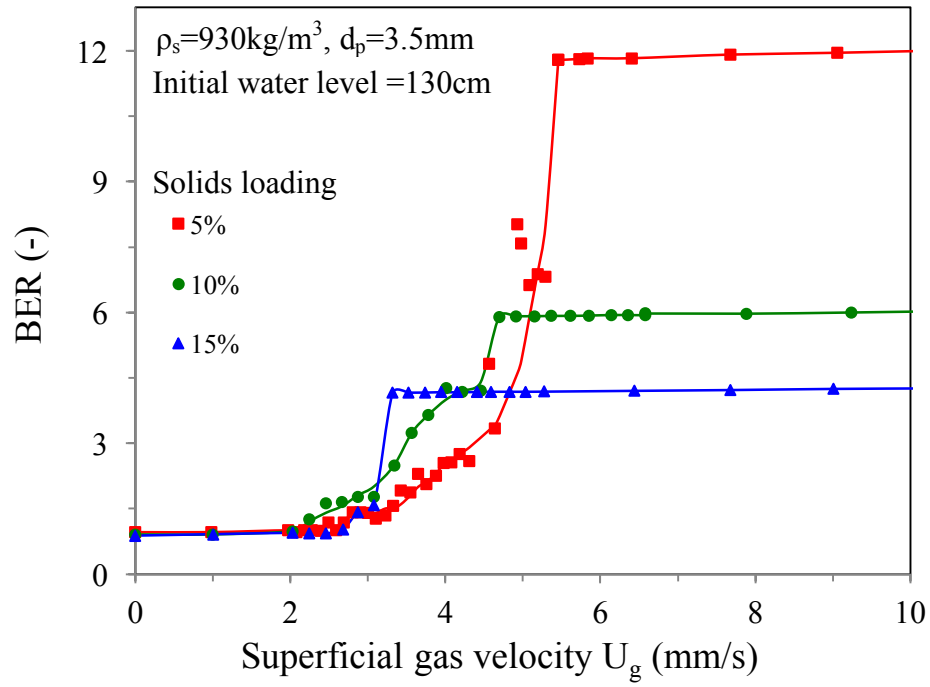
(a)
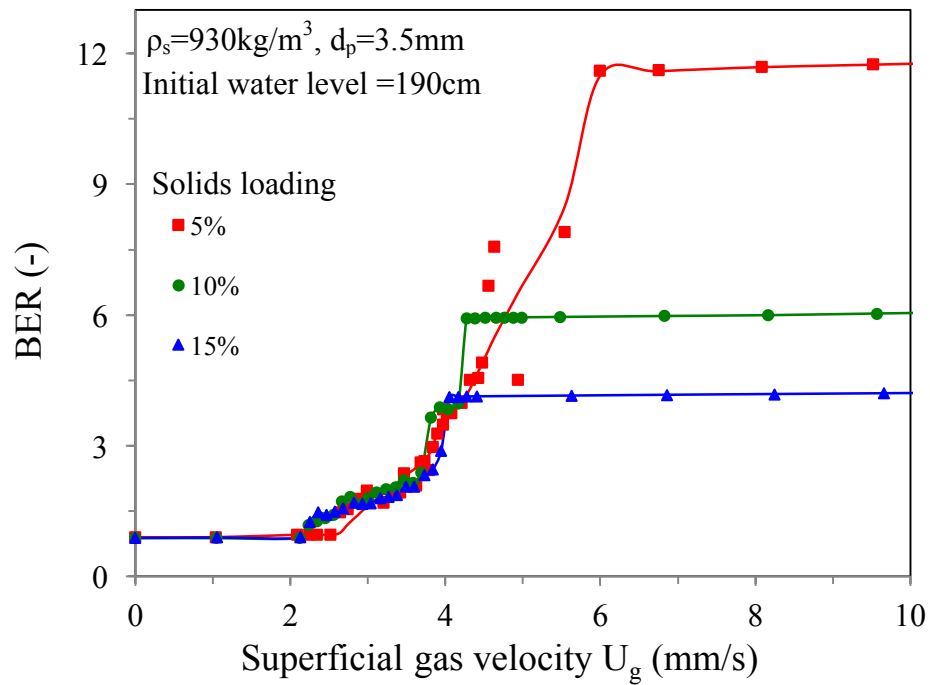
(b)
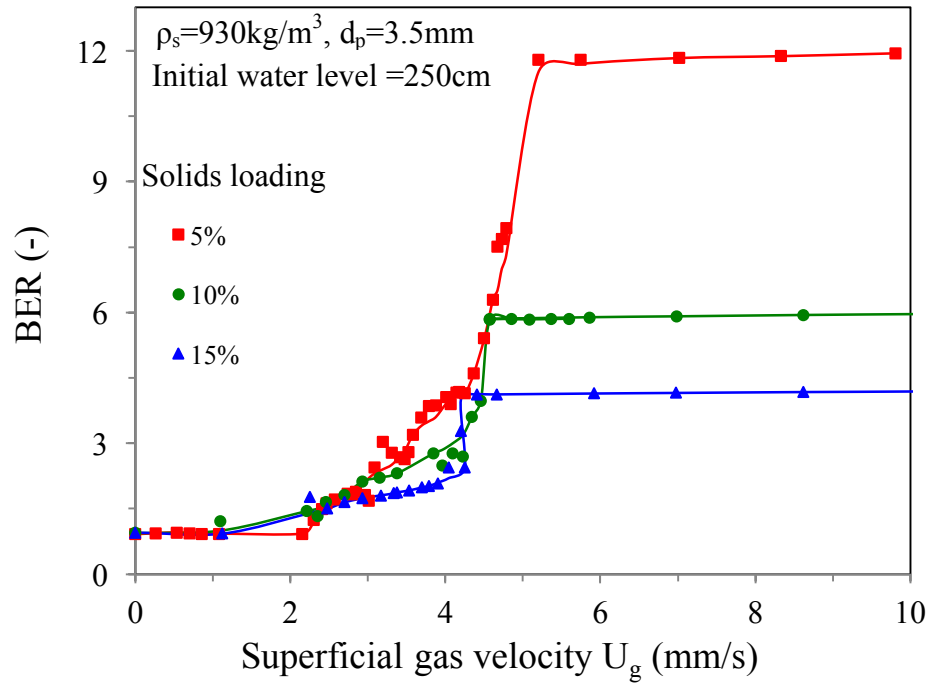
(c)

Figure 5.4 The variations of bed expansion ratio as a function of superficial gas velocity for three solids loadings: (a) 130cm, (b) 190cm and (c) 250cm.

However, the limit of the column height is not an important parameter, to avoid the effect of column height limitation, bed expansion percentage should be used. The bed

expansion percentage is calculated as $\dfrac{\dfrac{H_{bed}}{H_0}}{\left(\dfrac{H_{bed}}{H_0}\right)_{max}}$. The variations of bed expansion

percentage as a function of superficial gas velocity for three solids loadings are shown in Fig 5.5.

(a)

(b)

(c)
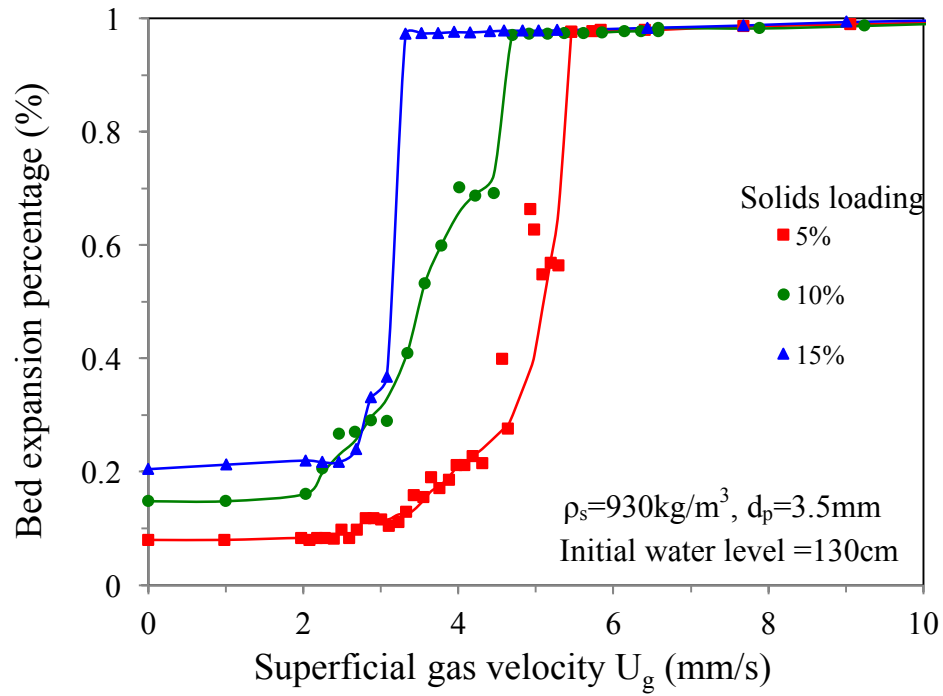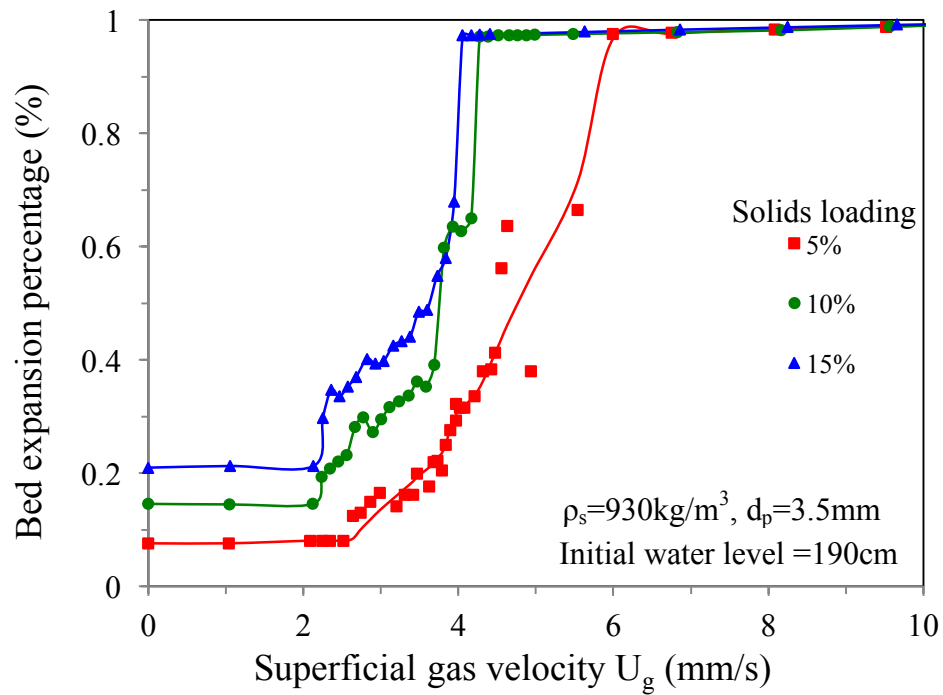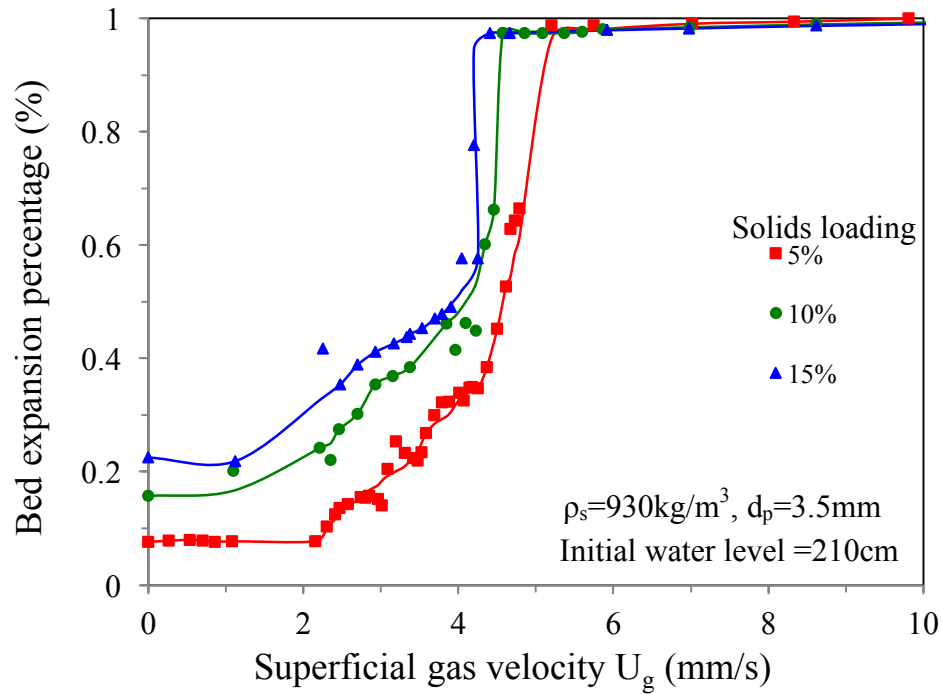
Figure 5.5 The variations of bed expansion percentage as a function of superficial gas velocity for three solids loadings: (a) 130cm, (b) 190cm and (c) 250cm.

Combined the Fig 5.4 and Fig 5.5, some results can be concluded. With increasing the solids loading, initial fluidization velocity is almost same, however, the full expansion velocity decreases. This phenomenon is caused by increasing the solids loading, more particles immerse into the water, which means the lowest layer particles are close to the gas distributor and are easier to fluidize. In three different initial water levels, the trends are similar with different solids loadings. As a result, initial fluidization velocity is not related to the solids loading, while full expansion velocity has a negative growth with solids loading.

Chapter 6

6 Experimental investigation on average phase holdups

Average phase holdups are important in the inverse operation since phase holdup is an essential parameter that is related to the fluidization efficiency. Lots of methods are used in the average phase holdups measurement.

In this project, the average phase holdups are investigated in the complete fluidization regime. Pressure probes mounted through the column are employed to record the changes between the highest and lowest pressure drop along the column. As mentioned in Chapter 3, to calculate the average phase holdups, a pressure balance equation between the top and bottom pressure taps is given based on Fig 6.1.

$$\rho_l g \Delta h + \rho_m g \Delta H = \rho_l g \Delta H \tag{6.1}$$
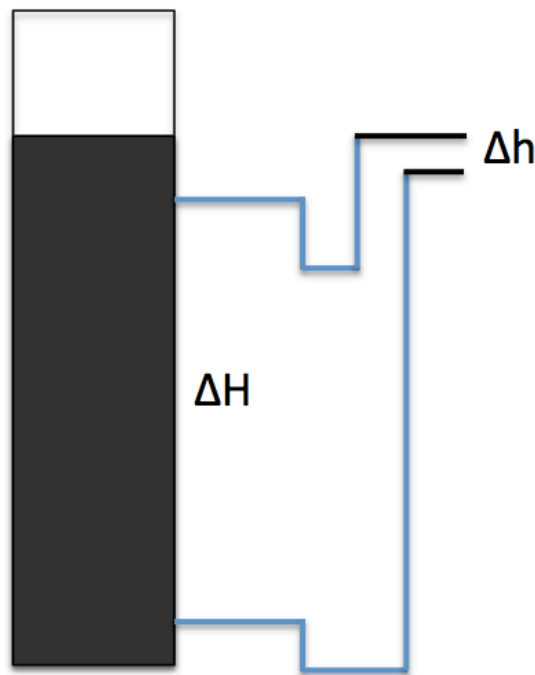
Figure 6.1 Schematic diagram of pressure drop through the column.

Meanwhile, the density of the mixture in the column including gas, liquid and solid phase can be calculated by

$$\rho_m = \rho_s \varepsilon_s + \rho_l \varepsilon_l + \rho_g \varepsilon_g \qquad (6.2)$$

and it is known that the amount of three terms is equal to 1.

$$\varepsilon_s + \varepsilon_l + \varepsilon_g = 1 \qquad (6.3)$$

The total height of bed is constant during the experiment, as the pressure taps can measure the pressure drop at same positions, also the pressure drop can be compared with different gas velocities. Meanwhile, to avoid the air binding among the packed bed, decreasing gas flow rate after the full fluidization is the optimal operating method.

Liquid added when decreasing gas velocity to remain the total bed height unchanged. The amount of added liquid is recorded to calculate the average liquid holdup.

$$\varepsilon_l = \frac{V_{water}}{V_{bed}} \qquad (6.4)$$

Therefore, with four equations and four unknown variables, column mixture density can be expressed with pressure drop, while gas holdup (ε_g) and solid holdup (ε_s) can use liquid holdup (ε_l) and column mixture density to obtain.

$$\varepsilon_g = \frac{(\rho_s - \rho_m) - (\rho_s - \rho_l)\varepsilon_l}{(\rho_s - \rho_g)} \qquad (6.5)$$

$$\varepsilon_s = \frac{(\rho_m - \rho_g) + (\rho_g - \rho_l)\varepsilon_l}{(\rho_s - \rho_g)} \qquad (6.6)$$

6.1 Compare average phase holdups in two-phase and three-phase system

Before three-phase fluidization, two-phase (gas-liquid) inverse fluidization has been finished as a blank experiment compared with three-phase system. The variations of

average phase holdups as a function of superficial gas velocity are shown in Fig 6.2. It is obvious that when gas flow rate is zero, there's no gas holdup, while liquid holdup is one. With increasing the gas velocity, liquid holdup decreases while gas holdup increases, because with increasing the gas flow rate, the bubbles become coalescence, then the bubble velocity decreases which results in gas holdup increasing. Meanwhile, as more and more bubbles are introduced into the two-phase system, liquid is replaced by the bubbles to keep the balance of the system, which causes liquid holdup decreases.
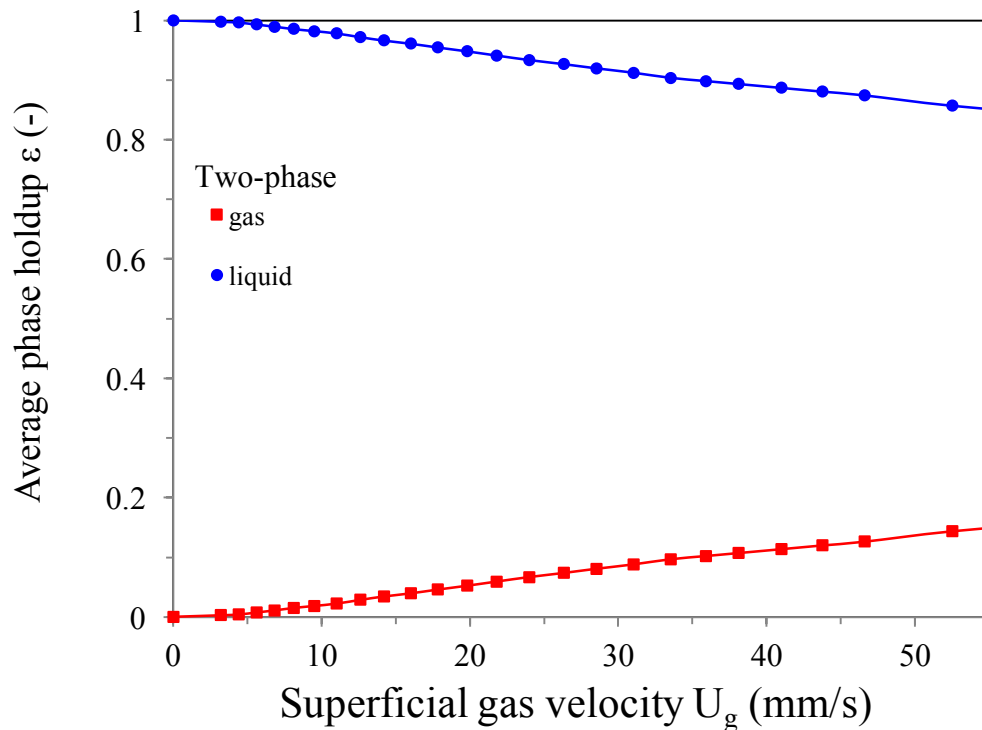
Figure 6.2 The variations of average phase holdups as a function of superficial gas velocity in two-phase (gas-liquid) system.

To examine the accuracy of the equation, the variations of calculated average liquid holdup as a function of actual average liquid holdup are shown in Fig 6.3. It is observed from the figure that the calculated liquid holdup is almost equal to the actual one, which means the equations are valid.
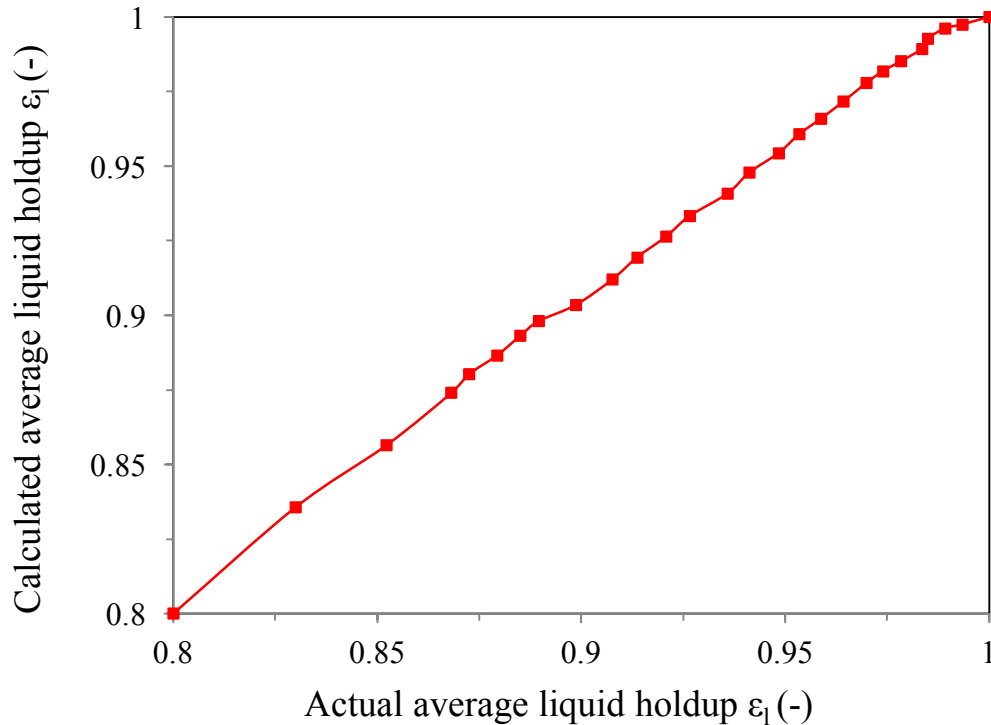
Figure 6.3 The variations of calculated average liquid holdup as a function of actual average liquid holdup in two-phase (gas-liquid) system.

Compared the phase holdups in two-phase and three-phase system (Fig 6.4), gas holdup remains constant, while liquid holdup of the three-phase system is lower than the two-phase system. The reason is that particles replace some positions of the liquid since the density of particles is close to the liquid. Gas holdup is only related to the gas flow rate regardless the presence of solids. The gas holdup increases and liquid holdup decreases both in two-phase and three-phase system because with increasing the gas velocity, more and more bubbles are introduced into the system and replace the position of liquid. Solids holdup in three-phase system remains constant when the gas velocity is higher than the complete fluidization velocity because all the particles are immersed in the three-phase system.
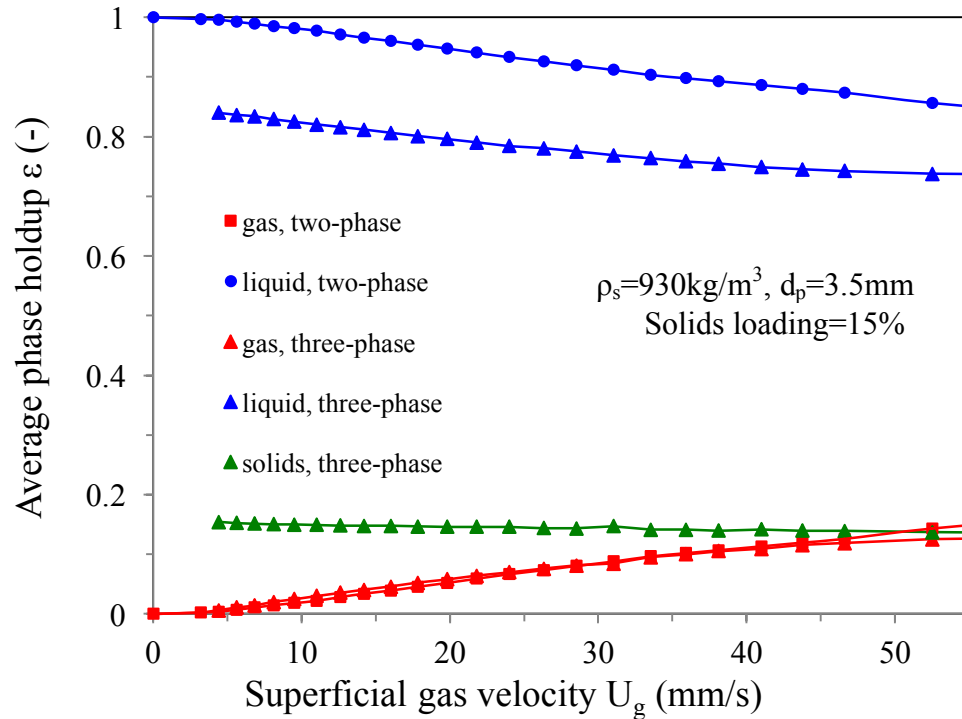
Figure 6.4 Compare the average phase holdup in two-phase (gas-liquid) system and three-phase (gas-liquid-solid) system, ρ_s=930kg/m^3, solids loading=15%.

6.2 The effect of particle property on average phase holdups

The variations of average phase holdup as a function of superficial gas velocity for three different particles at solids loading = 15% are shown in Fig 6.5. For all three particles, gas holdup increases, liquid holdup decreases and solids holdup remains constant with increasing gas velocity. Because with increasing gas velocity, more and more bubbles become coalescence, which results in the bubble velocity decreases, therefore, gas holdup increases. To remain the total bed height constant, water should be removed from the system with increasing the gas flow rate, which leads liquid holdup decreases. Meanwhile, some bubbles replace the position of liquid, which also cause liquid holdup decreases. Solids holdup remains constant as all the particles are immersed in the system after the complete fluidization velocity. As the phase holdup among three types of particles does not have a big difference, the effect of the particle property can be neglected.

It is observed from the Fig 6.5 that the particles whose density is close to the liquid density require lower complete fluidization velocity. Moreover, particle size is also a parameter affecting the complete fluidization velocity. In addition, bigger particles require higher complete fluidization velocity.
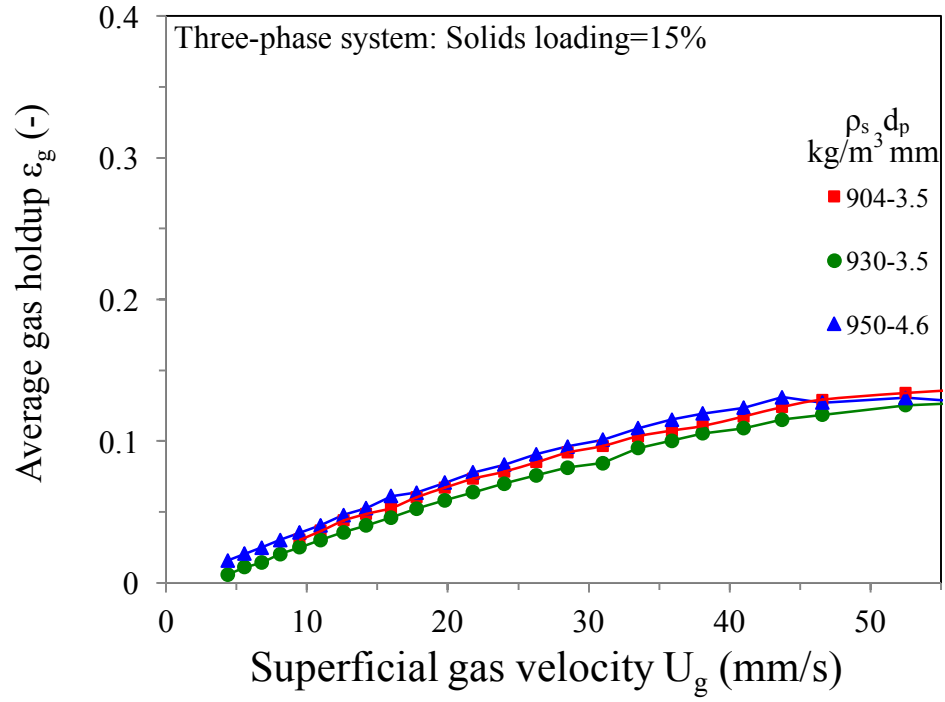
(a)

(b)
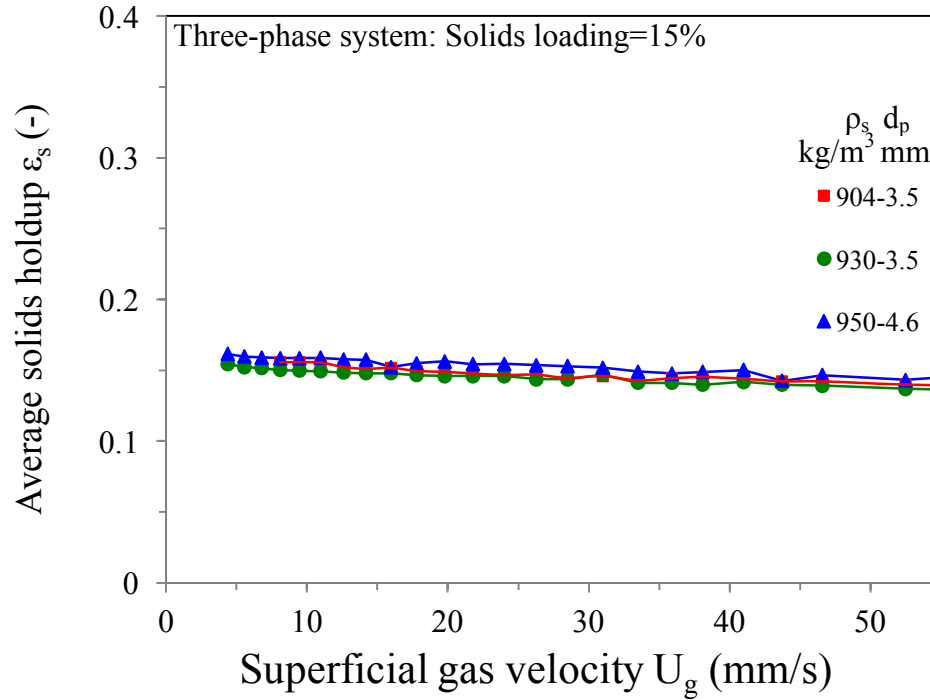
(c)

Figure 6.5 The variations of average phase holdup as a function of superficial gas velocity for three different particles at solids loading = 15%: (a) gas holdup, (b) liquid holdup and (c) solids holdup.

6.3   The effect of solids loading on average phase holdups

To investigate the effect of solids loading on average phase holdups, three particles are employed into the three-phase system, respectively. The variations of average phase holdups as a function of superficial gas velocity for different loadings of P2 (930kg/m^3) are shown in Fig 6.6. For all solids loadings, average gas holdup increases and liquid holdup decreases while solids holdup remains constant. The average phase holdups have the same trends as different solids loadings. With increasing solids loading, gas holdup is almost constant and liquid holdup decreases whereas solids holdup increases. With increasing solids loading, more particles are introduced into the three-phase system, therefore, solids holdup increases. In addition, the density of particles is close to the liquid, thus, the increasing particles replace part of the position of liquid, thereafter liquid holdup decreases. Gas holdup is only related to the gas flow rate, so the solids loadings have little effect on average gas holdup.
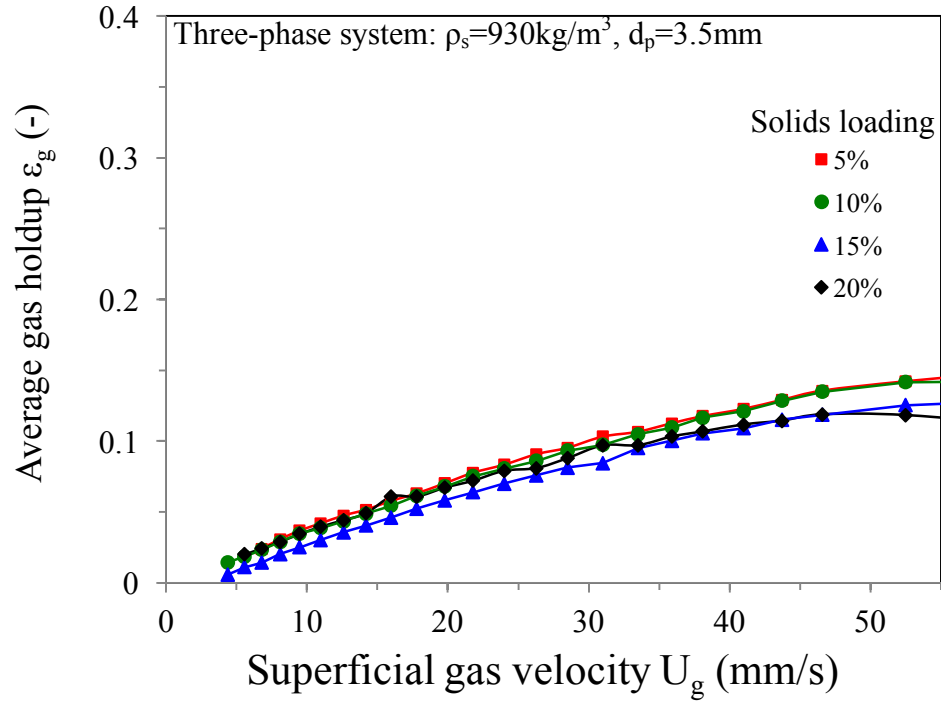
(a)
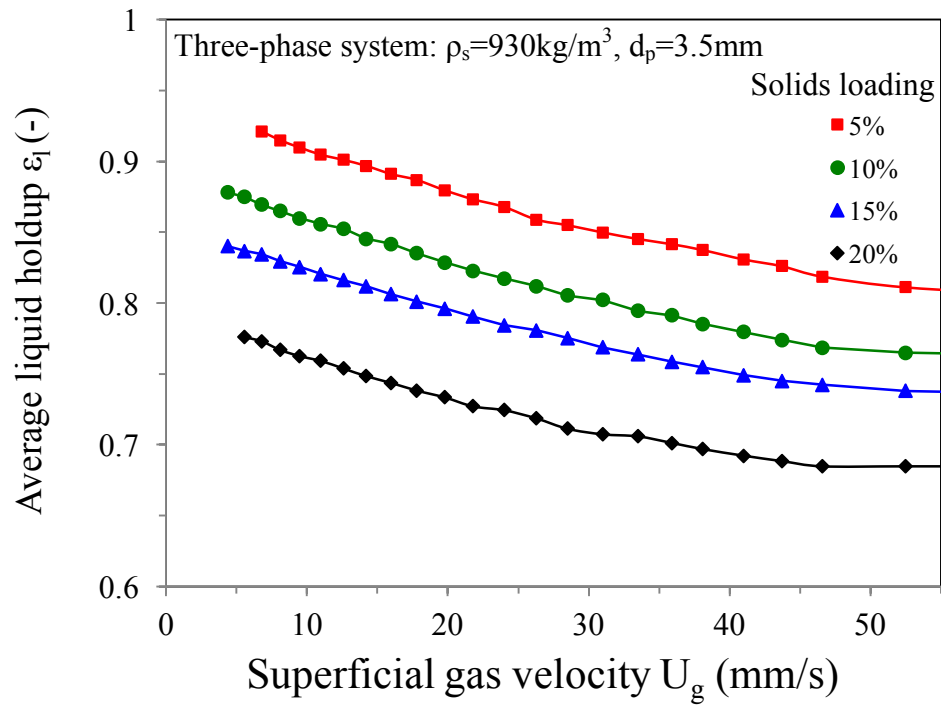
(b)
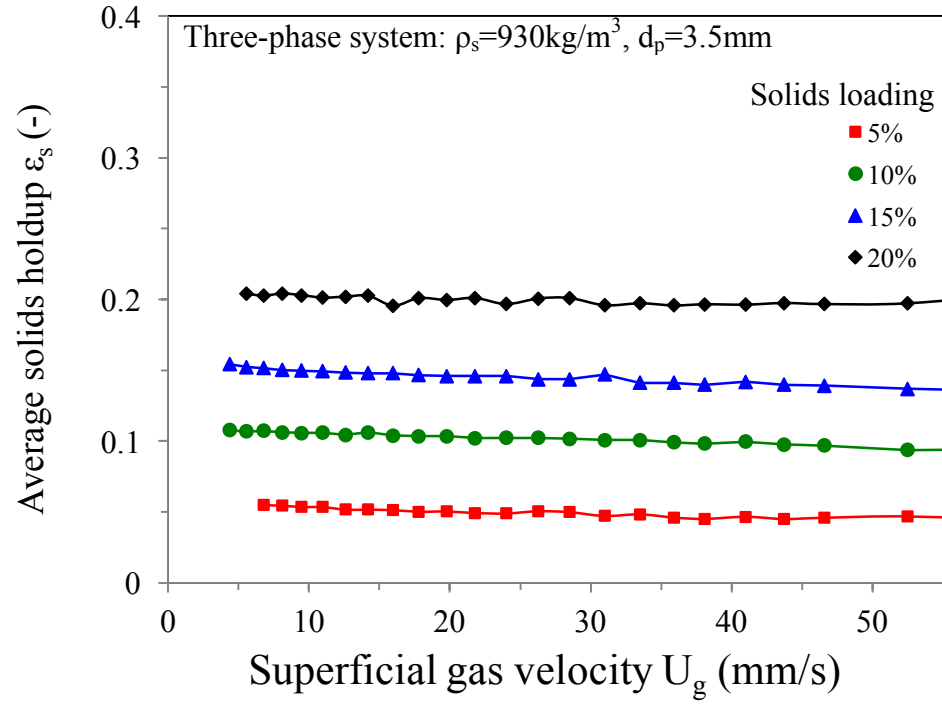
(c)

Figure 6.6 The variation of average phase holdups as a function of superficial gas velocity for different loadings, ρ_s=930kg/m^3: (a) gas holdup, (b) liquid holdup and (c) solids holdup.

Chapter 7

7   Experimental investigation on local phase holdups

Local phase holdups, especially local solids holdup, is the most direct parameter to investigate solids concentration. In another word, local phase holdups are one of the important arguments in inverse fluidization operation. However, due to the difficulty of measuring, little has been done in the literature regarding local phase holdups.

The effective height of the column is 2.1m, separated into four sections: 10-70cm, 70-130cm, 130-190cm and 190-210cm depending on the positions of pressure taps.

The equations of average phase holdups can be used in calculating local phase holdups. Based on the main assumption that liquid is uniformly distributed through the column as liquid is the continuous phase, thus the liquid holdup of each section is same as the average liquid holdup.

Based on the pressure balance equation in each section (Fig 7.1), some equations can be used in calculating the local phase holdups.

$$\rho_l g \Delta h + \rho_m g \Delta H = \rho_l g \Delta H \tag{7.1}$$

Meanwhile, the density of the mixture in the column including gas, liquid and solid phase can be calculated by

$$\rho_m = \rho_s \varepsilon_{s,local} + \rho_l \varepsilon_{l,local} + \rho_g \varepsilon_{g,local} \tag{7.2}$$

and it is known that the amount of three terms is equal to 1.

$$\varepsilon_{s,local} + \varepsilon_{l,local} + \varepsilon_{g,local} = 1 \tag{7.3}$$

Therefore, local phase holdups can be calculated by the following equations

$$\varepsilon_l = \frac{V_{water}}{V_{bed}} \tag{7.4}$$

$$\varepsilon_{l,local} = \varepsilon_l \tag{7.5}$$

$$\varepsilon_{g,local} = \frac{(\rho_s - \rho_m) - (\rho_s - \rho_l)\varepsilon_{l,local}}{(\rho_s - \rho_g)} \tag{7.6}$$

$$\varepsilon_{s,local} = \frac{(\rho_m - \rho_g) + (\rho_g - \rho_l)\varepsilon_{l,local}}{(\rho_s - \rho_g)} \tag{7.7}$$

7.1 Compare local phase holdups in two-phase and three-phase system

Compared with two-phase (gas-liquid) system, the local phase holdups in three-phase system from 130cm to 190cm are shown in Fig 7.1. With increasing the gas velocity, the local gas holdup increases whereas local liquid holdup decreases both in two-phase and three-phase system. In addition, local solids holdup remains constant after the gas velocity is over complete fluidization velocity. The local gas holdup of two-phase and three-phase system is almost same because gas holdup is only related with gas flow rate. After adding solids into the system, local liquid holdup reduces as the density of particles is close to the liquid and particles replace part positions of the liquid. Moreover, solids holdup remains constant after complete fluidization velocity, the reason is that all particles are introduced into the system after the complete fluidization.
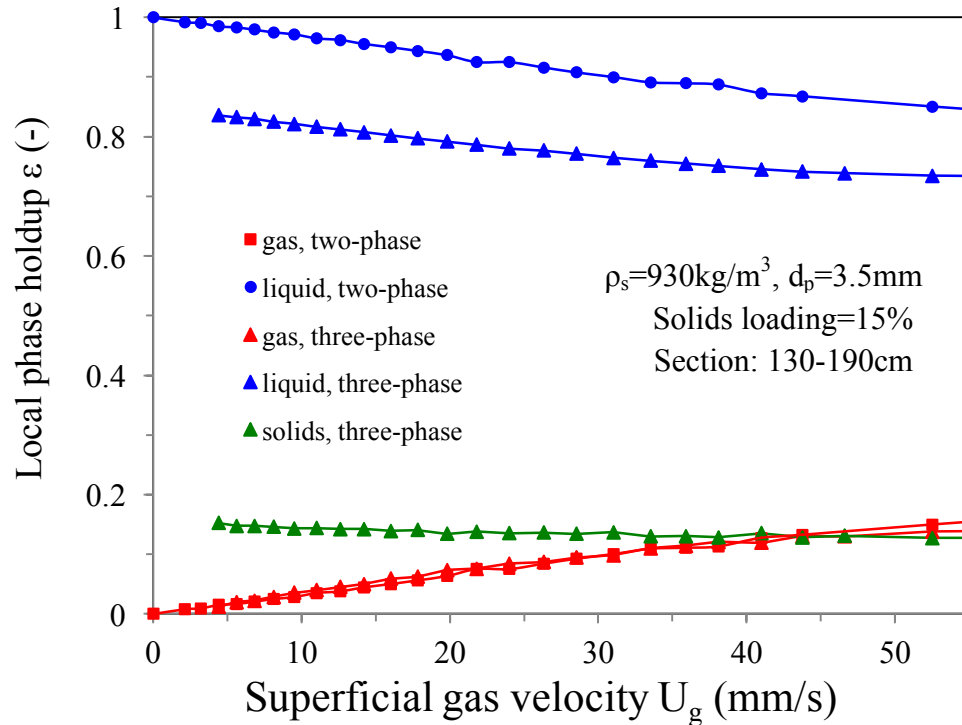
Figure 7.1 Compare the local phase holdup in two-phase (gas-liquid) system and three-phase (gas-liquid-solid) system, ρ_s=930kg/m3, solids loading=15%, from 130cm to 190cm.

7.2 The effect of particle property on local solids holdup

As the solids holdup is the direct parameter associating with the solids concentration, the variations of local solids holdup as a function of superficial gas velocity for three different particles are shown in Fig7.2. For all particles, local solids holdup is around solids loading because after complete fluidization velocity all particles are immersed into three-phase system. For P3 (950kg/m3), the local solids holdup in the lowest section is lower than the upper ones, while one possible reason is that some particles are removed from the system since the particles are packed under the gas distributor at higher gas velocity. In addition, the complete fluidization velocity decreases with increasing the density of particles or decreasing the size of particles.
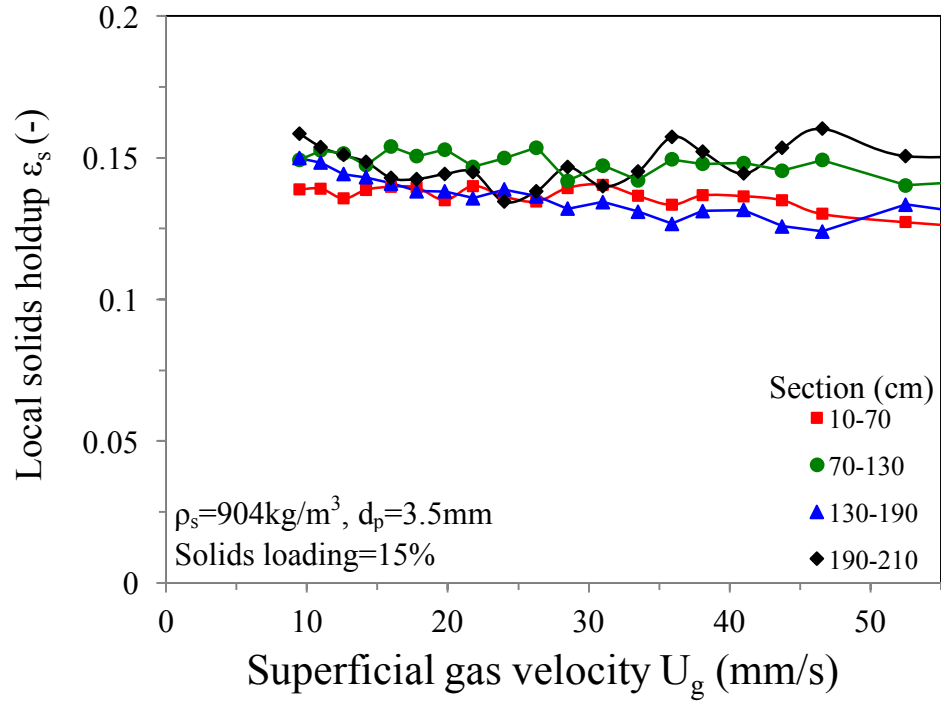
(a)
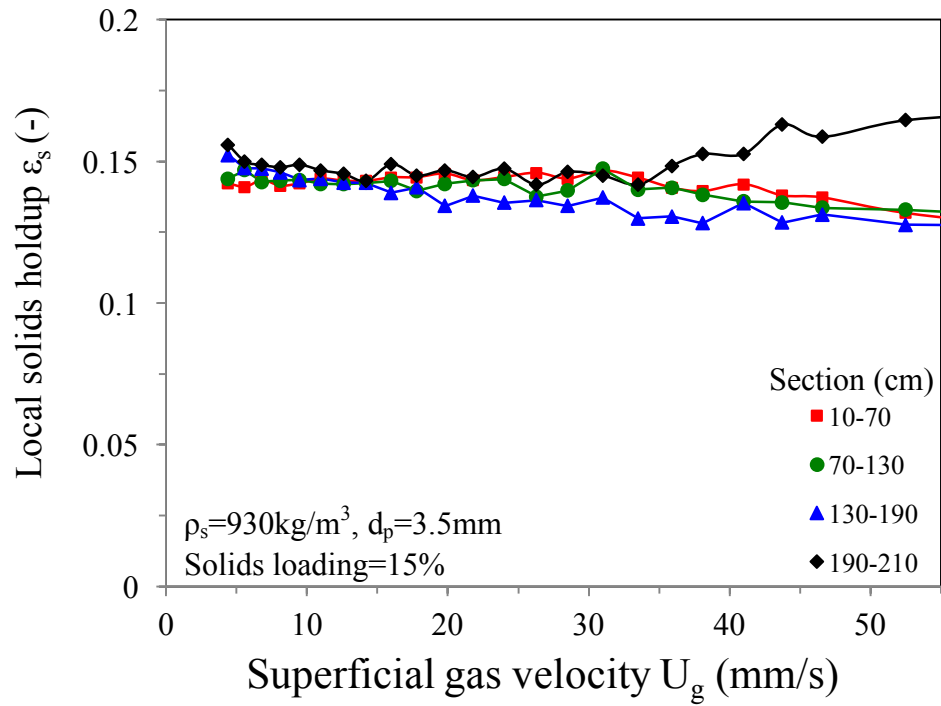
(b)
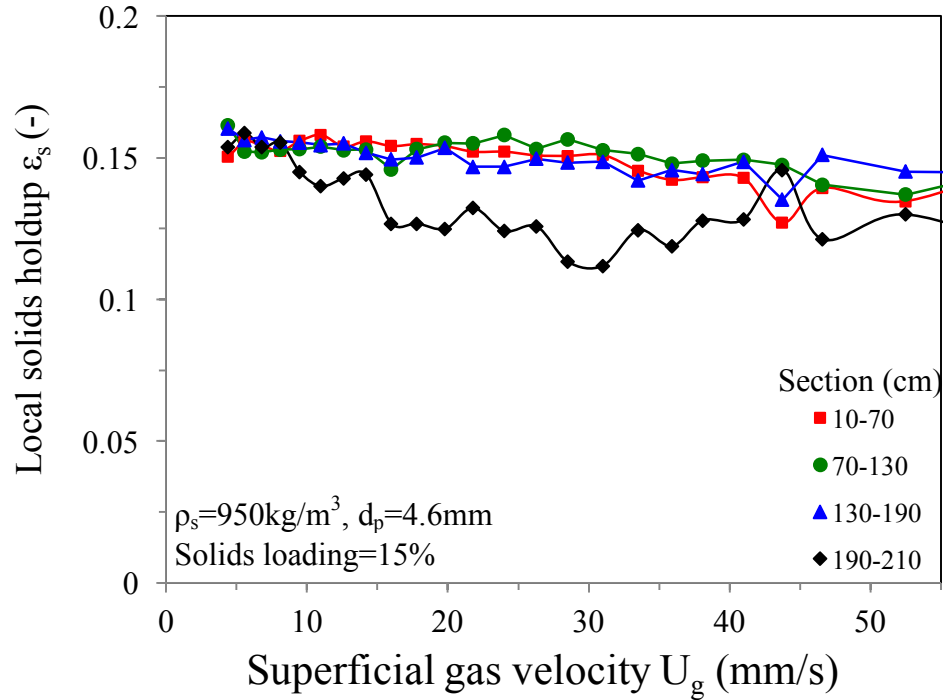
(c)

Figure 7.2 The variations of local phase holdup as a function of superficial gas velocity for three different particles at solids loading = 15%: (a) 904kg/m³, (b) 930kg/m³ and (c) 950kg/m³.

Obviously, when superficial gas velocity is in range from 0 to 21.8mm/s, the local solids holdup increases from top to bottom through the column, which means the particles are fluidized from top to bottom. However, from 24 to 62mm/s, the local solids holdup decreases from 40 cm to 160 cm, while the value of the lowest position is much higher than the upper. It maybe that at higher gas flow rate, the turbulence enhances around the gas distributor, which leads to a higher mass transfer between this region and its adjacent area increase. Hence, the local solids holdup of the lowest one is much higher than the upper one.
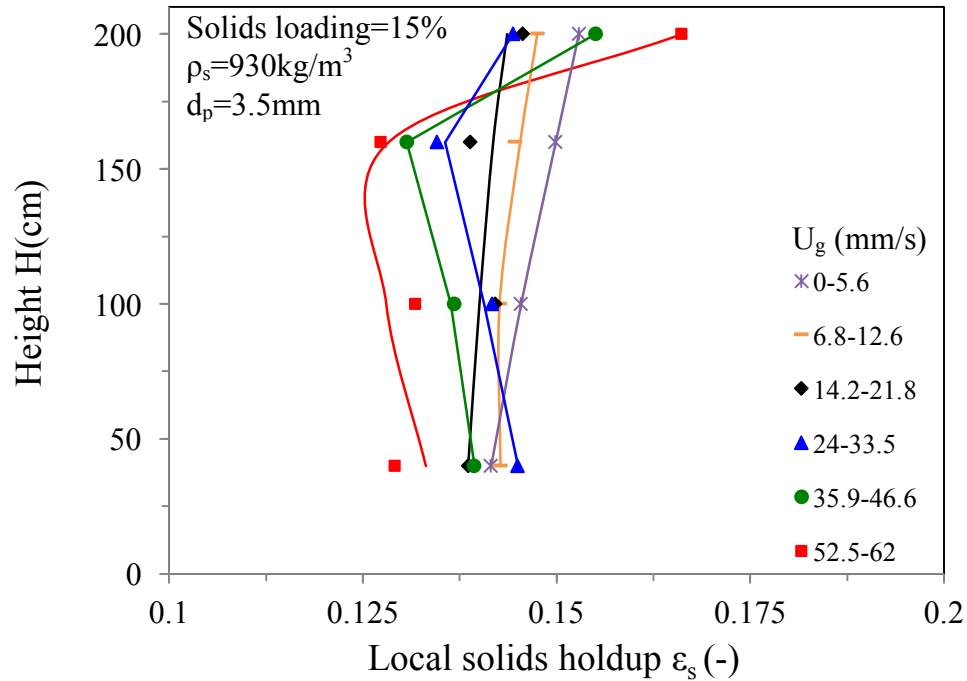
Figure 7.3 The variations of height as a function of local solids holdup at different superficial gas velocity, solids loading = 15%, ρ_s=930kg/m^3.

The variations of local solids holdup as a function of superficial gas velocity for different sections are shown in Fig 7.4. For the top three sections, local solids holdup of P3 is higher than P1 and P2, however, for the lowest section, the local solids holdup of P3 is much lower than the others. The most probable reason for this phenomenon is that P3 is much bigger than P1 and P2 and easier to stack under the gas distributor then remove from the system. Besides, the complete fluidization velocity of P1 is higher than P2 and P3 as the density of P1 is lower than P2 and P3. Also, particle size affects the complete fluidization velocity, therefore, the Ug3 of P2 and P3 is close.
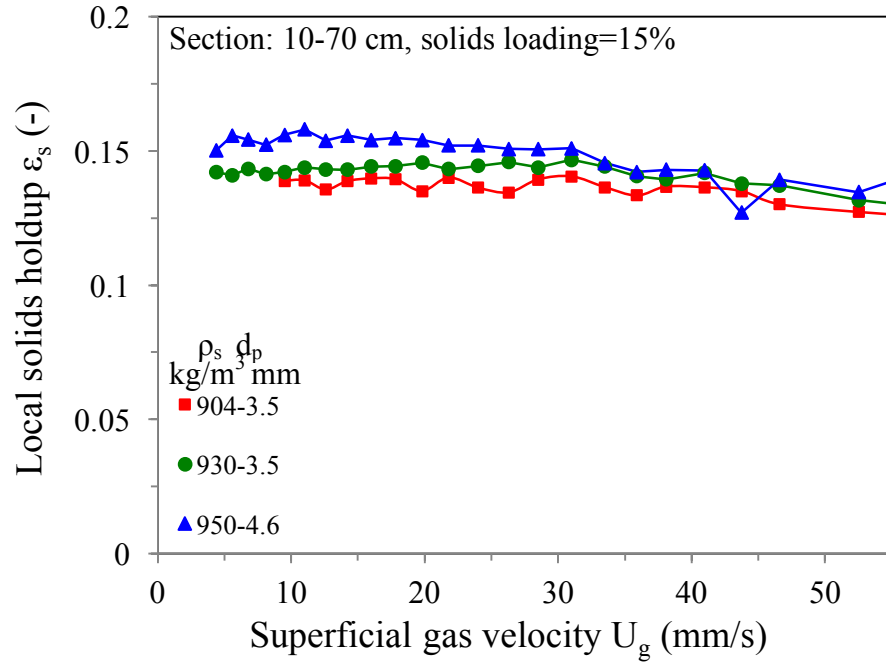
(a)
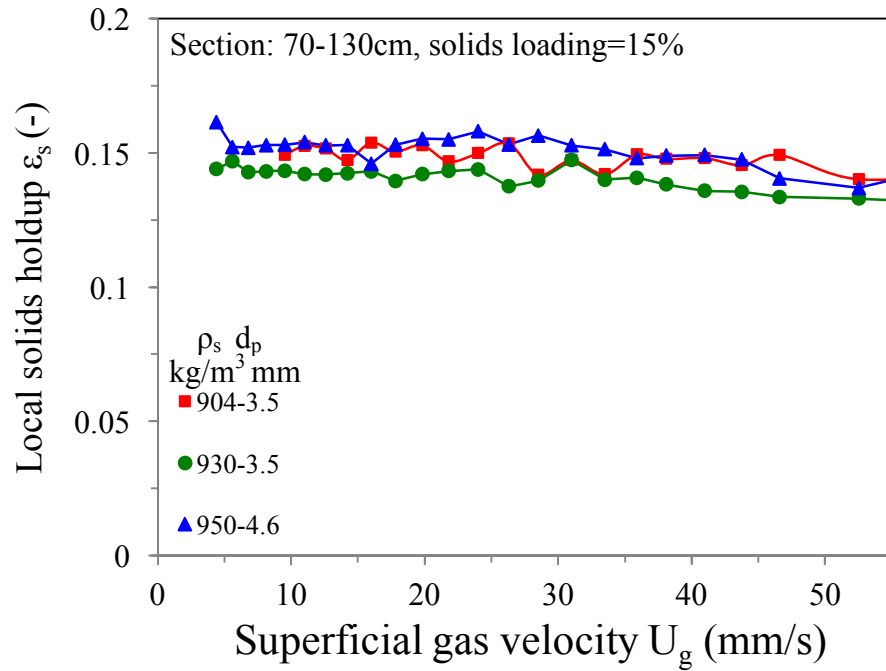
(b)
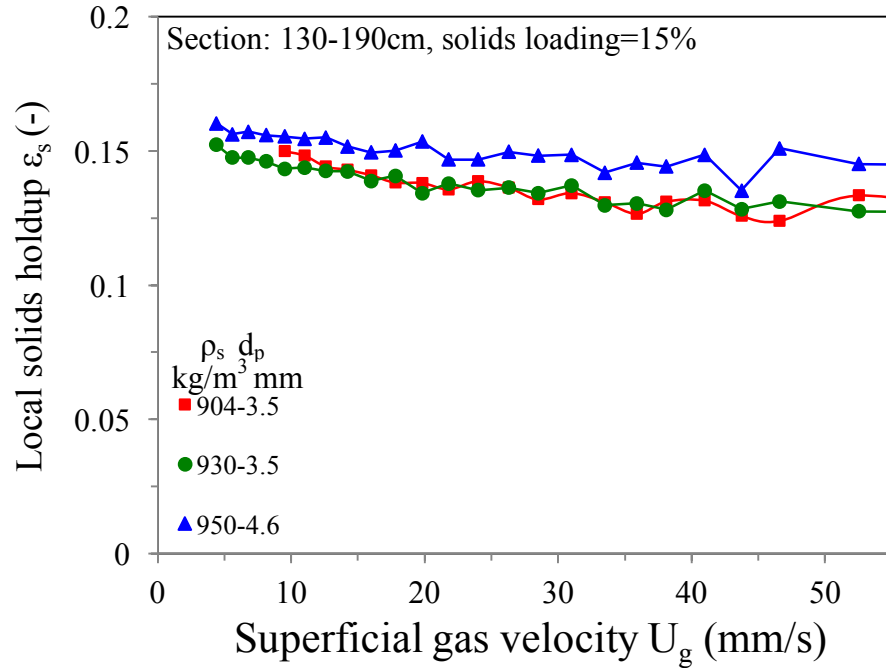
(c)
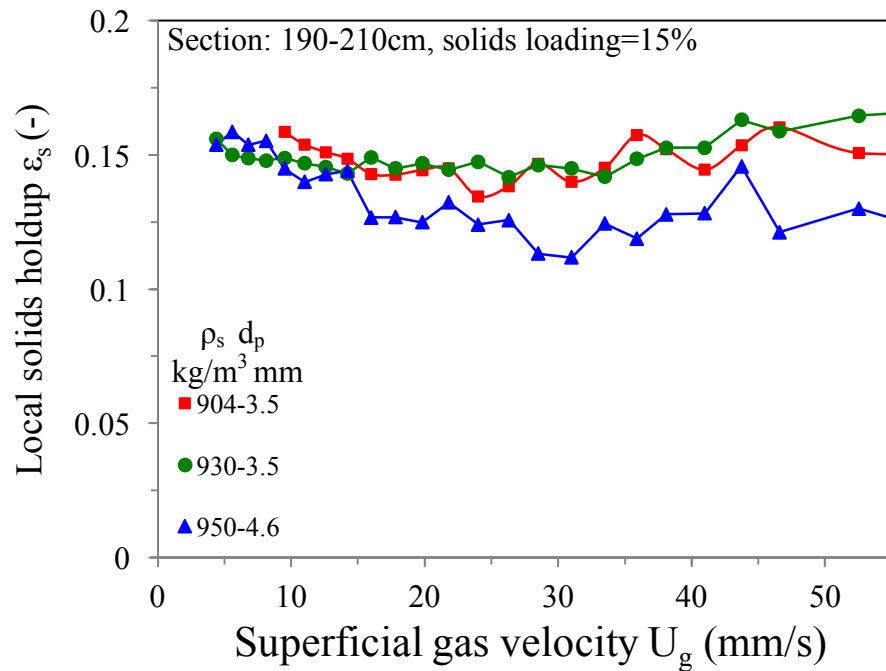
(d)

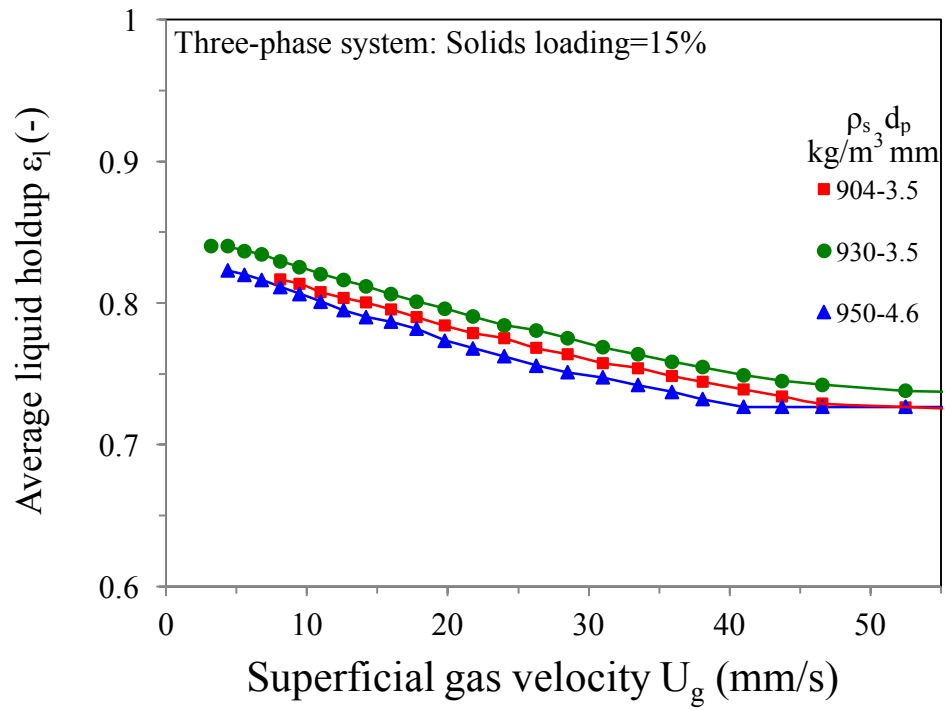**Figure 7.4 The variations of local solids holdup as a function of superficial gas velocity for three different particles, solids loading = 15%: (a) 10-70cm, (b) 70-130cm, (c) 130-190cm, (d) 190-210cm.**

In addition, it is obvious that from Fig 7.5, under the average local solids holdup in each section, the local solids holdup of P1 (904kg/m3) and P2 (930kg/m3) increases through the column, which means the solids concentration increases from top to the bottom of the column. However, the local solids holdup of P3 (950kg/m3) is almost same in the top section, but very small in the lowest one. The most likely reason is that with particles fluidizing to the lower position, some particles are stacked under the gas distributor then remove from the system.
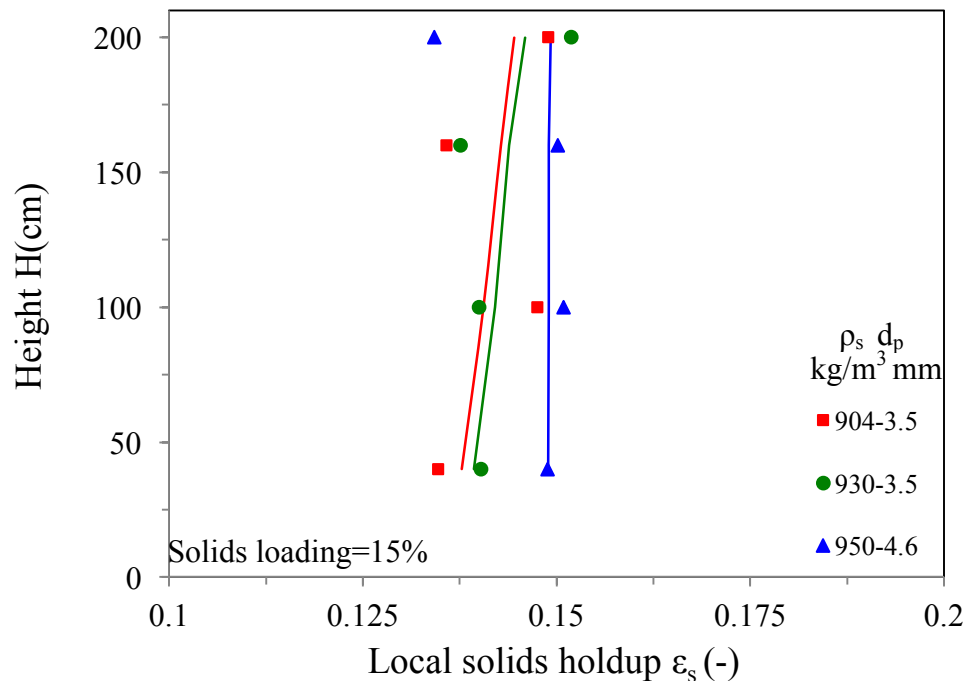
Figure 7.5 The variations of height as a function of local solids holdup for three different particles at solids loading = 15%: 904kg/m³, 930kg/m³ and 950kg/m³.

Comparing the calculated local solids holdup and the actual solids holdup, the trends of them are almost same. The most likely error is the limit of assumption and the human error.
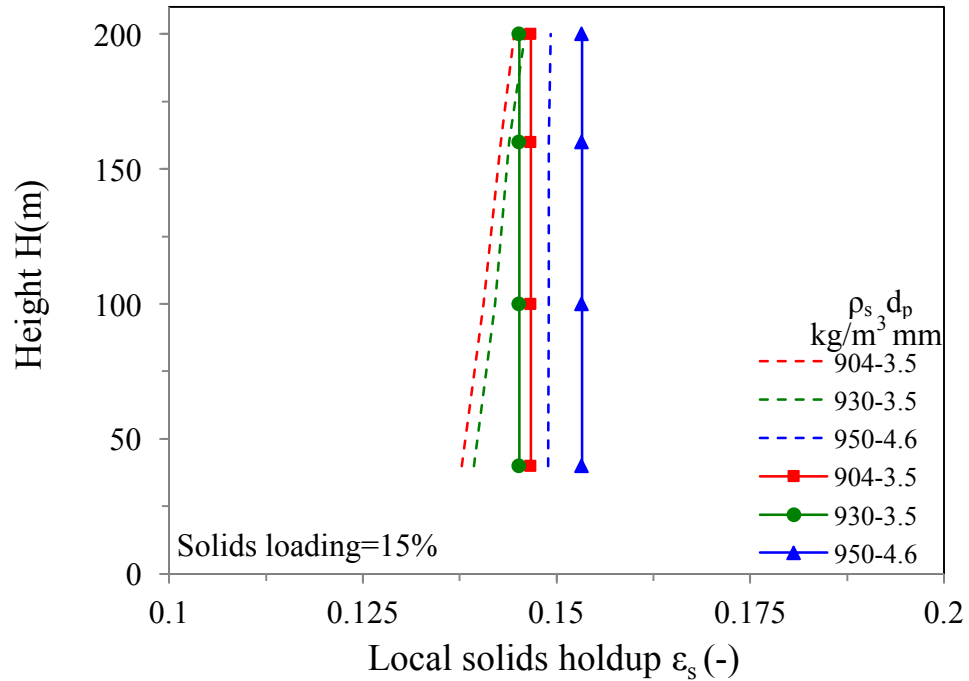
Figure 7.6 Compare the calculated local solids holdup and actual solids holdup

- - - calculated local solids holdup, ⎯⎯ actual solids holdup.

7.3   The effect of solids loading on local solids holdup

The variations of local solids holdup as a function of the superficial gas velocity are shown in Fig 7.7. It is observed from the Fig 7.7 (a)-(c) that with increasing the solids loading, the local solids holdup increases, while with increasing the superficial gas velocity, the local solids holdup remains constant after the complete fluidization velocity. For the lowest position, the local solids holdup at solids loading=5% decreases because there are lots of bubbles in the lowest region which is near the gas distributor. However, the effect of bubbles disappears with increasing solids loadings. In addition, the complete fluidization velocity decreases with increasing solids loading.
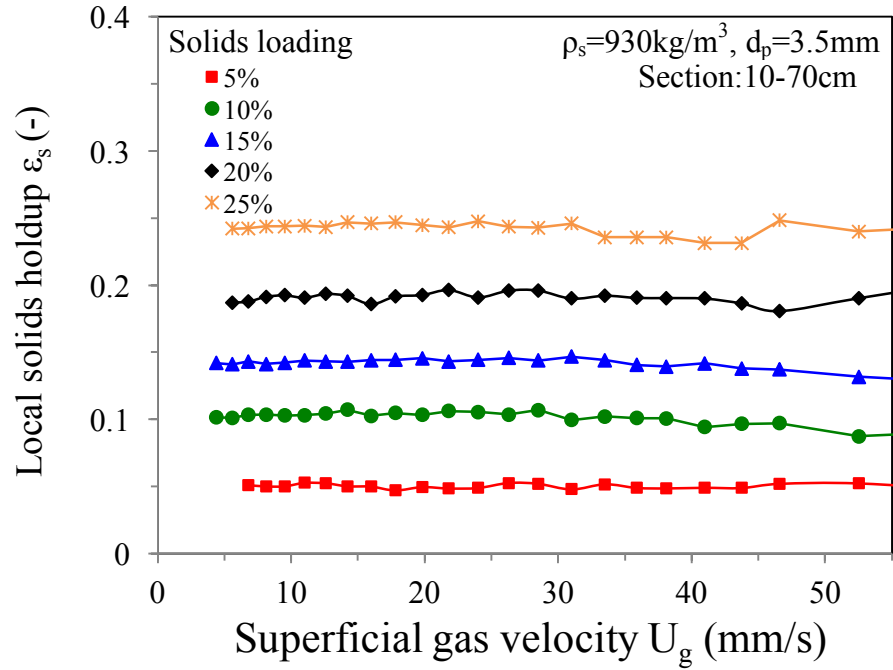
(a)
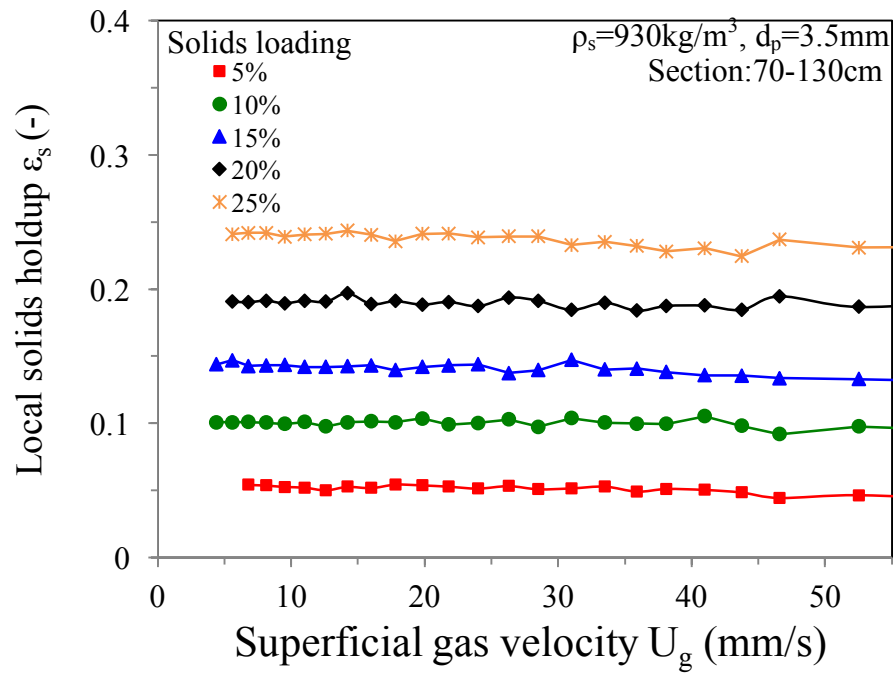
(b)
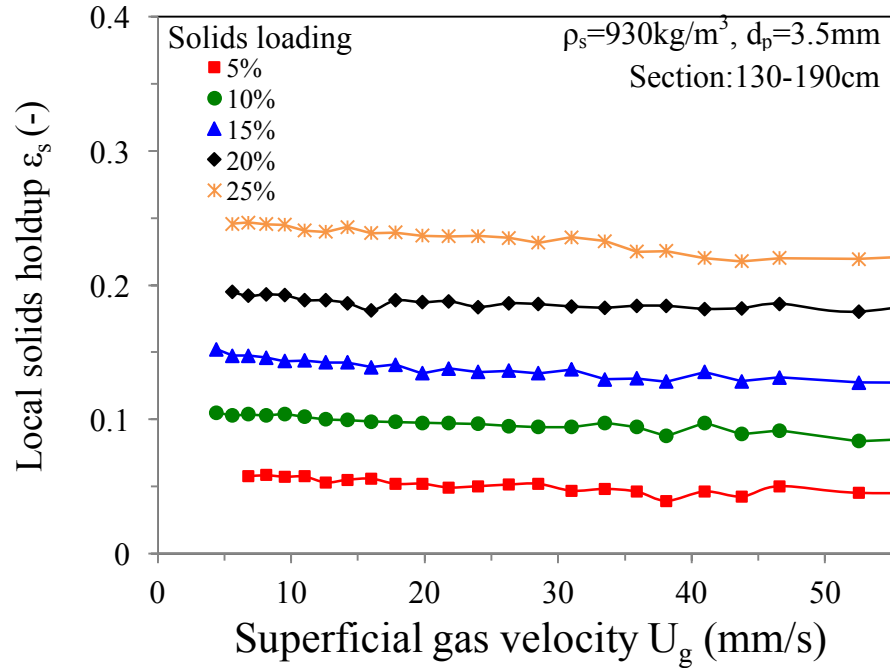
(c)
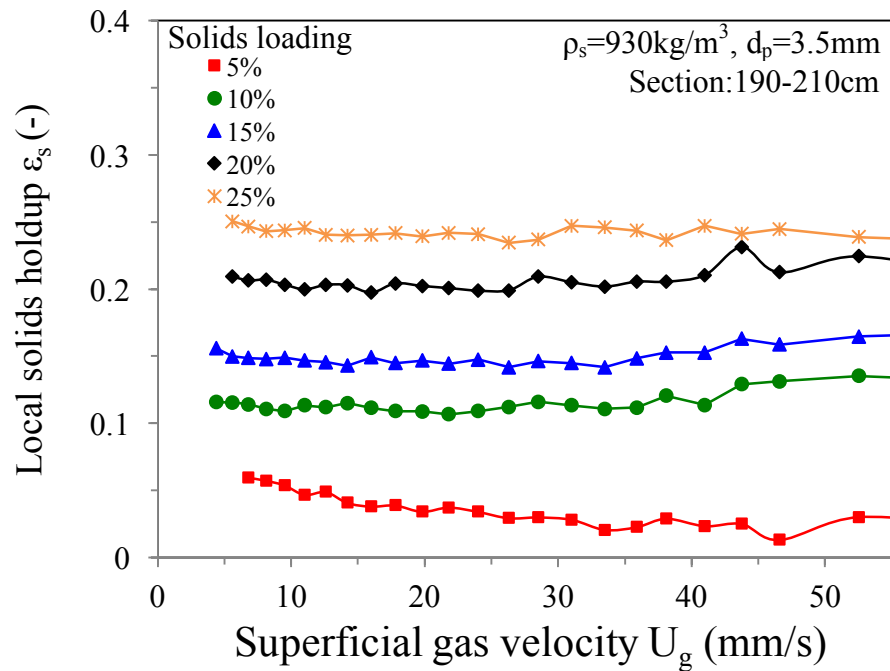
(d)

Figure 7.7 The variations of local solids holdup as a function of superficial gas velocity for different solids loadings, ρ_s=930kg/m^3: (a) 10-70cm, (b) 70-130cm, (c) 130-190cm, (d) 190-210cm.

From the Fig 7.8, it is observed that the local solids holdups from the 40cm to 160cm are almost same, however, the local solids holdups are lower at solids loading=5%, whereas higher for the other loadings. The most likely reason is that at lower solids loadings, as the lowest position is near the gas distributor, the bubbles affect the solids distribution, while this effect disappears with increasing solids loadings.
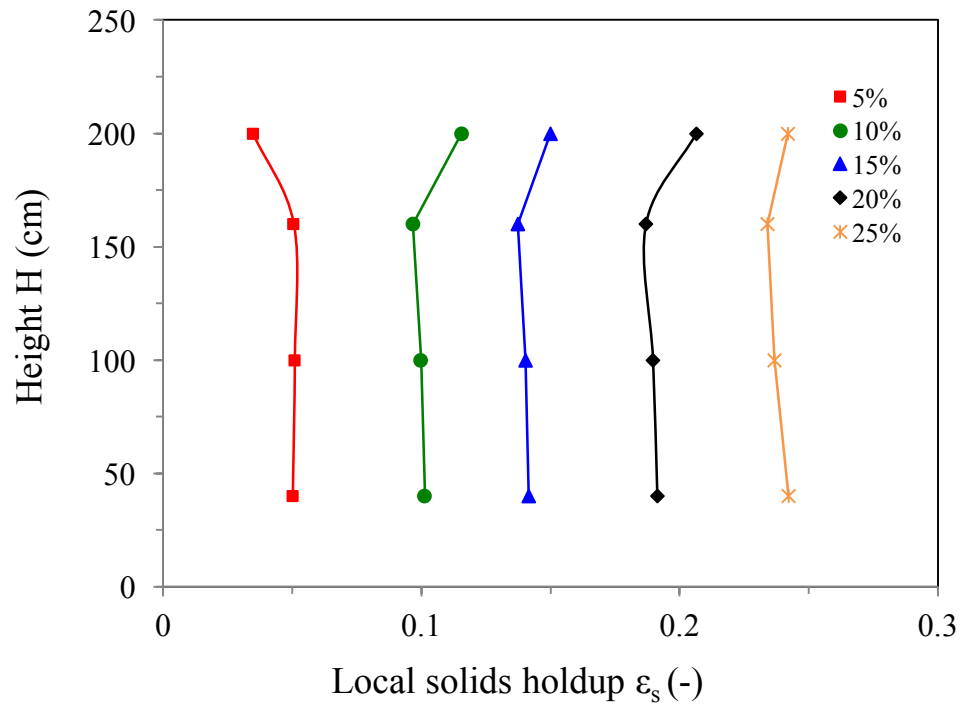
Figure 7.8 The variations of height as a function of local solids holdup for five different solids loadings, ρ_s=930kg/m^3.

Chapter 8

8   Preliminary modeling

In the above analysis, the basic concept of the flow regimes is found. Meanwhile, the effects of particle property and solids loadings have been studied. Among all the present models, the Richardson and Zaki model is the most acceptable one as its simplicity and good agreement with most experimental data. This model is based on the following equation:

$$\varepsilon^n = \frac{U_l}{U_i}$$

(8.1)

where the exponent n is determined by the correlated equations [Karamanev and Nikolov,1992].

$$n = (4.4 + 18\frac{d}{D})\mathrm{Re}_t^{-0.1}$$

(8.2)

for 1 < Ret < 200;

$$n = 4.4\,\mathrm{Re}_t^{-0.1}$$

(8.3)

for 200 < Ret < 500;

$$n = 2.4$$

(8.4)

for Ret > 500.

In addition, Ui is the extrapolated value of Ul as ε approaches one [Karamanev and Nikolov,1992],

$$U_i = U_t / 10^{\frac{d_p}{D}}$$

(8.5)

However, R-Z equation is widely used in liquid-solid system, for the three-phase system, R-Z equation has some limitations. Based on the R-Z equation, a primary model for inverse three-phase system has been built.

Some assumptions including:

Each bubble has a wake and the ratio of the wake to bubble is same.

All the bubbles go upwards with their wake, while the solids only go downward with the downward liquid.

The downward liquid volume flow rate is equal to the upward liquid volume flow rate.

A schematic diagram for this model is shown in Fig 8.1. Phase 1 is bubble phase, with upward bubbles, and the gas flow rate is measured by the rotameter. Phase 2 is the wake phase, which is the upward liquid regarding to the bubble phase. In addition, phase 3 and 4 are the liquid-solid region that the R-Z equation can be applied in this region.
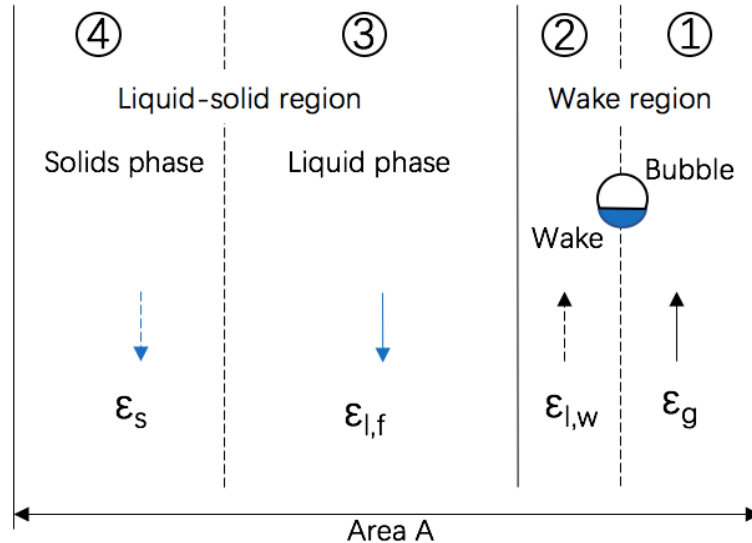
Figure 8.1 A schematic diagram of the bubble-induced three-phase system.

Based on the assumptions, some equations can be achieved. The ratio of the bubble to the wake is assumed as k, the upward liquid volume flow rate can be calculated by the following equation:

$$Q_l = kQ_g \tag{8.6}$$

$$U_l = \frac{Q_l}{A(\varepsilon_s + \varepsilon_{l,f})} \tag{8.7}$$

Ql (Eq.8.5) can be substituted into the Eq.8.6. Therefore, Ul can be expressed as

$$U_l = \frac{kQ_g}{A(\varepsilon_s + \varepsilon_{l,f})} \tag{8.8}$$

In addition, the volume gas flow rate can be calculated with the superficial gas velocity

$$Q_g = AU_g \tag{8.9}$$

Combined the Eq.8.7 and Eq.8.8, the common A can be canceled.

$$U_l = \frac{kU_g}{(\varepsilon_s + \varepsilon_{l,f})} \tag{8.10}$$

Furthermore, applying Eq8.9 to Eq8.1, the R-Z equation can be transferred as

$$\varepsilon^n = \frac{kU_g}{(\varepsilon_g + \varepsilon_{l,f})U_i} \tag{8.11}$$

The porosity in the left can be presented as

$$\varepsilon = \frac{\varepsilon_{l,f}}{\varepsilon_{l,f} + \varepsilon_s} \tag{8.12}$$

as the porosity in the downward liquid phase is

$$\varepsilon_{l,f} = 1 - \varepsilon_s - \varepsilon_g - \varepsilon_{l,w} = 1 - \varepsilon_s - \varepsilon_g - k\varepsilon_g = 1 - \varepsilon_s - (k+1)\varepsilon_g \tag{8.13}$$

Therefore, Eq8.11 can be calculated as

$$\varepsilon = \frac{1 - \varepsilon_s - (k+1)\varepsilon_g}{1 - (k+1)\varepsilon_g}$$

(8.14)

Finally, the expression of R-Z equation is shown as

$$\left[\frac{1 - \varepsilon_s - (k+1)\varepsilon_g}{1 - (k+1)\varepsilon_g}\right]^n = \frac{kU_g}{\left[1 - (k+1)\varepsilon_g\right]U_i}$$

(8.15)

The coefficients of three types particles are presented in Table 8.1.

Table 8.1 The coefficients of three types particles

Particle	U_i (cm/s)	Re_t	n	k
P1(904kg/m^3)	6.40	251.04	2.53	0.7
P2(930kg/m^3)	5.44	234.07	2.55	0.7
P3(950kg/m^3)	5.16	384.93	2.43	0.7

Based on the photograph of the bubbles, most of the wake ratio is from 0.6 to 0.8. In order to fit the experimental results, the wake ratio is determined as 0.7 in this model.

Combined the experimental results, a preliminary model has been built based on the R-Z equations and some assumptions.

8.1   The accuracy of model

To validate the proposed model, data from the experiments are used. Compared the average solids holdup of the experiment and the model with different particles is shown in Fig8.3. For all particles, compared with the experimental data, the max deviation of the model is about 1.81% and 4.67% for the P1 and P2, respectively. The deviation error is acceptable, in another word, this model is available for different kind of particles.
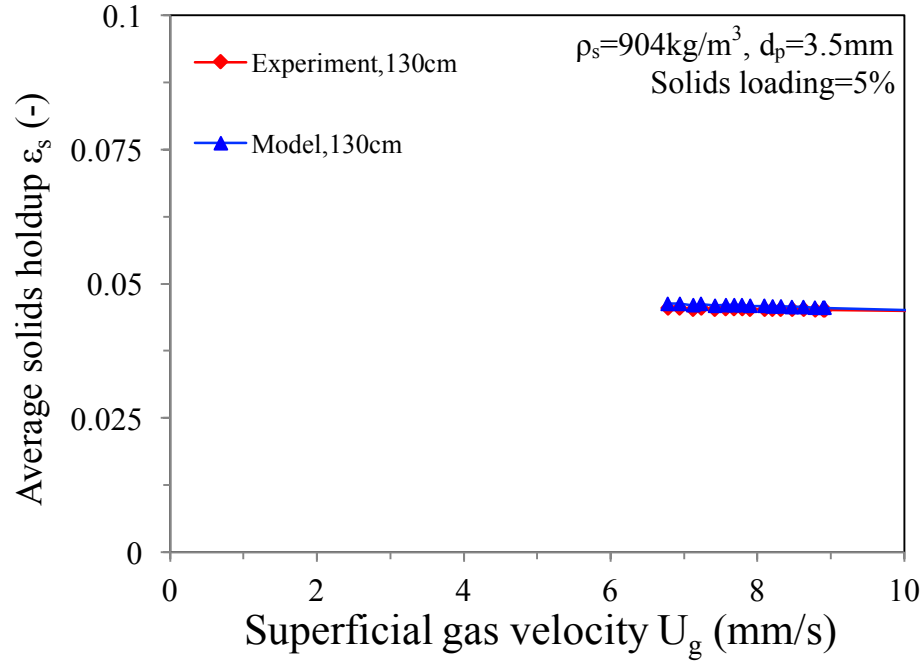
(a)
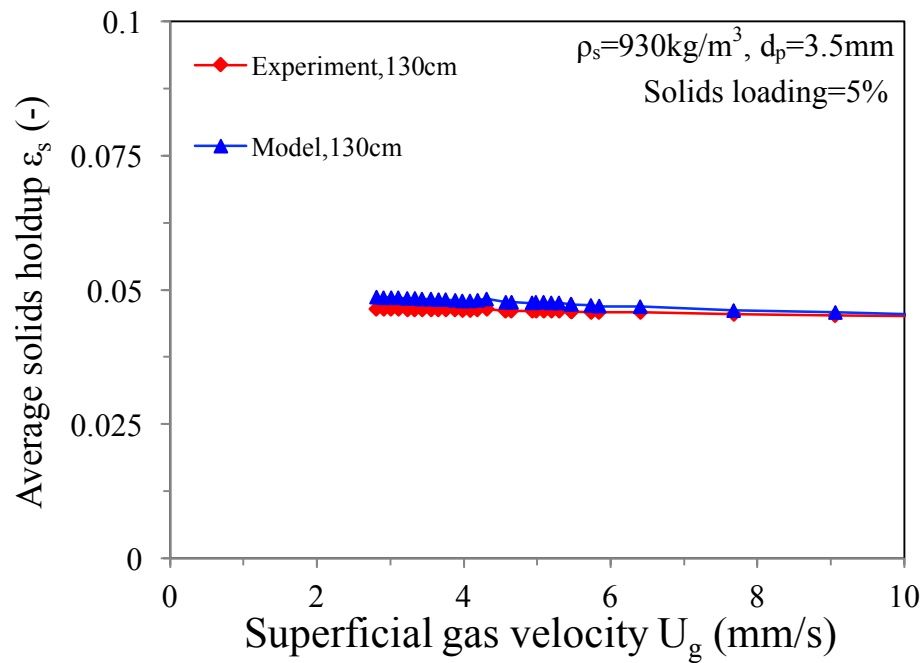
(b)

Figure 8.2 Compare the average solids holdup in experiment and model system for different kind of particles: (a)904kg/m³, (b) 930kg/m³.

The average solids holdup with different solids loadings are investigated in Fig 8.4. For lower solids loadings, such as 5% and 10%, the max deviation is 4.67% and 3.10%, respectively, which means the model can be applied for different solids loadings.
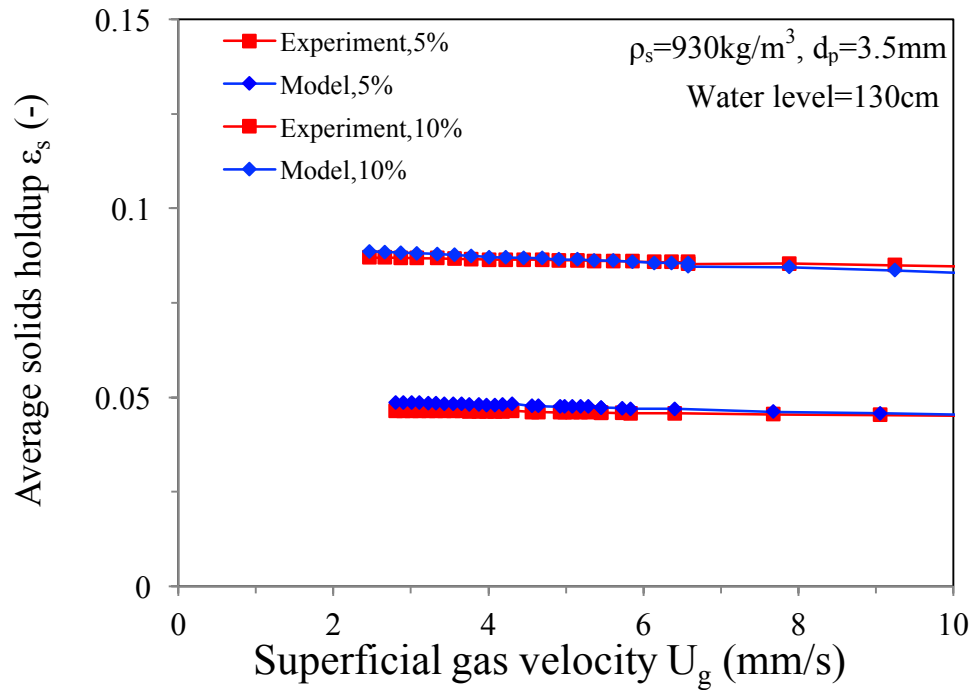
Figure 8.3 Compare the average solids holdup in experiment and model system for different solids loadings.

To exam the effect of the water level, the solids holdup with water level in 130cm and 190cm is shown in Fig8.5. As the max deviation of the 130cm and 190cm is 4.67% and 3.29%, this model also can be used for different water level.
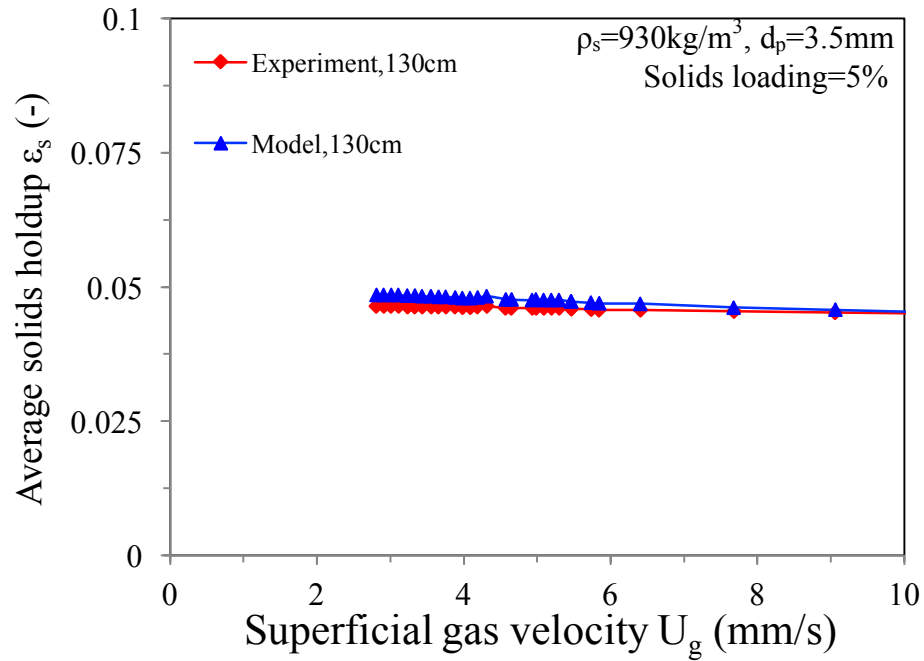
(a)
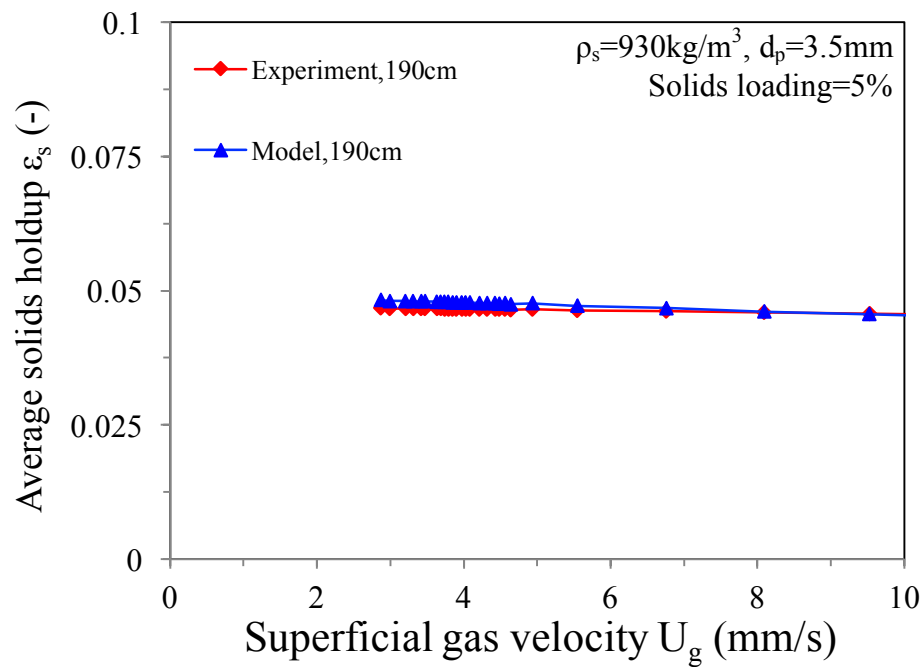
(b)

Figure 8.4 Compare the average solids holdup in experiment and model system for different water level: (a) 130cm, (b) 190cm.

In a word, a preliminary model based on the R-Z equation is achieved.

$$\left[\frac{1-\varepsilon_s-(k+1)\varepsilon_g}{1-(k+1)\varepsilon_g}\right]^n = \frac{kU_g}{\left[1-(k+1)\varepsilon_g\right]U_i} \tag{8.16}$$

where

k=0.7 in this thesis.

Chapter 9

9 Conclusion and recommendations

9.1 Conclusion

The flow regimes in bubble-induced inverse three-phase fluidized bed have been defined and a basic concept of the effect of particle density, particle size, solids loadings and water levels on superficial gas velocities is discussed. Based on the experimental phenomenon, four special superficial gas velocities including initial fluidization velocity, full expansion velocity, complete fluidization velocity have been studied. Three fluidization velocities decrease with increasing the particle density to the fluid density; whereas, superficial gas velocities increase with decreasing the particle size. For all particles, initial fluidization velocity is less than full expansion velocity, which is also lower than the complete fluidization velocity. With increasing the solids loading, three fluidization velocities decrease. In addition, water level has a positive relationship with fluidization velocities.

Moreover, based on the flow regimes map, the operating gas velocities range in a processing operation is higher than the full expansion velocity (4-7mm/s) or complete fluidization velocity (6-9mm/s) depending on the demand. Because the particles reach the bottom but not uniform distribution in full expansion velocity, the operating range is the whole column, but the efficiency of particle is not very high. In complete fluidization velocity, particles are distributed through the whole column, which means the reaction area is larger than the initial expansion regime. A concept of higher superficial gas velocity called top freeboard velocity (>50mm/s) has been given.

In the bed expansion regime, the bed expansion characteristics of bubble-induced inverse gas-liquid-solid fluidized bed have been studied and are similar to that of the conventional fluidization. The initial fluidization velocity and full expansion velocity decrease with increasing the particle density or decreasing the particle size. The effect of water level on the bed expansion can be neglected. In addition, there is a negative

correlation between the full expansion velocity and solids loadings, while the initial fluidization velocity is almost same with increasing the solids loadings.

In the complete fluidization regime, the average phase holdups in the bubble-induced inverse three-phase fluidized bed have been studied. For all particles, with increasing gas velocity, average gas holdup increases, liquid holdup decreases and solids holdup remains constant. Compared to the two-phase (gas-liquid) system, gas holdup is almost same, liquid holdup decreases as particles replace the part position of the liquid. The density and size of particles have little effect on the average phase holdups. In addition, with increasing solids loading, solids holdup increases while liquid holdup decreases as more particles are introduced into the three-phase system. However, gas holdup doesn't change much with increasing solids loading. In a word, gas holdup is only related to the gas flow rate.

Also, the local phase holdups are studied in the complete fluidization regime. For all particles, with increasing gas velocity, local gas holdup increases, local liquid holdup decreases and local solids holdup are same. Compared with gas-liquid system, gas holdup remains constant, liquid holdup decreases. For the effect of density and size of the particles, it is obvious that the superficial gas velocity from 0 to 21.8mm/s, the local solids holdup increases from top to bottom through the column, however, from 24 to 62mm/s, the local solids holdup decreases from 40 cm to 160 cm, while the value of the lowest position is much higher than the upper. In addition, local solids holdup increases with increasing the solids loadings. The bubbles near the gas distributor influence the local solids holdup at low solids loading, whereas, with higher solids loading (great or equal to 10%), this effect disappears. Compared with average phase holdups, the local phase holdups have the same trends.

Combined all the parameters, a preliminary model based on Richardson-Zaki equation has been built. From this model, the solids holdup can be calculated by the superficial gas velocity and the deviation error is acceptable.

The basic information offers some perspectives on future research interest in industrial applications. After realizing the effects of the hydrodynamic parameters, the theory

should be applied to practice and the application of new technique in industrial will be examined in the future work.

9.2   Recommendations

In this research, only three types of particles were employed. Therefore, it is necessary to exam more kinds of particles sharing common properties for accurate the effects of each property. In addition, the model should be exanimated with more experimental data for an improved one. Besides, bubble behaviors including bubble size and bubble velocity may be needed for the future work. Moreover, to confirm the effect of different parameter, real waste water should be used to instead of the tap water. In brief, more work is essential to complete for understanding the hydrodynamic characters and potential applications of this novel fluidization bed.

Nomenclature

a	Specific interfacial area (m^{-1})
A	Sectional area (m^2)
Ar	Archimedes number, dimensionless
BER	Bed expansion ratio, dimensionless
C	Empirical constant, dimensionless
C_D	Drag coefficient
C_i	Tracer concentration (mg/L)
C_p	Heat capacity of the liquid phase, J/(kg*K)
$C(\theta)$	Oxygen concentration (mg/L)
D_0	Bottom diameter of tapped bed (m)
D_1	Top diameter of tapered bed (m)
d_p	Particle diameter (m)
$E(\theta)$	Exit age distribution, dimensionless
F_b	Bubble frequency (m/s)
g	Gravitational acceleration on earth (m/s^2)
H	Henry constant, $mol/(m^3*atm)$
h	Heat transfer coefficient, $W/(m^2*K)$
ΔH	Height difference between pressure taps (m)
Δh	Height difference of pressure drop (m)
H_b	Bed height (m)
h_s	Initial static height of the particle bed (m)
H_w	Water level (m)
J	Flux density molar, mol $O^2*m^{-2}*s$
k_g	Gas mass transfer coefficient (m/s)
k_l	Liquid mass transfer coefficient (m/s)

k	Wake ratio, dimensionless
L_b	Bubble length (m)
n	The amount of substance of gas (mol)
Nu	Nusselt number, dimensionless
ΔP	Absolute pressure drop (Pa)
Q	Volumatic flow rate (m^3/s)
Q_g	Volumatic gas flow rate (m^3/s)
Q_l	Volumatic liquid flow rate (m^3/s)
R	Ideal, or universal, gas constant
T	Temperature (K)
t_a	Average detention time (s)
t_i	Time (s)
U_b	Bubble rising velocity (m/s)
U_g	Superficial gas velocity (m/s)
U_{g0}	Initial gas velocity (m/s)
U_{g1}	Initial fluidization velocity (mm/s)
U_{g2}	Full expansion velocity (mm/s)
U_{g3}	Complete fluidization velocity (mm/s)
U_l	Liquid velocity (mm/s)
U_{l0}	Initial liquid velocity (m/s)
U_{mf}	Minimum fluidization velocity (m/s)
U_t	Terminal velocity (m/s)
V	Volume (m^3)
V_{bed}	Bed volume (m^3)
V_{water}	Water volume (m^3)
Δz	Height difference (m)
σ	Surface tension (mN/m)

Abbreviations

BIITPFB   Bubble-induced inverse three-phase fluidized bed

Greek letters

ε Phase holdup, dimensionless

ε_s Solids holdup, dimensionless

ε_l Liquid holdup, dimensionless

ε_g Gas holdup, dimensionless

ε_{s0} Initial solids holdup, dimensionless

ρ_s Particle density (kg/m^3)

ρ_f Fluid density (kg/m^3)

ρ_{bed} Bed density (kg/m^3)

ρ_l Liquid density (kg/m^3)

ρ_g Gas density (kg/m^3)

ρ_m Mix fluid density (kg/m^3)

Φ Particle sphericity

μ_l Liquid viscosity being $1.002\times10-3$ Pa.s at 20℃ (Pa.s)

μ_g Gas viscosity

Subscripts

ac   Actual

st   Standard

g   Gas

l   Liquid

P   Particle

b   Bed

f   Fluid

f,ls   Liquid-solid fluidized bed

t   Terminal

References or Bibliography

Bandaru, Krishna S.V.S.R., D.V.S. Murthy, and K. Krishnaiah. "Some Hydrodynamic Aspects Of 3-Phase Inverse Fluidized Bed". *China Particuology* 5.5 (2007): 351-356.

Bello, Mustapha Mohammed, Abdul Aziz Abdul Raman, and Monash Purushothaman. "Applications Of Fluidized Bed Reactors In Wastewater Treatment – A Review Of The Major Design And Operational Parameters". *Journal of Cleaner Production* 141 (2017): 1492-1514.

Briens, C.L. et al. "Effect Of Coalescence Inhibitors On The Performance Of Three-Phase Inverse Fluidized-Bed Columns". *Chemical Engineering Science* 54.21 (1999): 4975-4980.

Briens, L.A. et al. "Minimum Liquid Fluidization Velocity In Gas-Liquid-Solid Fluidized Beds Of Low-Density Particles". *Chemical Engineering Science* 52.21-22 (1997): 4231-4238.

Buffière, Pierre, and René Moletta. "Collision Frequency And Collisional Particle Pressure In Three-Phase Fluidized Beds". *Chemical Engineering Science* 55.22 (2000): 5555-5563.

Buffière, Pierre, and René Moletta. "Some Hydrodynamic Characteristics Of Inverse Three Phase Fluidized-Bed Reactors". *Chemical Engineering Science* 54.9 (1999): 1233-1242.

Campos-Díaz, K.E., E.R. Bandala-González, and R. Limas-Ballesteros. "Fluid Bed Porosity Mathematical Model For An Inverse Fluidized Bed Bioreactor With Particles Growing Biofilm". *Journal of Environmental Management* 104 (2012): 62-66.

Cho, Yong Jun et al. "Heat Transfer And Hydrodynamics In Two- And Three-Phase Inverse Fluidized Beds". *Industrial & Engineering Chemistry Research* 41.8 (2002): 2058-2063.

Das, Bimal, Uma Prasad Ganguly, and Sudip Kumar Das. "Inverse Fluidization Using Non-Newtonian Liquids". *Chemical Engineering and Processing: Process Intensification* 49.11 (2010): 1169-1175.

Das, Bimal et al. "Holdup Prediction In Inverse Fluidization Using Non-Newtonian Pseudoplastic Liquids: Empirical Correlation And ANN Modeling". *Powder Technology* 273 (2015): 83-90.

Ergun, S., "Fluid Flow Through Packed Columns", Chem. Eng. Prog., 48, 89 (1952).

Fahim, Sameh et al. "Oxygen Transfer In Three Phase Inverse Fluidized Bed Bioreactor During Biosurfactant Production By Bacillus Subtilis". *Biochemical Engineering Journal* 76 (2013): 70-76.

Fan, Liang-Shih, Katsuhiko Muroyama, and Song-Hsing Chern. "Hydrodynamic Characteristics Of Inverse Fluidization In Liquid—Solid And Gas—Liquid—Solid Systems". *The Chemical Engineering Journal* 24.2 (1982a): 143-150.

Fan, Liang-Shih, K. Muroyama, and S.H. Chern. "Some Remarks On Hydrodynamics Of Inverse Gas-Liquid-Solid Fluidization". *Chemical Engineering Science* 37.10 (1982b): 1570-1572.

Fan, Liang - Shih. Gas - Liquid - Solid Fluidization Engineering. *Boston: Butterworths*, 1989.

Femin Bendict, R. J., G. Kumaresan, and M. Velan. "Bed Expansion And Pressure Drop Studies In A Liquid-Solid Inverse Fluidised Bed Reactor". *Bioprocess Engineering* 19.2 (1998): 137.

Garcia-Ochoa, Felix, and Emilio Gomez. "Bioreactor Scale-Up And Oxygen Transfer Rate In Microbial Processes: An Overview". *Biotechnology Advances* 27.2 (2009): 153-176.

Hamdad, Imran et al. "Oxygen Transfer And Hydrodynamics In Three-Phase Inverse Fluidized Beds". *Chemical Engineering Science* 62.24 (2007): 7399-7405.

Han, S.J., R.B.H. Tan, and K.C. Loh. "Hydrodynamic Behaviour In A New Gas-Liquid-Solid Inverse Fluidization Airlift Bioreactor". *Food and Bioproducts Processing* 78.4 (2000): 207-215.

Karamanev, D. G., and L. N. Nikolov. "Bed Expansion Of Liquid-Solid Inverse Fluidization." *AIChE Journal* 38.12 (1992): 1916-1922.

Karamanev, D. G. "Equations for calculation of the terminal velocity and drag coefficient of solid spheres and gas bubbles". *Chemical Engineering Communications* 147.1 (1996): 75-84.

Karamanev, D. G., and L. N. Nikolov. "Application Of Inverse Fluidization In Wastewater Treatment: From Laboratory To Full-Scale Bioreactors". *Environmental Progress* 15.3 (1996): 194-196.

Khan, M.J.H. et al. "CFD Simulation Of Fluidized Bed Reactors For Polyolefin Production – A Review". *Journal of Industrial and Engineering Chemistry* 20.6 (2014): 3919-3946.

Kim S D，Kang Y. Hydrodynamics，"heat and mass transfer in inverse and circulating three-phase fluidized-bed reactors for wastewater treatment." *Stud. Surf. Sci. Catal.*，159(2006)：103-108.

Lacroix, Nicolas, Daniel R Rousse, and Robert Hausler. "Anaerobic Digestion And Gasification Coupling For Wastewater Sludge Treatment And Recovery". *Waste Management & Research* 32.7 (2014): 608-613.

Lee, Dong-Hyun, Norman Epstein, and John R. Grace. "Hydrodynamic Transition From Fixed To Fully Fluidized Beds For Three-Phase Inverse Fluidization". *Korean Journal of Chemical Engineering* 17.6 (2000): 684-690.

Myre, Denis, and Arturo Macchi. "Heat Transfer And Bubble Dynamics In A Three-Phase Inverse Fluidized Bed". *Chemical Engineering and Processing: Process Intensification* 49.5 (2010): 523-529.

Narayanan, C. M. et al. "Studies On Performance Analysis And Computer Aided Design Of Inverse Fluidized Bed Bioreactors With Nanosupport Particles". *International Journal of Chemical Reactor Engineering* 12.1 (2014).

Nikolov, L., and D. Karamanev. "Experimental Study Of The Inverse Fluidized Bed Biofilm Reactor". *The Canadian Journal of Chemical Engineering* 65.2 (1987): 214-217.

Richardson, J.F. and Zaki, W.N., *Trans. Inst. Chem. Engrs*,32,35 (1954)

Sánchez, Omar et al. "Liquid Mixing And Gas–Liquid Mass Transfer In A Three-Phase Inverse Turbulent Bed Reactor". *Chemical Engineering Journal* 114.1-3 (2005): 1-7.

Sau, D.C., S. Mohanty, and K.C. Biswal. "Experimental Studies And Empirical Models For The Prediction Of Bed Expansion In Gas–Solid Tapered Fluidized Beds". *Chemical Engineering and Processing: Process Intensification* 49.4 (2010): 418-424.

Shin I.S.，Son S.M.，Kang，et al. "Phase holdup characteristics of viscous three-phase inverse fluidized beds". *Journal of Industrial and Engineering Chemistry*, 13-6：971-978 (2007).

Sokół, Włodzimierz, and Belay Woldeyes. "Evaluation Of The Inverse Fluidized Bed Biological Reactor For Treating High-Strength Industrial Wastewaters". *Advances in Chemical Engineering and Science* 01.04 (2011): 239-244.

Son, Sung Mo et al. "Bubble Properties In Three-Phase Inverse Fluidized Beds With Viscous Liquid Medium". *Chemical Engineering and Processing: Process Intensification* 46.8 (2007): 736-741.

Yang, W.-C. Handbook Of Fluidization And Fluid-Particle Systems. *New York: Marcel Dekker*, 2003

Zhang, J.-P,N. Epstein, J. R. Grace, and Zhu, J., "Minimum Liquid Fluidization Velocity of Gas-Liquid Fluidized beds" *Trans IChemE*, 73, Part A, 347 (1995).

Zhang, J.-P., N. Epstein, and J.R. Grace. "Minimum Fluidization Velocities For Gas— Liquid—Solid Three-Phase Systems". *Powder Technology* 100.2-3 (1998): 113-118.

Zhiping Zhu, Na Yongjie, and Lu Qinggang. "Effect Of Pressure On Minimum Fluidization Velocity". *Journal of Thermal Science* 16.3 (2007): 264-269.

Appendices

Appendix A Calibration curve for the gas rotameter

In order to measure the accuracy of the gas rotameter, the calibration of this gas rotameter is shown in Appendix A1. The actual gas flow rate is almost same as the gas rotameter scales and the average error is less than 4.7 %, which means the scales of the gas rotameter can be trusted.
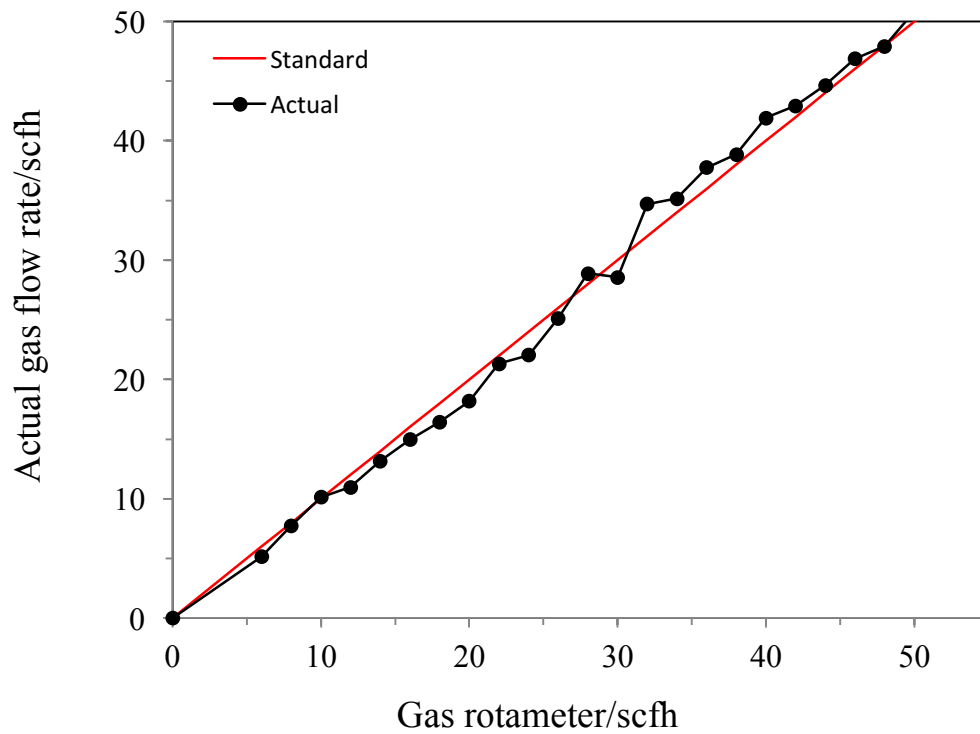
Appendix A1 The calibration curve for the gas rotameter

Appendix B Examples of error analysis

To estimate the possible experimental errors associate with the experimental data and to provide an appropriate analyses for the experimental errors, we have repeated some of the experiments repeatedly.

For example, the bed expansion ratio with error bars for P1 particles (904kg/m^3) at 5% solids loading is shown in Appendix B1. The average experimental error is less than 8%, providing good accuracy for the rest of experiments.
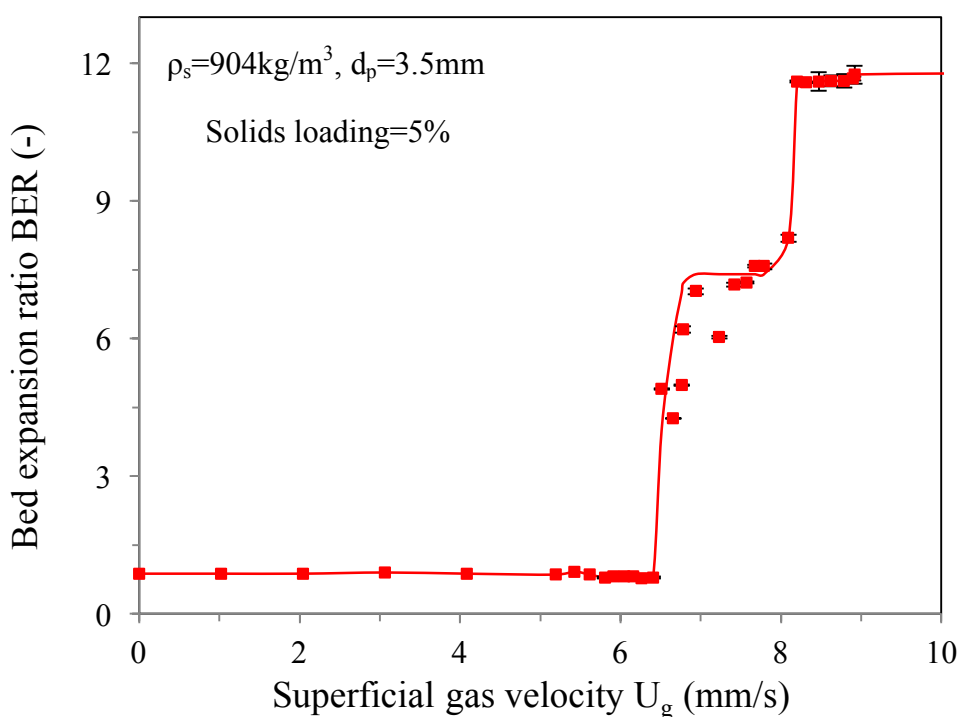
Appendix B1 The bed expansion ratio versus superficial gas velocity with error bars for particles with a density of 904 kg/m^3, solids loading=5%.

In order to ensure the accuracy of solids holdup, liquid holdup and gas holdup, preliminary measurements and analyses of standard error were taken for 930kg/m^3 particles at 15% solids loading. Appendix B2 shows an example of error bars for average solid holdup, average liquid holdup and average gas holdup measurements respectively.
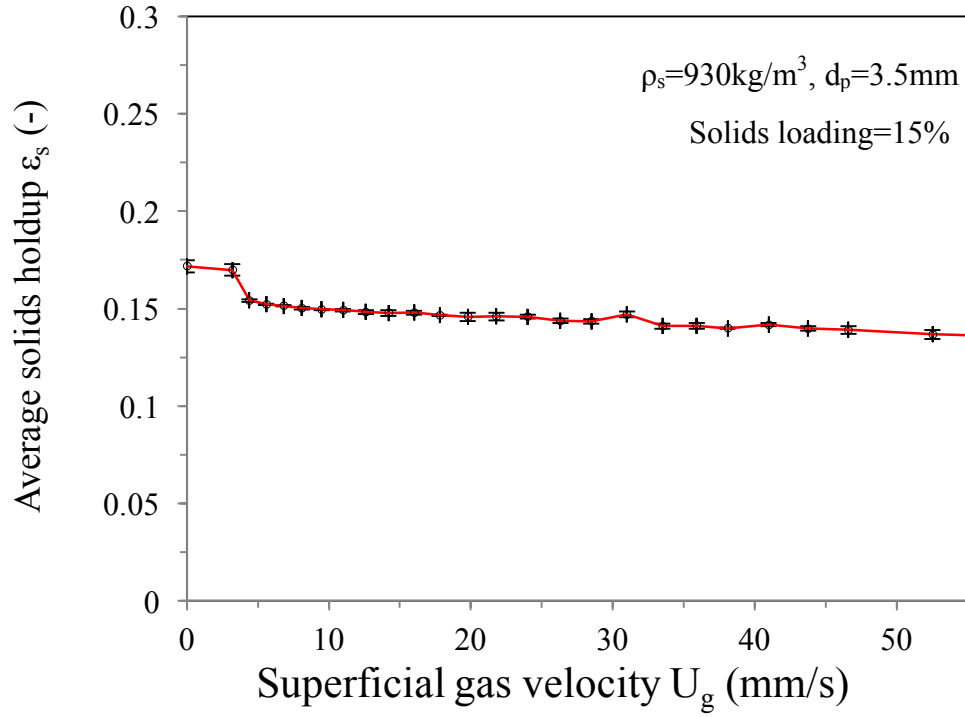
(a)
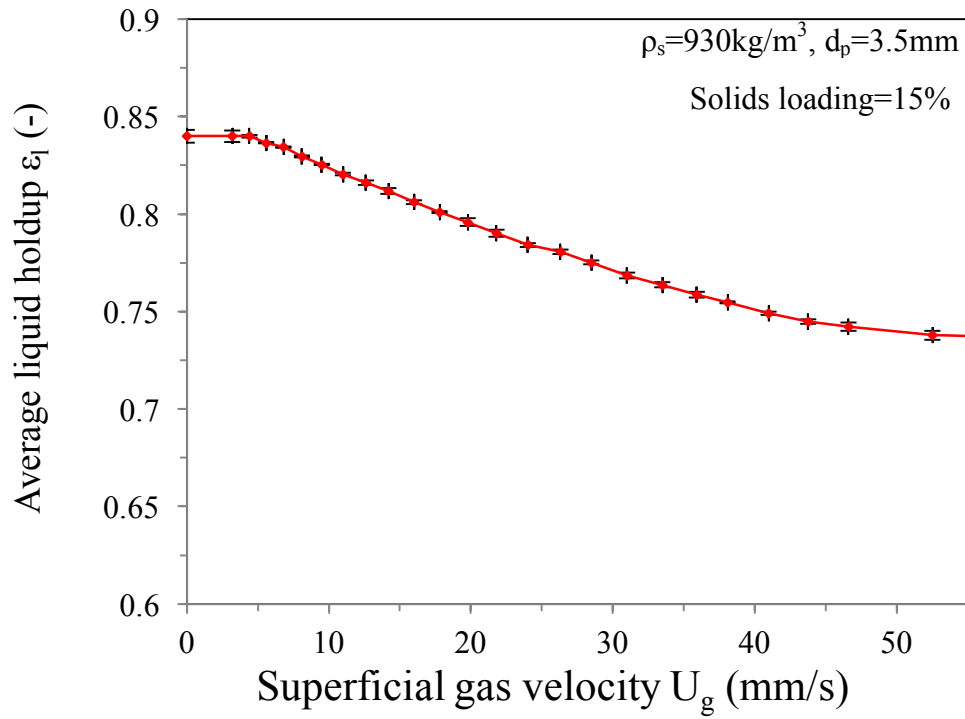
(b)
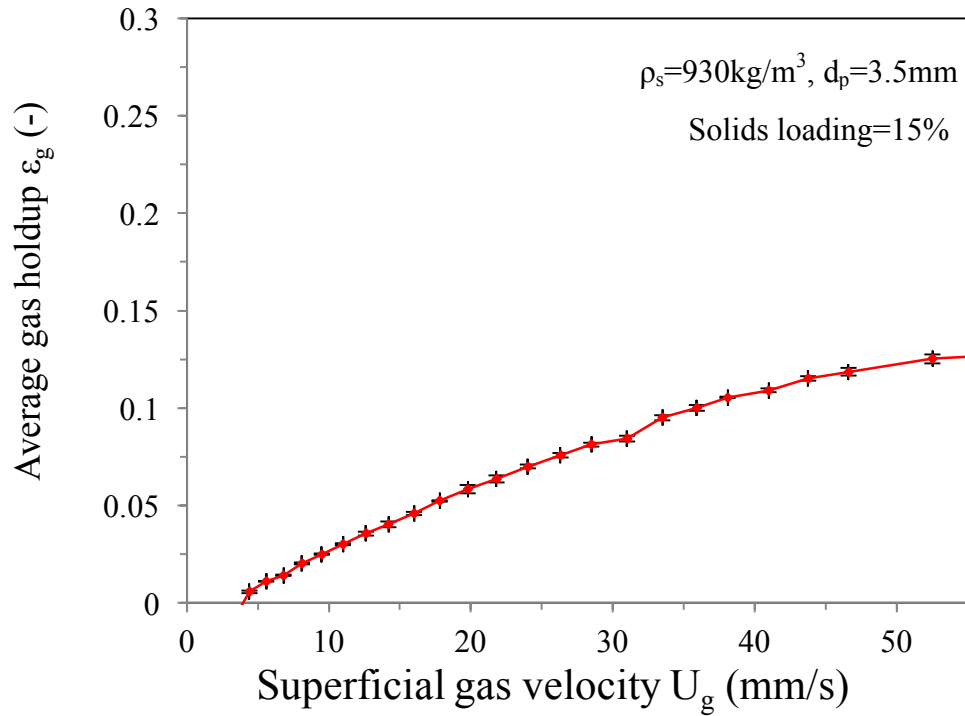
(c)

Appendix B2 The average phase holdups versus superficial gas velocity with error bars for particles with a density of 930 kg/m³, solids loading=15% (a) average solids holdup; (b) average liquid holdup; (c) average gas holdup.

The local solids holdup with error bars for P2 (930 kg/m³) at 15% solids loading is shown in Appendix B3. The average error for each position from bottom to top is 0.09%,0.12%,0.12% and 0.13% respectively, which affords good accuracy and reliability for the remaining experiments.
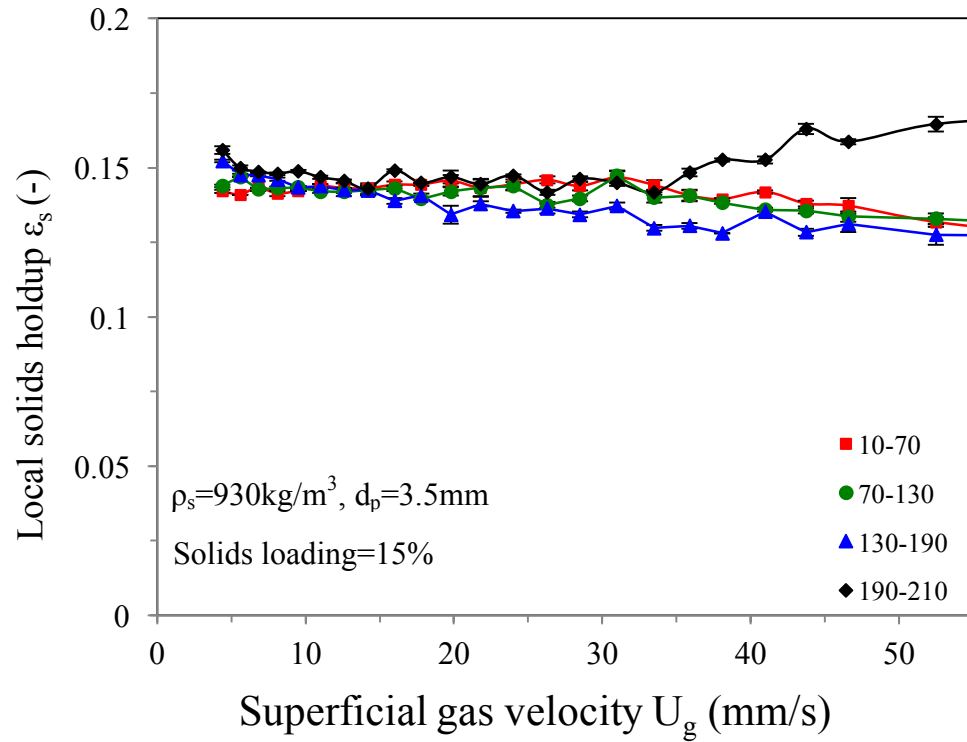
Appendix B3 The local solids holdup versus superficial gas velocity with error bars for particles with a density of 930 kg/m³, solids loading=15%.

Appendix C Initial fluidization velocity, full expansion velocity and complete fluidization velocity

Solids loading=5%

Superficial gas velocity (mm/s)	Particle density (kg/m^3)	Water level (cm)		
		130	190	250
Initial fluidization velocity	904	2.841	3.203	3.344
	930	2.082	2.520	2.413
	950	1.983	2.548	2.194
Full expansion velocity	904	7.642	8.687	8.384
	930	4.187	4.212	3.697
	950	5.430	7.300	7.507
Complete fluidization velocity	904	8.204	8.872	8.500
	930	5.840	6.758	6.922
	950	6.476	7.092	8.000

P2,930-0.35

Superficial gas velocity (mm/s)	Water level (cm)	Solids loading		
		5%	10%	15%
Initial fluidization velocity	130	2.082	2.245	2.684
	190	2.520	2.123	2.254
	250	2.413	2.103	2.126
Full expansion velocity	130	4.187	4.226	4.156
	190	4.212	4.171	3.603
	250	3.697	3.705	4.672
Complete fluidization velocity	130	5.840	6.143	4.410
	190	6.758	5.485	4.278
	250	6.922	7.145	4.670

Appendix D Bed expansion ratio

P1,904-0.35; Solids loading=5%

130cm		190cm		250cm	
U_g	H_{total}/H_0	U_g	H_{total}/H_0	U_g	H_{total}/H_0
12.03	11.79	8.40	11.90	7.78	11.66
8.92	11.75	8.31	11.89	7.66	11.66
12.03	11.79	8.20	11.88	7.54	11.66
8.92	11.75	8.05	11.88	7.35	11.66
8.90	11.67	7.90	11.86	7.23	11.66
8.78	11.62	7.79	11.85	7.11	4.50
8.63	11.62	7.68	11.82	6.99	4.58
8.47	11.60	7.59	11.82	6.87	4.37
8.31	11.59	7.57	11.86	6.72	4.26
8.20	11.60	7.51	11.84	6.60	4.37
8.09	8.19	7.42	11.85	6.48	4.32
7.79	7.57	7.06	6.49	6.34	4.33
7.68	7.58	6.87	6.47	6.19	4.18
7.57	7.22	6.64	6.07	6.04	4.32
7.42	7.17	6.53	5.74	5.92	4.23
7.23	6.03	6.42	4.55	5.81	4.00
6.94	7.03	6.27	0.82	5.66	3.94

6.78	6.20	6.16	0.90	5.55	3.77
6.76	4.99	6.05	0.84	5.40	3.83
6.66	4.26	5.91	0.84	5.26	0.81
6.51	4.90	5.77	0.95	5.15	0.86
6.41	0.79	5.62	0.94	5.03	0.87
6.26	0.77	5.51	0.94	4.92	0.89
6.16	0.81	5.37	0.99	4.78	0.95
6.05	0.81	5.27	0.95	4.64	0.95
5.91	0.81	5.05	0.97	4.53	0.94
5.81	0.79	4.77	0.97	4.28	0.94
5.62	0.85	4.56	0.99	4.05	0.94
5.43	0.92	4.34	0.97	3.83	0.95
5.19	0.85	3.74	0.94	3.60	0.93
4.08	0.88	3.20	0.99	3.34	0.95
3.06	0.90	2.62	0.97	2.76	0.95
2.04	0.88	2.09	0.95	2.19	0.91
1.02	0.88	1.04	0.97	1.08	0.91
0.00	0.88	0.00	0.90	0.00	0.93

P2,930-0.35; Solids loading=5%

130cm		190cm		250cm	
U_g	H_{total}/H_0	U_g	H_{total}/H_0	U_g	H_{total}/H_0
5.73	11.82	9.53	11.75	4.67	7.51
5.46	11.79	8.09	11.69	4.62	6.29
5.46	11.79	6.76	11.63	4.51	5.40
5.30	6.82	5.54	7.90	4.37	4.60
5.19	6.88	4.94	4.52	4.26	4.15
5.09	6.63	4.64	7.56	4.18	4.17
4.98	7.58	4.56	6.68	4.15	4.16
4.93	8.02	4.48	4.91	4.07	3.89
4.65	3.33	4.43	4.56	4.01	4.05
4.57	4.82	4.32	4.52	3.88	3.87
4.31	2.59	4.21	3.99	3.79	3.85
4.18	2.75	4.08	3.75	3.69	3.58
4.08	2.56	4.03	3.75	3.58	3.20
3.98	2.55	3.97	3.83	3.53	2.80
3.88	2.25	3.97	3.48	3.47	2.63
3.75	2.07	3.90	3.29	3.42	2.68
3.65	2.30	3.84	2.98	3.31	2.79

3.55	1.87	3.79	2.44	3.20	3.03
3.43	1.91	3.74	2.65	3.09	2.44
3.33	1.56	3.68	2.62	3.02	1.68
3.23	1.34	3.63	2.10	2.96	1.81
3.11	1.26	3.47	2.37	2.85	1.88
3.01	1.40	3.42	1.93	2.80	1.84
2.91	1.42	3.31	1.93	2.74	1.85
2.81	1.42	3.20	1.69	2.58	1.71
2.69	1.18	2.99	1.97	2.47	1.63
2.59	1.00	2.87	1.78	2.41	1.49
2.49	1.18	2.75	1.55	2.30	1.24
2.39	0.99	2.64	1.48	2.16	0.92
2.28	1.00	2.52	0.96	1.08	0.92
2.18	1.00	2.35	0.96	0.86	0.91
2.08	0.96	2.24	0.96	0.70	0.93
1.97	1.00	2.09	0.96	0.54	0.95
0.98	0.96	1.04	0.90	0.27	0.93
0.00	0.96	0.00	0.90	0.00	0.91

P3,950-0.46; Solids loading=5%

130cm		190cm		250cm	
U_g	H_{total}/H_0	U_g	H_{total}/H_0	U_g	H_{total}/H_0
5.26	9.03	12.67	12.25	5.92	11.57
5.09	8.60	11.09	12.19	5.81	11.58
5.01	2.22	9.53	12.10	5.69	11.58
4.83	3.47	8.17	12.09	5.55	11.57
4.78	2.77	8.17	12.09	5.43	11.56
4.72	2.48	8.01	12.08	5.32	11.56
4.67	2.85	7.86	12.09	5.17	11.55
4.59	2.76	7.74	12.07	5.03	11.56
4.54	2.07	7.59	12.06	4.92	8.19
4.49	2.95	7.47	12.06	4.78	8.89
4.44	3.48	7.28	12.09	4.67	7.57
4.39	2.32	7.13	12.03	4.53	7.58
4.34	2.38	7.09	12.07	4.39	7.22
4.28	2.00	6.94	12.05	4.28	7.17
4.21	2.24	6.83	12.06	4.17	6.03
4.11	1.98	6.76	12.03	3.94	7.03
3.98	1.89	6.71	12.05	3.83	6.20

3.88	1.86	6.53	9.12	3.72	4.99
3.78	1.75	5.97	8.53	3.60	4.26
3.65	1.56	4.72	6.45	3.47	4.90
3.55	1.26	4.61	6.29	3.36	0.79
3.45	1.07	4.50	5.71	3.25	0.77
3.35	1.07	4.39	5.60	3.12	0.81
3.25	1.02	4.26	4.84	3.01	0.81
3.13	1.06	4.10	4.66	2.90	0.81
3.01	1.12	3.99	3.52	2.77	0.79
2.81	1.01	3.20	0.96	2.66	0.85
2.59	1.04	2.97	0.99	2.52	0.92
2.44	1.06	2.76	0.98	2.41	0.85
2.29	1.01	2.60	0.94	2.30	0.88
2.19	0.99	2.32	0.93	2.19	0.90
1.98	0.98	2.10	0.94	1.09	0.88
0.98	0.93	1.04	0.90	0.54	0.88
0.00	0.90	0.00	0.89	0.00	0.88

P2,930-0.35, water level=130cm

5%		10%		15%	
U_g	H_{total}/H_0	U_g	H_{total}/H_0	U_g	H_{total}/H_0
5.46	11.79	6.58	5.94	11.85	4.27
5.46	11.79	6.36	5.94	10.40	4.26
5.30	6.82	6.14	5.94	9.01	4.25
5.19	6.88	5.86	5.93	7.68	4.22
5.09	6.63	5.61	5.92	6.44	4.20
4.98	7.58	5.37	5.92	5.28	4.19
4.93	8.02	5.15	5.91	5.04	4.18
4.65	3.33	4.91	5.91	4.83	4.18
4.57	4.82	4.70	5.90	4.59	4.18
4.31	2.59	4.46	4.21	4.41	4.18
4.18	2.75	4.22	4.18	4.15	4.17
4.08	2.56	4.01	4.26	3.95	4.17
3.98	2.55	3.78	3.64	3.74	4.16
3.88	2.25	3.57	3.24	3.53	4.16
3.75	2.07	3.34	2.49	3.32	4.16
2.49	1.18	3.08	1.76	3.08	1.57
2.39	0.99	2.87	1.77	2.87	1.42
2.28	1.00	2.67	1.65	2.68	1.03

2.18	1.00	2.46	1.62	2.46	0.93
2.08	0.96	2.25	1.25	2.25	0.93
1.97	1.00	2.03	0.98	2.03	0.94
0.98	0.96	1.00	0.90	1.01	0.91
0.00	0.96	0.00	0.90	0.00	0.88

P2,930-0.35, water level=190cm

5%		10%		15%	
U_g	H_{total}/H_0	U_g	H_{total}/H_0	U_g	H_{total}/H_0
8.09	11.69	5.48	5.95	13.08	4.24
6.76	11.63	4.99	5.95	11.25	4.22
5.54	7.90	4.88	5.94	9.67	4.20
4.32	4.52	4.77	5.94	8.25	4.18
4.21	3.99	4.66	5.94	6.86	4.17
4.08	3.75	4.52	5.94	5.63	4.15
4.03	3.75	4.39	5.93	4.41	4.13
3.97	3.83	4.28	5.93	4.28	4.13
3.97	3.48	4.17	3.97	4.17	4.12
3.90	3.29	4.04	3.83	4.06	4.12
3.84	2.98	3.93	3.88	3.95	2.88
3.79	2.44	3.82	3.65	3.84	2.46

3.74	2.65	3.69	2.39	3.73	2.32
3.68	2.62	3.58	2.15	3.60	2.07
3.63	2.10	3.47	2.21	3.49	2.06
3.47	2.37	3.36	2.05	3.38	1.87
3.42	1.93	3.24	2.00	3.27	1.83
3.31	1.93	3.11	1.93	3.16	1.80
3.20	1.69	3.01	1.80	3.04	1.69
2.99	1.97	2.90	1.67	2.93	1.67
2.87	1.78	2.78	1.82	2.82	1.70
2.75	1.55	2.67	1.72	2.68	1.57
2.64	1.48	2.56	1.42	2.58	1.50
2.52	0.96	2.46	1.35	2.47	1.42
2.35	0.96	2.35	1.27	2.36	1.47
2.24	0.96	2.24	1.18	2.25	1.26
2.09	0.96	2.12	0.89	2.14	0.90
1.04	0.90	1.05	0.89	1.06	0.90
0.00	0.90	0.00	0.89	0.00	0.89

P2,930-0.35, water level=250cm

5%		10%		15%	
U_g	H_{total}/H_0	U_g	H_{total}/H_0	U_g	H_{total}/H_0
5.75	11.80	8.62	5.94	13.32	4.23
5.20	11.80	6.99	5.91	11.72	4.22
4.79	7.93	5.87	5.89	10.09	4.19
4.73	7.69	5.60	5.86	8.62	4.18
4.67	7.51	5.37	5.85	6.98	4.16
4.62	6.29	5.08	5.84	5.92	4.14
4.51	5.40	4.85	5.85	4.67	4.12
4.37	4.60	4.58	5.85	4.41	4.12
4.26	4.15	4.58	5.84	4.20	3.29
4.18	4.17	4.46	3.98	4.25	2.44
3.31	2.79	4.35	3.61	4.04	2.44
3.20	3.03	4.23	2.69	3.91	2.08
3.09	2.44	4.10	2.77	3.79	2.02
3.02	1.68	3.96	2.49	3.70	1.99
2.47	1.63	3.85	2.77	3.54	1.92
2.41	1.49	3.38	2.31	3.38	1.88
2.30	1.24	3.15	2.22	3.33	1.85
2.16	0.92	2.93	2.12	3.17	1.81

1.08	0.92	2.70	1.81	2.93	1.74
0.86	0.91	2.46	1.65	2.70	1.65
0.70	0.93	2.35	1.32	2.48	1.50
0.54	0.95	2.22	1.45	2.25	1.76
0.27	0.93	1.10	1.21	1.13	0.93
0.00	0.91	0.00	0.94	0.00	0.95

Appendix E Average phase holdups

P1,904-0.35

Ug (mm/s)	5%			10%			15%			20%		
	ε_s	ε_g	ε_l	ε_s	ε_g	ε_l	ε_s	ε_g	ε_l	ε_s	ε_g	ε_l
62.0	0.047	0.151	0.802	0.099	0.151	0.751	0.138	0.140	0.723	0.202	0.122	0.676
52.5	0.048	0.146	0.807	0.096	0.138	0.766	0.140	0.134	0.726	0.195	0.129	0.676
46.6	0.046	0.143	0.811	0.096	0.138	0.766	0.142	0.129	0.729	0.199	0.125	0.676
43.7	0.047	0.133	0.820	0.098	0.130	0.772	0.142	0.124	0.734	0.201	0.119	0.679
41.0	0.044	0.130	0.826	0.094	0.126	0.780	0.144	0.117	0.739	0.200	0.117	0.683
38.1	0.046	0.124	0.830	0.096	0.120	0.784	0.145	0.111	0.744	0.201	0.111	0.688
35.9	0.049	0.117	0.834	0.098	0.114	0.788	0.144	0.107	0.748	0.206	0.106	0.688
33.5	0.048	0.113	0.839	0.099	0.109	0.793	0.143	0.103	0.754	0.203	0.103	0.694
31.0	0.050	0.101	0.849	0.096	0.105	0.799	0.146	0.097	0.758	0.205	0.097	0.699
28.5	0.050	0.096	0.854	0.096	0.098	0.806	0.144	0.092	0.764	0.203	0.093	0.703
26.3	0.051	0.091	0.859	0.098	0.090	0.812	0.147	0.085	0.768	0.202	0.089	0.709
24.0	0.051	0.085	0.863	0.098	0.084	0.818	0.147	0.078	0.775	0.200	0.084	0.716
21.8	0.052	0.078	0.871	0.097	0.079	0.824	0.148	0.073	0.779	0.204	0.076	0.720
19.8	0.054	0.069	0.877	0.097	0.072	0.831	0.149	0.067	0.784	0.203	0.072	0.726
17.8	0.055	0.063	0.882	0.099	0.065	0.836	0.149	0.060	0.790	0.204	0.066	0.731
16.0	0.056	0.055	0.890	0.100	0.058	0.841	0.152	0.053	0.795	0.202	0.062	0.736
14.2	0.055	0.049	0.896	0.099	0.054	0.847	0.151	0.049	0.800	0.205	0.054	0.741
12.6	0.055	0.044	0.900	0.100	0.047	0.852	0.152	0.044	0.804	0.203	0.051	0.746
11.0	0.053	0.039	0.907	0.101	0.042	0.857	0.155	0.037	0.808	0.205	0.044	0.750
9.5	0.052	0.035	0.913	0.101	0.037	0.862	0.156	0.031	0.814	0.205	0.040	0.755
8.1	0.053	0.028	0.918	0.105	0.028	0.867	0.156	0.028	0.817	0.207	0.033	0.760
6.8	0.053	0.024	0.923	0.120	0.012	0.867	0.156	0.021	0.822	0.213	0.027	0.760
5.6	0.057	0.018	0.926	0.127	0.005	0.867	0.183	0.013	0.822	0.244	0.021	0.760
4.4	0.062	0.013	0.926	0.135	0.012	0.867						
3.2	0.065	0.008	0.928									
2.1	0.078	0.006	0.929									
0	0.064	0	0.942	0.128	0	0.884	0.196	0.000	0.822	0.265	0	0.760

P2,904-0.35

Ug (mm/s)	5%			10%			15%			20%		
	ε_s	ε_g	ε_l	ε_s	ε_g	ε_l	ε_s	ε_g	ε_l	ε_s	ε_g	ε_l
62.0	0.043	0.151	0.806	0.095	0.143	0.763	0.135	0.129	0.736	0.205	0.110	0.685
52.5	0.047	0.142	0.811	0.094	0.142	0.765	0.137	0.125	0.738	0.197	0.118	0.685
46.6	0.046	0.136	0.819	0.097	0.135	0.769	0.139	0.119	0.742	0.197	0.119	0.685
43.7	0.045	0.129	0.826	0.098	0.128	0.774	0.140	0.115	0.745	0.197	0.114	0.688
41.0	0.047	0.123	0.831	0.099	0.121	0.779	0.142	0.109	0.749	0.196	0.112	0.692
38.1	0.045	0.118	0.837	0.098	0.117	0.785	0.140	0.105	0.755	0.196	0.107	0.697
35.9	0.046	0.112	0.842	0.099	0.110	0.791	0.141	0.100	0.759	0.196	0.103	0.701
33.5	0.048	0.106	0.845	0.101	0.105	0.794	0.141	0.095	0.764	0.197	0.097	0.706
31.0	0.047	0.103	0.850	0.101	0.097	0.802	0.147	0.084	0.769	0.196	0.097	0.707
28.5	0.050	0.095	0.855	0.102	0.093	0.805	0.144	0.081	0.775	0.201	0.088	0.711
26.3	0.051	0.091	0.859	0.102	0.086	0.812	0.144	0.076	0.781	0.201	0.081	0.719
24.0	0.049	0.083	0.868	0.102	0.081	0.817	0.146	0.070	0.784	0.197	0.079	0.724
21.8	0.049	0.078	0.873	0.102	0.075	0.823	0.146	0.064	0.790	0.201	0.072	0.727
19.8	0.050	0.070	0.880	0.103	0.068	0.829	0.146	0.058	0.796	0.200	0.067	0.733
17.8	0.050	0.063	0.887	0.103	0.061	0.835	0.147	0.052	0.801	0.201	0.061	0.738
16.0	0.051	0.058	0.891	0.104	0.054	0.842	0.148	0.046	0.806	0.196	0.061	0.744
14.2	0.052	0.052	0.897	0.106	0.049	0.845	0.148	0.040	0.812	0.202	0.049	0.748
12.6	0.052	0.047	0.901	0.104	0.043	0.852	0.148	0.036	0.816	0.202	0.044	0.754
11.0	0.053	0.042	0.905	0.106	0.038	0.856	0.149	0.030	0.821	0.201	0.040	0.759
9.5	0.054	0.037	0.910	0.106	0.035	0.860	0.150	0.025	0.825	0.203	0.035	0.763
8.1	0.054	0.031	0.915	0.106	0.029	0.865	0.150	0.020	0.830	0.204	0.029	0.767
6.8	0.055	0.024	0.921	0.107	0.023	0.870	0.151	0.014	0.834	0.203	0.024	0.773
5.6	0.060	0.019	0.921	0.107	0.018	0.875	0.152	0.011	0.837	0.204	0.020	0.776
4.4	0.062	0.015	0.923	0.108	0.014	0.878	0.154	0.006	0.840	0.204	0.014	0.782
3.2	0.063	0.014	0.927	0.115	0.014	0.880	0.170	0.002	0.840	0.224	0.010	0.782
0	0.067	0	0.938	0.129	0	0.880	0.172	0	0.840	0.234	0	0.782

P3,950-0.46

Ug (mm/s)	5%			10%			15%			20%		
	ε_s	ε_g	ε_l	ε_s	ε_g	ε_l	ε_s	ε_g	ε_l	ε_s	ε_g	ε_l
62.0	0.044	0.162	0.794	0.099	0.144	0.757	0.150	0.124	0.727	0.208	0.114	0.678
52.5	0.051	0.150	0.799	0.095	0.148	0.757	0.143	0.130	0.727	0.198	0.123	0.678
46.6	0.050	0.140	0.810	0.103	0.138	0.759	0.146	0.127	0.727	0.199	0.122	0.678
43.7	0.045	0.135	0.820	0.103	0.133	0.764	0.143	0.131	0.727	0.195	0.121	0.683
41.0	0.046	0.129	0.825	0.104	0.127	0.769	0.150	0.123	0.727	0.196	0.116	0.688
38.1	0.045	0.126	0.830	0.105	0.122	0.773	0.149	0.119	0.732	0.198	0.111	0.691
35.9	0.048	0.118	0.834	0.105	0.115	0.780	0.148	0.115	0.737	0.195	0.107	0.698
33.5	0.049	0.112	0.839	0.104	0.109	0.787	0.149	0.109	0.742	0.197	0.101	0.702
31.0	0.048	0.106	0.846	0.106	0.102	0.793	0.152	0.101	0.747	0.197	0.097	0.706
28.5	0.049	0.098	0.853	0.107	0.096	0.797	0.153	0.096	0.751	0.199	0.092	0.710
26.3	0.048	0.093	0.859	0.105	0.092	0.803	0.154	0.091	0.756	0.199	0.087	0.714
24.0	0.050	0.085	0.865	0.107	0.085	0.808	0.154	0.083	0.762	0.200	0.082	0.718
21.8	0.050	0.079	0.871	0.106	0.080	0.814	0.154	0.078	0.768	0.201	0.074	0.725
19.8	0.050	0.073	0.878	0.107	0.072	0.820	0.156	0.070	0.773	0.201	0.069	0.730
17.8	0.050	0.066	0.884	0.107	0.068	0.825	0.155	0.063	0.782	0.201	0.064	0.735
16.0	0.053	0.059	0.889	0.109	0.060	0.830	0.152	0.061	0.787	0.202	0.058	0.740
14.2	0.053	0.053	0.894	0.109	0.054	0.837	0.157	0.052	0.790	0.202	0.053	0.745
12.6	0.054	0.047	0.899	0.110	0.048	0.842	0.158	0.048	0.795	0.202	0.049	0.749
11.0	0.054	0.041	0.904	0.111	0.042	0.847	0.159	0.040	0.801	0.202	0.043	0.755
9.5	0.054	0.036	0.910	0.110	0.037	0.853	0.158	0.035	0.806	0.200	0.040	0.760
8.1	0.054	0.031	0.915	0.112	0.033	0.855	0.159	0.030	0.811	0.201	0.034	0.765
6.8	0.063	0.023	0.915	0.113	0.028	0.859	0.159	0.025	0.816	0.202	0.029	0.770
5.6	0.063	0.018	0.919	0.118	0.022	0.859	0.160	0.020	0.820	0.202	0.024	0.774
4.4	0.066	0.003	0.924	0.121	0.021	0.865	0.162	0.016	0.823	0.202	0.021	0.778
3.2							0.159	0.011	0.829	0.203	0.015	0.782
2.1							0.165	0.008	0.836	0.217	0.011	0.782
0	0.070	0	0.933	0.135	0	0.871	0.173	0	0.836	0.228	0	0.782

Appendix B4. Local solids holdup

Ug (mm/s)	904-0.35				930-0.35				950-0.46			
	10-70	70-130	130-190	190-210	10-70	70-130	130-190	190-210	10-70	70-130	130-190	190-210
62.0	0.124	0.143	0.127	0.152	0.127	0.131	0.127	0.168	0.150	0.148	0.145	0.116
52.5	0.127	0.140	0.133	0.151	0.132	0.133	0.128	0.165	0.135	0.137	0.145	0.130
46.6	0.130	0.149	0.124	0.160	0.137	0.134	0.131	0.159	0.139	0.140	0.151	0.121
43.7	0.135	0.145	0.126	0.153	0.138	0.136	0.128	0.163	0.127	0.147	0.135	0.146
41.0	0.136	0.148	0.132	0.144	0.142	0.136	0.135	0.153	0.143	0.149	0.149	0.128
38.1	0.137	0.148	0.131	0.152	0.139	0.138	0.128	0.153	0.143	0.149	0.144	0.128
35.9	0.133	0.149	0.127	0.157	0.141	0.141	0.131	0.148	0.142	0.148	0.146	0.119
33.5	0.137	0.142	0.131	0.145	0.144	0.140	0.130	0.142	0.145	0.151	0.142	0.124
31.0	0.140	0.147	0.134	0.140	0.147	0.147	0.137	0.145	0.151	0.153	0.149	0.112
28.5	0.139	0.142	0.132	0.147	0.144	0.140	0.134	0.146	0.151	0.156	0.148	0.113
26.3	0.135	0.154	0.136	0.138	0.146	0.138	0.136	0.142	0.151	0.153	0.150	0.126
24.0	0.136	0.150	0.139	0.134	0.144	0.144	0.135	0.147	0.152	0.158	0.147	0.124
21.8	0.140	0.147	0.136	0.145	0.143	0.143	0.138	0.144	0.152	0.155	0.147	0.132
19.8	0.135	0.153	0.138	0.144	0.146	0.142	0.134	0.147	0.154	0.155	0.154	0.125
17.8	0.139	0.151	0.138	0.143	0.144	0.140	0.141	0.145	0.155	0.153	0.150	0.127
16.0	0.140	0.154	0.141	0.143	0.144	0.143	0.139	0.149	0.154	0.146	0.149	0.127
14.2	0.139	0.147	0.143	0.149	0.143	0.142	0.142	0.143	0.156	0.153	0.152	0.144
12.6	0.136	0.152	0.144	0.151	0.143	0.142	0.143	0.146	0.154	0.153	0.155	0.143
11.0	0.139	0.153	0.148	0.154	0.144	0.142	0.144	0.147	0.158	0.154	0.155	0.140
9.5	0.139	0.149	0.150	0.158	0.142	0.143	0.143	0.149	0.156	0.153	0.155	0.145
8.1	0.133	0.150	0.153	0.160	0.141	0.143	0.146	0.148	0.152	0.153	0.156	0.155
6.8	0.134	0.153	0.151	0.160	0.143	0.143	0.147	0.149	0.154	0.152	0.157	0.154
5.6	0.174	0.180	0.171	0.166	0.141	0.147	0.148	0.150	0.156	0.152	0.156	0.159
4.4					0.142	0.144	0.152	0.156	0.150	0.161	0.160	0.154
3.2					0.161	0.164	0.159	0.169	0.136	0.157	0.166	0.168
2.1									0.156	0.162	0.162	0.162
0	0.186	0.186	0.186	0.186	0.164	0.164	0.164	0.164	0.169	0.169	0.169	0.169

Curriculum Vitae

Name: Xiliang Sun

Post-secondary   The University of Western Ontario
Education and   London, Ontario, Canada
Degrees: 2016-2017 MA.Sc

                       Tianjin University
                       Nankai, Tianjin, China
                       2012-2016 B.Eng

Honours and   Excellent student scholarship, Tianjin University
Awards: 2012-2015

Related Work   Teaching Assistant
Experience   The University of Western Ontario
                       2016-2017

                       Research Assistant
                       The University of Western Ontario
                       2016-2017